Analysis of surface roughness in agricultural soils using in-situ measurements and remote sensing techniques

Alex Martinez de Agirre

December 2017

Supervisors:
Jesús Álvarez Mozos
Rafael Giménez Díaz

upna
Universidad Pública de Navarra
Nafarroako Unibertsitate Publikoa

Thesis submitted in fulfillment of the requirements for the degree of Doctor (PhD) in Science and Industrial Technologies from the Public University of Navarre

upna
Universidad Pública de Navarra
Nafarroako Unibertsitate Publikoa

upna
Universidad Pública de Navarra
Nafarroako Unibertsitate Publikoa

ACKNOWLEDGEMENTS

En primer lugar, me gustaría agradecer la labor de mis supervisores, los profesores Jesús Álvarez Mozos y Rafael Giménez Díaz del Departamento de Proyectos e Ingeniería Rural de la Universidad Pública de Navarra, por su inestimable ayuda y apoyo moral durante el desarrollo de toda la tesis. Eskerrik asko!

También me gustaría agradecer a todos los compañeros del Laboratorio de Hidráulica por los buenos momentos compartidos a la hora del café y por las innumerables charlas mantenidas a modo de "terapia" que tanta falta nos han hecho. Y por supuesto, a todos los compañeros que hemos compartido día tras días las comidas en el comedor de la universidad.

Me gustaría agradecer de manera especial a José Antonio Malpica Velasco, quien me descubrió el "gusanillo" de la investigación y tan injustamente se nos fue, y a María Concepción Alonso Rodríguez, del Departamento de Física y Matemáticas de la Universidad de Alcalá, por su apoyo en los inicios de mi carrera investigadora.

Also, I am very grateful to the Laboratory of Hydrology and Water Management of Ghent University for hosting me and kindly sharing their knowledge with me during three months. I want to especially acknowledge Doctor Niko Verhoest and Hans Lievens for helping me in the analysis of SAR data during the summer of 2014.

In the same way, I am very grateful to the Photogrammetry research group of the Department of Geodesy and Geoinformation (GEO) in Technische Universität Wien. I want to especially acknowledge Doctor Norbert Pfeifer and Milutin Milenkovic for supporting me with the TLS data processing during the spring of 2016.

Eskerrak eman nahi dizkiet ere Gasteiz eta Iruñeko lagunei, urte hauetan zehar hainbeste momentu zuekin konpartitzeagatik. Batez ere, Kutxiko poteoan, Juevintxoan eta Mendizorrotzako harmailan nirekin egoten zaretenoi. Mila esker!

Así mismo, quisiera agradecer a mi familia el apoyo recibido durante estos años. Me gustaría tener presente a la gente que nos ha dejado en el tiempo en el que se ha

desarrollado esta tesis. Sobre todo, a la tía Mari, que se nos ha ido pocos días antes del depósito de esta tesis.

Por último, me gustaría agradecer de manera especial a mis padres, Felix y Rosa, por estar siempre a mi lado y por haberme enseñado a ser cómo soy. ¡Os estaré siempre agradecido!

Eta nola ez, zuri, Miren, eskerrik asko bihotz-bihotzez beti hor egoteagatik eta zaren modukoa izateagatik!

Gasteiz & Iruñea,
Alex Martinez de Agirre

TABLE OF CONTENTS

LIST OF FIGURES

upna
Universidad Pública de Navarra
Nafarroako Unibertsitate Publikoa

LIST OF TABLES

upna
Universidad Pública de Navarra
Nafarroako Unibertsitate Publikoa

LIST OF ABBREVIATIONS AND ACRONYMS

2D	Two Dimensions
3D	Three Dimensions
ASAR	Advanced Synthetic Aperture Radar
BC	Box Counting method
CH	Chisel
dB	Decibel
DEM	Digital Elevation Model
ENVISAT	Environmental Satellite
ESA	European Space Agency
FFT	Fast Fourier Transform
FWO	Research Foundation Flanders
GOM	Geometrical Optics Model
HC	Harrowed Compacted
HH	Horizontal transmit horizontal receive polarization mode
HH-VV	Alternative Polarization mode of ENVISAT/ASAR
HR	Harrowed Rough
HS	Harrowed Smooth
ICP	Iterative Closest Point
IEEE	Institute of Electrical and Electronics Engineers
IEM	Integral Equation Model
IGARSS	International Geoscience and Remote Sensing Symposium
IS	Image Swath of ENISAT/ASAR
LiDAR	Light Detection And Ranging
MAP	Maximum A Posteriori
MP	Mouldboard Plough
N	North
OPALS	Orientation and Processing of Airborne Laser Scanning
P	Planted
P*	Parallel (chapter 6)
PC	Planted Compacted
PM	Planted Modified
PRO	Laser Profilometer
PS	Power Spectrum method

PU	Planted Unmodified
RGB	Red, Green and Blue
RMS	Root Mean Square method
RMSE	Root Mean Square Error
RS	Rescaled range method
SAR	Synthetic Aperture Radar
SfM	Structure from Motion
SM	Soil Moisture
SMV	Semivariogram method
SSR	Soil Surface Roughness
T	Perpendicular or Transverse
TDR	Time Domain Reflectometry
TLS	Terrestrial Laser Scanner
TOPLATS	TOPMODEL based Land-Atmosphere Transfer Scheme
VV	Vertical transmit vertical receive polarization mode
W	West

LIST OF NOTATIONS

$\gamma(h)$	Semivariogram for spatial lag h
θ	Local Incidence angle
θ_{ref}	Reference incidence angle
k	Specific roughness spectral component
λ	Wavelength
π	Ratio of circle circumference to diameter
$\rho(h)$	Autocorrelation for spatial lag h
$\rho'(0)$	Initial slope of the autocorrelation function
σ^0	Backscattering coefficient
$\sigma^0_{\theta_{ref}}$	Linear backscatter observation at reference incidence angle
σ^0_{norm}	Normalized backscattering coefficient
D	Fractal dimension
D_{BC}	Fractal dimension (box counting method)
D_{JM}	Jeffries-Matusita Distance
D_{PS}	Fractal dimension (power spectrum method)
D_{RMS}	Fractal dimension (root mean square method)
D_{RS}	Fractal dimension (rescaled range method)
D_{SMV}	Fractal dimension (semivariogram method)
e	Euler's number
fBm	Fractal Brownian motion
H	Hurst coefficient
L_0	Profile horizontal projection length
L_1	Profile perimeter length
l	Correlation length
l_{ACF}	Correlation length
LD	Limiting elevation difference
l_{RMS}	Crossover length (root mean square method)
LS	Limiting slope
l_{SMV}	Crossover length (semivariogram method)
F	Peak frequency
MI	Microrelief Index
MIF	Römkens and Wang (1986) proposed parameter
MUD	Mean Upslope Depression

Q	Linden et al. (1998) proposed parameter
R	Spearman correlation coefficient
R^2	Coefficient of determination
Range	Range of the semivariogram
s	Standard deviation of heights
Sill	Sill of the semivariogram
T_S	Tortuosity index of Saleh (1993)
Z_S	Zribi and Dechambre (2003) proposed parameter

ABSTRACT

The term soil surface roughness is used to describe the variations in soil surface elevation (micro-relief). Roughness affects different important hydrological processes such as surface depression storage, infiltration, overland flow and soil erosion. At the same time, it strongly affects the scattering of microwaves at the soil surface and determines the backscattering coefficient observed by radar sensors. Then, its characterization and quantification is relevant for different sciences areas. However, the current knowledge about this issue is far from being complete and universally accepted. Besides, the natural micro-relief of agricultural soils can be also affected by tillage action in many different ways. In this thesis, field experiments were carried out in agricultural soils affected by different types of conventional tillage, pursuing the following objectives. (i) The evaluation and characterization of different roughness parameters. (ii) The analysis of the influence of roughness measurement scale on radar backscattering. (iii) The analysis of the influence of roughness sample size on radar backscattering. (iv) The evaluation of Terrestrial Laser Scanner and Structure from Motion techniques for quantifying surface roughness.

First, a detailed evaluation of different roughness parameters proposed in the literature was performed. In total, twenty one roughness parameters (divided into four categories) were analyzed. For this purpose, a database of 164 profiles (5-m-long), measured in 5 different roughness classes, was used. Four of these classes corresponded to typical tillage operations (i.e., mouldboard, harrow, seedbed, etc.), and the fifth corresponded to a seedbed soil modified by rainfall. The roughness parameters which best separated the different roughness classes were the limiting elevation difference (*LD*) and the mean upslope depression (*MUD*). However, the roughness parameters most sensitive to roughness changes caused by rainfall were the limiting slope (*LS*) and the crossover lengths obtained by the semivariogram method (l_{SMV}) and the root mean square method (l_{RMS}). On the other hand, many of the roughness parameters showed high correlation values, thus providing the same information.

Secondly, the influence of surface roughness measurement scale on radar backscattering in different agricultural soils was analyzed. To do this, a database of 132 profiles (5-m-long) measured on agricultural soils with different tillage

operations was used, coinciding with a series of ENVISAT/ASAR C-band observations. With this aim, the influence of measurement range (profile length) and the influence of low and high frequency roughness components on radar backscatter were explored. For each of these issues, eight roughness parameters values were computed, and their correlation with the backscatter coefficient and the goodness-of-fit with the Oh model were evaluated. Most of the parameters showed a significant correlation with the backscatter coefficient, especially the fractal dimension (D), the peak frequency (F) and the initial slope of the auto-correlation function ($\rho'(0)$). The medium frequency roughness components (scale of 5-100 cm) showed the highest influence in the radar backscatter observations at C-band.

On the other hand, the sample size required to accurately measure surface roughness for radar applications in agricultural soils was studied. In this case, a database of 1-m-long 635 profiles obtained over five different agricultural soils, and coinciding with ten ENVISAT/ASAR observations, was used. This time, the analysis was carried out considering different surface roughness sample sizes from 1 to 20 profiles. The behavior of the two commonly used roughness parameters (standard deviation of heights (s) and the correlation length (l)), their correlation with the backscatter coefficient and the goodness-of-fit of different backscatter models (IEM, GOM and Oh) were addressed. A sample size of 10-15 profiles could be considered sufficient for an accurate estimation of the standard deviation of heights (s), while 20 profiles have not seemed sufficient to accurately estimate the correlation length (l). The IEM and GOM models showed worse results than the Oh model, probably due to a greater uncertainly of the correlation length (l).

Finally, the in-situ characterization of the surface roughness in agricultural soils using different measurement techniques was assessed. For this, Terrestrial Laser Scanner (TLS) and Structure from Motion (SfM) measurements were carried out in in the filed in three experimental plots (5 x 5 meters) representing different roughness conditions. Laser profilometer measurements were co-registered to TLS and SfM ones to assess the accuracy and suitability of the latter for quantifying surface roughness over agricultural soils. The results showed the ability of both TLS and SfM techniques to measure surface roughness over agricultural soils. However, both techniques (especially SfM) presented a loss of high frequency roughness information that affected the values of some roughness parameters. Altogether, both TLS and SfM

techniques provide very useful 3D surface roughness information that enables a detailed directional analysis, being relevant for hydrological and soil erosion processes or radar remote sensing applications.

With all this, it is expected that this thesis will contribute to a better understanding of the soil surface roughness phenomenon and its characterization in agricultural soils.

upna
Universidad Pública de Navarra
Nafarroako Unibertsitate Publikoa

RESUMEN

El término rugosidad superficial del suelo es utilizado para describir las variaciones de elevación de la superficie del suelo (micro-relieve). La rugosidad afecta diferentes procesos hidrológicos importantes como el almacenamiento superficial, la infiltración, la escorrentía y la erosión del suelo. Al mismo tiempo, la rugosidad superficial también afecta la retrodispersión de las microondas en la superficie del suelo y determina el coeficiente de retrodispersión observado por los sensores radar. Debido a esto, su caracterización y cuantificación es relevante en diferentes áreas científicas. Sin embargo, el conocimiento actual sobre esta cuestión está lejos de ser completo y aceptado universalmente. Además, el micro-relieve natural de los suelos agrícolas puede verse afectado también de muy diferentes maneras por la acción del laboreo. En esta tesis doctoral, se ha llevado a cabo experimentación en suelos agrícolas afectados por diferentes tipos de tratamientos de laboreo, persiguiendo los siguientes objetivos: (i) La evaluación y caracterización de diferentes parámetros de rugosidad. (ii) El análisis de la influencia de la escala de medida de la rugosidad en la retrodispersión radar. (iii) El análisis de la influencia del tamaño de la muestra de rugosidad en la retrodispersión radar. (iv) La evaluación de las técnicas de Laser Escáner Terrestre y la denominada "Structure from Motion" para cuantificar la rugosidad superficial.

Primero, se ha realizado una evaluación detallada de los diferentes parámetros de rugosidad propuestos en la literatura. En total, se han analizado 21 parámetros de rugosidad (divididos en cuatro categorías). Con este propósito, se ha utilizado una base de datos de 164 perfiles (de 5 m de longitud) medidos en 5 diferentes clases de rugosidad. Cuatro de estas clases han correspondido a operaciones típicas de laboreo (es decir, vertedera, rastra, siembra, etc.) y la quinta ha correspondido a un suelo sembrado modificado por la precipitación. Los parámetros de rugosidad que mejor han separado las diferentes clases de rugosidad han sido la diferencia de elevación límite (*LD*) y el índice *MUD*. Sin embargo, los parámetros de rugosidad más sensibles a los cambios de rugosidad causados por la precipitación han sido la pendiente límite (*LS*) y las longitudes de cruce l_{SMV} y l_{RMS}. Por otro lado, muchos de los parámetros de rugosidad han mostrado altos valores de correlación, proporcionando así la misma información.

En segundo lugar, se ha analizado la influencia de la escala de medición de la rugosidad superficial en la retrodispersión radar en diferentes suelos agrícolas. Para ello, se ha utilizado una base de datos de 132 perfiles (de 5 m de longitud) medidos en suelos agrícolas con diferentes operaciones de labranza, coincidiendo con una serie de observaciones ENVISAT/ASAR en banda C. Con este objetivo, se ha explorado la influencia del rango de medida (longitud del perfil) y la influencia de los componentes de rugosidad de baja y alta frecuencia en la retrodispersión radar. Para cada una de estas cuestiones, se han calculado los valores de ocho parámetros de rugosidad, y se ha evaluado su correlación con el coeficiente de retrodispersión y el grado de ajuste con el modelo de Oh. La mayoría de los parámetros han mostrado una correlación significativa con el coeficiente de retrodispersión, especialmente la dimensión fractal (D), la frecuencia de picos (F) y la pendiente inicial de la función de auto-correlación ($\rho'(0)$). Los componentes de rugosidad de media frecuencia (escala de 5-100 cm) han mostrado la mayor influencia en las observaciones de retrodispersión radar en banda C.

Por otro lado, se ha estudiado el tamaño de muestra requerido para medir con precisión la rugosidad superficial para aplicaciones radar en suelos agrícolas. En este caso, se ha utilizado una base de datos de 635 perfiles de 1 m de longitud obtenida en cinco suelos agrícolas diferentes y que coincide con diez observaciones ENVISAT/ASAR. Esta vez, el análisis se ha llevado a cabo teniendo en cuenta diferentes tamaños de muestra de rugosidad superficial de 1 a 20 perfiles. Para ello, han sido abordados el comportamiento de los dos parámetros de rugosidad más utilizados (la desviación estándar de las alturas (s) y la longitud de correlación (l)), su correlación con el coeficiente de retrodispersión y el grado de ajuste de diferentes modelos de retrodispersión (IEM, GOM y Oh). Un tamaño de muestra de 10-15 perfiles podría considerarse suficiente para una estimación precisa de la desviación estándar de las alturas (s), mientras que 20 perfiles podrían no ser suficientes para estimar la longitud de correlación (l) con precisión. Los modelos IEM y GOM han mostrado peores resultados que el modelo de Oh, probablemente debido a una mayor incertidumbre de la longitud de correlación (l).

Por último, se ha evaluado la caracterización in-situ de la rugosidad superficial en suelos agrícolas utilizando diferentes técnicas de medición. Para esto, se han llevado a cabo mediciones con un láser escáner terrestre (TLS) y con la técnica denominada

“Structure from Motion” sobre tres parcelas experimentales (de 5 x 5 m de superficie) que han representado diferentes condiciones de rugosidad. Medidas de perfilómetro laser se han co-registrado a las de TLS y SfM para evaluar la precisión e idoneidad de estas últimas para cuantificar la rugosidad superficial en suelos agrícolas. Los resultados han mostrado la capacidad de las técnicas TLS y SfM para medir la rugosidad superficial de suelos agrícolas. Sin embargo, ambas técnicas (especialmente SfM) han presentado una pérdida de información de rugosidad de alta frecuencia que ha afectado los valores de algunos parámetros de rugosidad. En conjunto, las técnicas TLS y SfM proporcionan una información muy valiosa de la rugosidad superficial 3D que permite un análisis detallado de la direccionalidad, siendo relevante en procesos hidrológico-erosivos de los suelos o en aplicaciones de teledetección radar.

Con todo ello, se espera que esta tesis doctoral contribuya a un mejor entendimiento del fenómeno de la rugosidad superficial del suelo y su caracterización en suelos agrícolas.

upna
Universidad Pública de Navarra
Nafarroako Unibertsitate Publikoa

LABURPENA

Lurrazalaren zimurtasun kontzeptua erabiltzen da lurrazalaren altueraren bariazioak (mikro-erliebea) deskribatzeko. Zimurtasunak prozesu hidrologiko garrantzitsuak eragiten ditu, hala nola, gainazaleko metatzea, infiltrazioa, isurketa, higadura, etab. Era berean, gainazalaren zimurtasunak eragina du gainazaleko mikrouhinen erretrodispertsioan eta radar sentsoreek behatutako erretrodispertsio koefizientea zehazten du. Hori dela eta, zimurtasunaren ezaugarritze eta kuantifikazioa esanguratsua da zenbait zientzia alorretan. Hala ere, gai honen inguruko ezagutza guztiz eta unibertsalki onartua izatetik urrun dago. Gainera, nekazal lurzoruen gainazaleko mikro-erliebe naturalak laborantza lanen eragin desberdinak jasan ditzake ere. Doktore-tesi honen esperimentazioa laborantza lanen eragina pairatu duten nekazal lurretan burutu da. Ondorengo helburu hauek jarraitu direlarik: (i) Zimurtasun parametroen ebaluazioa eta ezaugarritzea. (ii) Zimurtasuna neurtzeko eskalaren eraginaren analisia radar erretrodispertsioan. (iii) Zimurtasun laginaren tamainaren eraginaren analisia radar erretrodispertsioan. (iv) Lurrazalaren zimurtasuna ezaugarritzeko "Terrestrial Laser Scanner" eta "Structure from Motion" tekniken ebaluazioa.

Lehenik, literaturan proposatutako zimurtasun parametroen ebaluazio zehatza egin da. Osotara, 21 zimurtasun parametro aztertu dira (lau kategoriatan banatuak). Horretarako, 164 profilez (5 m luzerakoak) osatutako datu basea erabili da, bost zimurtasun klase desberdinetan neurtuak. Horietako lau laborantza lanei lotutako klaseak izan dira, eta bosgarren klase bat prezipitazioak aldatutako ereindako lurra izan da. Zimurtasun klase desberdinak bereizteko zimurtasun parametrorik onenak "goratze muga desberdintasuna" (*LD*) eta *MUD* indizea izan dira. Hala ere, prezipitazioek eragindako zimurtasun aldaketekiko parametrorik sentikorrenak "malda muga" (*LS*) eta l_{SMV} eta l_{RMS} gurutze luzerak izan dira. Bestalde, zimurtasun parametro askok korrelazio balio altuak eman dituzte, eta, modu honetan, informazio bera eman dute.

Bigarrenik, nekazal lurren gainazalaren zimurtasuna neurtzeko eskalaren eragina aztertu da radar erretrodispertsioan. Horretarako, laborantza teknika desberdinekin landutako nekazal lurzoruetan jasotako 132 profilez (5 m luzerakoak) osatutako datu basea erabili da, C bandan egindako ENVISAT/ASAR behaketekin bat etorriz. Helburu

honekin miatu dira; alde batetik, neurketa tartea (profilaren luzera); eta, bestetik, maiztasun baxuko eta altuko zimurtasun osagaien eragina radar erretrodispertsioan. Gai horietako bakoitzarekin, zortzi zimurtasun parametroren balioak kalkulatu dira, eta hauen korrelazioa erretrodispertsio koefizientearekin eta Oh modeloaren doitze maila ebaluatu dira. Parametro gehienek korrelazio esanguratsua erakutsi dute erretrodispertsio koefizientearekiko, batez ere, dimentsio fraktalak (D), tontor maiztasunak (F) eta auto-korrelazio funtzioaren hasierako maldak ($\rho'(0)$). Maiztasune ertaineko zimurtasun osagaiek (5-100 cm eskala) erakutsi dute eraginik handiena C bandako radar erretrodispertsio behaketetan.

Bestalde, nekazal lurren gainazalaren zimurtasuna zehaztasunez neurtzeko beharrezkoa den laginaren tamaina radar aplikazioetan ikertu da. Kasu honetan, bost nekazal lurzoru desberdinetan neurtutako 1 m luzerako 635 profilez osatutako datu basea erabili da, hamar ENVISAT/ASAR behaketekin bat egiten duena. Oraingo honetan, analisia 1 eta 20 bitarteko profilen zimurtasun lagineko tamaina kontuan hartuz burutu da. Horretarako, zimurtasun parametrorik erabilienen (altueren desbideraketa estandarra (s) eta korrelazio luzera (l)) portaera, hauen korrelazioa erretrodispertsioarekin, eta erretrodispertsio modelo desberdinen doitasun maila aztertu dira. Altueren desbideraketa estandarraren (s) estimazio zehatza egiteko 10-15 profilen lagina nahikoa izan liteke, korrelazio luzera (l) estimatzeko, ordea, 20 lagin ez lirateke nahikoak izango. IEM eta GOM modeloek Oh modeloak baino emaitza kaxkarragoak erakutsi dituzte, seguruenik, korrelazio luzeraren (l) ziurgabetasun handiagoa dela medio.

Azkenik, nekazal lurren gainazalaren zimurtasunaren ezaugarritzea ebaluatu da, in-situ neurketa teknika anitzak erabili direlarik. Horretarako, “Terrestrial Laser Scanner” (TLS) eta “Structure from Motion” (SfM) teknikekin egin dira neurketak, zimurtasun baldintza desberdinak irudikatu dituzten hiru partzelatan (5 x 5 m azalerakoak). Profilometroz jasotako neurketak ko-erregistratu egin dira TLS eta SfM teknikekin jasotakoekin, azkeneko horien egokitasuna ebaluatzeko zimurtasuna ezaugarritzean. Emaitzek erakutsi dute TLS eta SfM tekniken gaitasuna nekazal lurren gainazalaren zimurtasuna neurtzeko. Hala ere, teknika biek (SfM batez ere) maiztasun altuko zimurtasuneko informazio galera erakutsi dute, eta, hortaz, eragin zuzena izan dute zimurtasun parametro batzuetan. Osotara, TLS eta SfM teknikek gainazaleko zimurtasunaren inguruko 3D informazio baliotsua eman dute; norabidearen inguruko

analisi zehatza ahalbidetzen baitute. Eta, hori, garrantzitsua da lurren higadura hidrologiko prozesuetan edota radar teledetekzio aplikazioetan.

Horrekin guztiarekin, doktore-tesi honek nekazal lurren gainazaleko zimurtasunaren fenomenoa eta berorren ezaugarritzea hobeto ulertzen lagunduko duela espero da.

upna
Universidad Pública de Navarra
Nafarroako Unibertsitate Publikoa

PUBLICATIONS

This thesis is presented as a compendium of publications on the topic of surface roughness characterization in agricultural soils. This set of articles has recently been published or are being considered for publications as follows:

- Martinez-Agirre, A., Álvarez-Mozos, J., Giménez, R., 2016. Evaluation of surface roughness parameters in agricultural soils with different tillage conditions using a laser profile meter. Soil & Tillage Research. 161, 19-30. Impact Factor: 3.401, Subject category: SOIL SCIENCE, rank 6 out of 34 (Q1).

- Martinez-Agirre, A., Álvarez-Mozos, J., Lievens, H., Verhoest, N.E.C., 2017. Influence of Surface Roughness Measurement Scale on Radar Backscattering in Different Agricultural Soils. IEEE Transactions on Geoscience and Remote Sensing. 55 (10), 5925-5936. Impact Factor: 4.942, Subject category: REMOTE SENSING, rank 3 out of 29 (Q1).

- Martinez-Agirre, A., Álvarez-Mozos, J., Lievens, H., Verhoest, N.E.C., Giménez, R., 2017. Influence of surface roughness sample size for C-band SAR backscattering applications on agricultural soils. IEEE Geoscience and Remote Sensing Letters, 14 (2), 2300-2304. Impact Factor: 2.761, Subject category: REMOTE SENSING, rank 11 out of 29 (Q2).

- Martinez-Agirre, A., Álvarez-Mozos, J., Milenkovic, M., Pfeifer, N., Giménez, R., Valle Melón, J.M., Rodríguez Miranda, A., 2017. Evaluation of Terrestrial Laser Scanner and Structure from Motion techniques for quantifying soil surface roughness parameters over agricultural soils. ISPRS Journal of Photogrammetry and Remote Sensing. Under Review. Impact Factor: 6.387, Subject category: REMOTE SENSING, rank 1 out of 29 (Q1).

upna
Universidad Pública de Navarra
Nafarroako Unibertsitate Publikoa

CHAPTER 1

INTRODUCTION

upna
Universidad Pública de Navarra
Nafarroako Unibertsitate Publikoa

1.1. State of the art

1.1.1. Surface roughness: definition and importance

Roughly speaking, soil roughness is a measure of the variation in surface elevation from a reference value (Ulaby et al., 1982). Soil surface roughness affects different hydrological processes such as surface depression storage, water infiltration, overland flow velocity, organization of overland flow (connectivity) and consequently soil erosion by water as well. Thus, the characterization and quantification of roughness is of paramount importance in different areas of hydrology and earth sciences. However, and although a wheal of studies addressing this important issue have been carried out, the current knowledge about it is far from being complete and universally accepted. Most of the current definitions of roughness recognized that it is a scale-dependent phenomenon (Zobeck and Poppham, 1998; Pardini, 2003). But, in general it can be said that roughness is the topographic expression of the surface at scales lower than the common resolution of the digital elevation models (Govers et al., 2000; Mushking and Gillespie, 2005). On the other hand, the natural micro-relief of agricultural soils – as a result of the soil particles and soil aggregates/clods arrangements– can be also strongly affected by tillage action.

One of the best known classifications of surface roughness was proposed by Römkens and Wang (1986), which takes into account not only the spatial scale but also the spatial pattern of the surface roughness. The following categories were defined:

- The micro-relief: surface variations due to individual particles or micro-aggregates. This type of roughness is uniform in all directions (isotropic). The surface variations are of the order of millimeter (0-2 mm).

- The random roughness: variations in the surface generated by soil clods caused by agricultural practices. This type or roughness is also non-directional (isotropic). The variations are of the order of 100 mm (can reach up to 200 mm).

- The oriented roughness: systematic differences in elevation due to agricultural works. These forms are one-directional or anisotropic with variations between 100-200 mm.

- The high-order roughness: elevation variations at field, basin or landscape level. These variations are usually non-directional (isotropic).

The term surface roughness will be used from now on only to refer to the random component of roughness, unless stated otherwise.

1.1.2. Surface roughness parameterization

The parameterization of surface roughness in agricultural soils is not straightforward, because each tillage practice causes a particular type of micro-relief even under identical soil conditions (in terms of texture, moisture, density, etc.). Thus, considering the wide range of possible soil conditions, a very large variety of roughness type could result in an agricultural soil immediately after tillage. Furthermore, the micro-relief generated by the different tillage practices is more or less susceptible to change throughout time due to the action of meteorological agents, e.g., precipitations (Della Rosa et al., 2012), wind and temperature changes in the low atmosphere (Pardini, 2003), or even by animal activity (e.g., earthworm).

Although there are many parameters and indices for quantifying surface roughness (e.g., Helming et al., 1993; Magunda et al., 1997; Kamphorst et al., 2000; Vermang et al., 2013), it is not surprising, as mentioned above, that there are none of a universal nature. The roughness parameters most used in the literature can be divided into four groups, following a criterion similar to that of Smith (2014): (1) parameters measuring the vertical dimension of roughness or the magnitude of the elevation variations of the points at the soil surface, (2) parameters measuring the horizontal dimension of roughness or the relation between the height of a point and that of its neighbors, (3) parameters combining both dimensions, and (4) parameters based on fractal theory, which measure self-affinity or the balance between height variations at different spatial scales.

In the first group (vertical parameters) we find the standard deviation of surface heights (*s*) (Currence and Lovely, 1970), the limiting elevation difference (*LD*) (Linden and Van Doren, 1986), the *Sill* of the semivariogram (Helming et al., 1993), and the microrelief index (*MI*) (Römkens and Wang, 1986). Those measuring the horizontal dimension of roughness (horizontal parameters) are: the correlation length (l_{ACF}) and the initial slope of the autocorrelation function ($\rho'(0)$) (Ulaby et al., 1982), the limiting slope (*LS*) (Linden and Van Doren, 1986), the *Range* of the semivariogram, and the peak frequency (*F*) (Römkens and Wang, 1986). Among the combined parameters we find: parameter Z_S (defined as the product of parameter *s* squared and l_{ACF}) (Zribi and Dechambre, 2003), parameter *Q* (defined as the root of the product of parameters *LD* and *LS*) (Linden et al., 1988), parameter *MIF* (defined as the product of the microrelief index and the peak frequency) (Römkens and Wang, 1986), Mean Upslope Depression index (*MUD*) index (Hansen et al., 1999), and the tortuosity index of Saleh (T_S) (Saleh et al, 1993). With regard to the fractal parameters, although the fractality concept does not represent exactly the surface roughness, the estimation of the self-affinity measured by these parameters can supply information of interest in roughness analysis. In fractal parameters we have: the fractal dimension and the crossover length calculated by the semivariogram method (D_{SMV}, l_{SMV}) and by the root mean square method (D_{RMS} , l_{RMS}) (Vidal Vázquez et al., 2005); and the fractal dimension calculated by the box counting (D_{BC}), power spectrum (D_{PS}) (Gneiteng et al., 2012) and rescaled range (D_{RS}) (Liu and Molz, 1996) methods.

All these parameters proposed in the literature are described and evaluated in detail in this thesis (chapter 3).

1.1.3. Surface roughness and radar backscatter

Radar remote sensing has a great potential for the estimation of surface roughness over large areas. The influence of surface roughness on the backscatter coefficient observed by this type of sensors has been known for decades (Ulaby et al., 1978). However, the estimation of surface roughness from radar imagery has been complicated because of the influence of other variables such as soil moisture or vegetation, and also for the difficulty for obtaining field measurements on a scale comparable to that of radar observations (Zribi et al., 2005; Verhoest et al., 2008). In recent years, the concept of effective roughness has been deepened by calibrating the

roughness parameters necessary to obtain a good fit in the soil moisture estimation (Su et al., 1997). This research line provided adequate results in terms of soil moisture estimation (Baghdadi et al., 2006a; Álvarez-Mozos et al., 2008; Lievens et al., 2011). However, it remains to be seen if the effective roughness parameters estimated correspond to the real roughness of the observed surfaces or are just fitting parameters to enable soil moisture content estimation.

Recently, Fung (2015) proposed that many natural surfaces, such as agricultural or sea surfaces, have multiscale roughness properties and not all roughness scale components contribute in the same way in the backscatter process. He proposed that only one specific roughness spectral component, $\kappa = (4\pi/\lambda)\sin\theta$, was responsible for microwave backscatter, where λ is the incident wavelength and θ is the incidence angle. Also, the spatial sampling of surface roughness measurements is an important factor which has been related to the wavelength of SAR sensors. In this aspect, Ulaby et al., (1982) recommended a sampling interval of $\sim 1/10$ of the wavelength and Barber et al., (2016) intervals of 15 mm for L-band and 5 mm for C-band, which is roughly coincident with Ulaby. Finally, due to the spatial variability of surface roughness, a minimum roughness sample size is required for accurately characterizing roughness parameters in agricultural soils. Regarding to this, Bryant et al., (2007) observed that at least 20 profiles were required to accurately determine s and Baghdadi et al., (2008a) reported 10% accuracy for parameter s and 20% accuracy for l when 10 profiles were used.

Radar backscattering is a present but also a future and promising technique since some recently launched polarimetric radar sensors could be used for surface roughness estimation (Allain et al., 2003). In fact, recent studies have demonstrated that some polarimetric parameters obtained from this type of images have a direct relationship with surface roughness. Regarding to this, Marzahn and Ludwig (2009) used observations acquired by airborne sensors to accurately estimate the surface roughness degree of different agricultural soils cultivated with cereal. However, some other studies demonstrated a rather low sensitivity of most polarimetric parameters to surface roughness of agricultural soils (Baghdadi et al., 2013).

In this thesis the surface roughness scales that most affect the radar backscattering process in C-band observations were studied, along with the sample size needed to accurately characterize the surface roughness.

1.1.4. Surface roughness measurement techniques

The complexity of roughness reflects the wide range of surface measurement techniques used for its parameterization (Smith, 2014). The resolution, extent and availability of surface elevation datasets have been spectacularly improved over the last years (Vericat et al., 2014).

The measurement techniques can be classified according to different criteria such us sensor type (contact/non-contact), precision (mm/cm) or dimensionality (2D/3D). However, most of the literature centered the classification by the sensor type into contact and non-contact devices (Govers et al., 2000; Verhoest et al., 2008; Aguilar et al., 2009; Thomsen et al., 2015; Nouwakpo et al., 2016). The most common contact techniques for characterizing soil surface roughness are the needle profilometers (e.g. Gilley and Kottwitz, 1995), the meshboard technique (Callens et al., 2004), the chain method –nowadays rather obsolete– (e.g. Saleh, 1993) and the automated relief meters (e.g. Hansen et al., 1999). The main benefits of these techniques are their low cost and easy handling. However, these techniques have a limited resolution and besides the physical contact between the instrument and the soil surface can cause measurement biases and experimental errors (Jester and Klik, 2005).

This last problem is avoided when using non-contact techniques. The laser profilometer is the non-contact technique that has been mostly used (Verhoest et al., 2008). However, nowadays, the most commonly used non-contact techniques for micro-topography measurements are laser scanners and image based 3D reconstruction technologies (Barneveld et al., 2013; Nouwakpo et al., 2016). Furthermore, laser based measurement techniques have been used since they enable a very high spatial resolution soil micro-topography measurements (Perez-Gutierrez et al., 2007; Aguilar et al., 2009; Castillo et al., 2012; Milenkovic et al., 2014; Nouwakpo et al., 2016). Specifically, Terrestrial Laser Scanner (TLS) technique presents accuracies of 0.1-0.5 mm for vertical measurements and 0.1-2 mm for horizontal ones (Aguilar et al., 2009). Although, the high acquisition cost and the bulky size of the

devices limited their used for field measurement campaigns (Nouwakpo et al., 2016), technical improvements in sensor design could improve this aspect in the near future. In recent years, different authors studied the suitability of TLS for surface roughness characterization in agricultural soils (e.g., Milenkovic et al., 2014; Thomsen et al., 2015; Rodríguez-Caballero et al., 2016).

On the other hand, image based 3D reconstruction technologies can be divided into traditional stereo-photogrammetry and Structure from Motion (SfM) photogrammetry (Nouwakpo et al., 2016). Traditional photogrammetric techniques required specific cameras, precise calibration and geometric constrains (Gilliot et al., 2017), while SfM relaxes some of these specifications making image acquisition and processing significantly faster and easier (Castillo et al., 2012; James and Robson, 2012; Woodget et al., 2015; Gomez et al., 2015). In the last years, the interest of scientists of different disciplines in this technology as a surface reconstruction tool has expanded since the development of readily available SfM software (e.g., Smith and Vericat, 2015; Nouwakpo et al., 2016).

Also, within non-contact techniques it could be included the surface elevation measurements obtained from remote sensors. This group includes optical sensors (Mushkin and Gillespie, 2005), radar sensors (e.g. Raju, 2008), airborne photogrammetric techniques (e.g. Taconet and Ciarletti, 2007), unmanned aerial vehicles (UAV) as a flexible tool for measurement and monitoring (e.g. Laliberte et al., 2010) and airborne laser scanners (Mallet and Bretar, 2009).

In this thesis, a laser profilometer and the newly developed TLS and SfM techniques were used for the in-situ characterization of surface roughness in agricultural soils, and the relationship between surface roughness and radar remote sensing was also explored.

1.2. Objectives

The general objective of this thesis was to gain insight into the surface roughness characterization in agricultural soils using the most advanced measurement

techniques. In order to achieve this general objective, some particulars objectives were established as well:

- The evaluation of the different parameters and the selection of the most suitable ones for characterizing and quantifying surface roughness on agricultural soils as affected by different types of conventional tillage.

- The analysis of the influence of surface roughness measurement scale on radar observations across different agricultural soils determining the roughness scales which contribute to backscatter.

- The analysis of the influence of surface roughness sample size on radar observations in agricultural soils, in order to determine the minimum number of profiles required in radar applications.

- The evaluation of Terrestrial Laser Scanner and Structure from Motion techniques, so as to assess their accuracy and suitability for quantifying surface roughness in different agricultural soils.

1.3. Structure of the thesis

The core of this thesis has been written as a collection of research papers published in or submitted to international scientific journals. Since each paper was intended to be read independently, some overlap may occur between the various papers, especially in the introduction and the materials and methods sections.

The **first chapter** consists of a general introduction in which the different works are presented and their thematic unit is justified and the **second chapter** describes the material and the methods used in this thesis. Next, the four central chapters are the published (or submitted) papers which correspond to the objectives presented above. The **third chapter** presents a detailed evaluation of different roughness parameters proposed in the literature, looking for the most suitable ones for surface roughness characterization in agricultural soils. The **fourth chapter** assesses the influence of surface roughness measurement scale on radar backscattering and the **fifth chapter**

the influence of the surface roughness sample size on radar backscattering. Finally, the **sixth chapter** presents an evaluation of Terrestrial Laser Scanner and Structure from Motion techniques for quantifying surface roughness on agricultural soils. To conclude, the specific conclusions obtained from the different analyses assessed and the general conclusions deducted throughout this thesis are presented.

CHAPTER 2

MATERIALS AND METHODS

upna
Universidad Pública de Navarra
Nafarroako Unibertsitate Publikoa

This chapter aims to introduce the reader to the materials used in the data acquisition process and the methods applied for the data analysis throughout the thesis. For this, the description of the different materials and methods sections in the presented publications has been compiled and synthesized.

2.1. Test sites

In this thesis two different test sites were used to obtain the data for the different analyses. On the one hand, the experimental watershed of La Tejería (Navarre, Spain), which was studied in chapters 3, 4 and 5 (Martinez-Agirre et al., 2016; Martinez-Agirre et al., 2017a; Martinez-Agirre et al., 2017b). On the other hand, the experimental fields at the School of Agricultural Engineers of the Public University of Navarre in Pamplona (Navarre, Spain), which was used in chapter 6 (Martinez-Agirre et al., 2017c). The location of the two study areas is shown in Fig. 2.1.

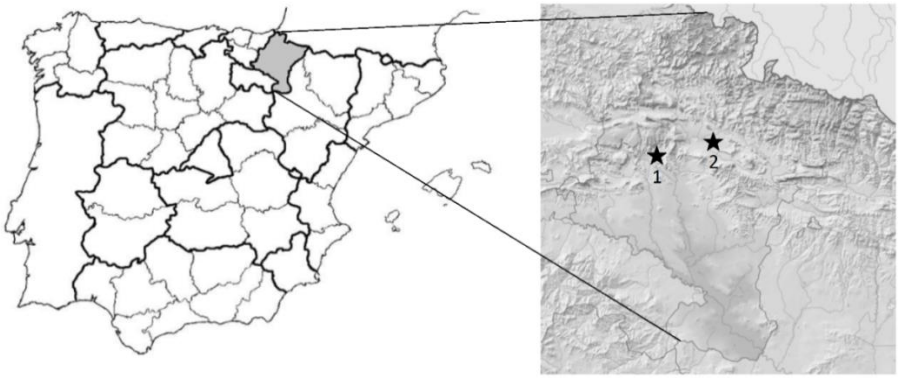

Fig. 2.1. Location of La Tejería experimental watershed (1) and the experimental fields at the School of Agricultural Engineers (2).

2.1.1. La Tejería experimental watershed (chapters 3, 4 and 5)

This watershed is part of the Experimental Agricultural Watershed Network of Navarre, created by the local Government of Navarre in 1993 for the study of the impact of agriculture on the hydrological processes (Casali et al., 2008) (Fig. 2.1), and can be considered representative of rain-fed cereal cropping areas in the region (Álvarez-Mozos et al., 2011). The watershed covers 169 ha with quite homogenous slopes of about 12% and an altitude ranging from 469 to 649 m. The climate is humid

sub-Mediterranean, with a mean annual temperature of 13 ºC. Soils have a silty-clay texture (approximately 5% sand, 52% silt and 43% clay).

Surface roughness measurements were performed over this site on 6 dates (Table 2.1). On the first three dates four different roughness classes (corresponding to different tillage classes) were measured: Mouldboard Plough (MP), Harrowed Rough (HR), Harrowed Smooth (HS) and Planted Unmodified (PU). On the forth date a cereal crop was sown and hence the tillage class was referred to as Planted Unmodified (PU) or Planted Compacted (PC). Some months after planting, soils exhibited the consequences of rainfall, and thus a last roughness class was considered, i.e., Planted Modified (PM). The description of the different roughness classes considered is given in Table 2.2.

Table 2.1. Roughness classes of the test field on the different measurement dates.

Test field	22/09/2004	08/10/2004	24/10/2004	12/11/2004	17/12/2004	01/03/2005
188	HR	HR	-	PU	PU*	PM
189	HR	HR	HS	PU	PU*	PM
193	HR	HR	PU*	PU	PU*	PM
194	-	HR	HR	PU	PU*	PM
199	MP	MP	MP	PU	PU*	PM
201	HS	HS	-	PU	PU*	PM
208	MP	-	-	-	PC	-
235	HS	HS	PU*	PU	PU*	PM
255	HS	HS	-	PU	PU*	PM
258	HR	-	-	PU	PU*	PM

* Planted Unmodified (PU) was referred to as planted (P) in chapters 4 and 5.

Table 2.2. Description of the different roughness classes analyzed in chapter 3, 4 and 5.

Tillage class	Acronym	Description
Mouldboard Plough	MP	Tillage operation performed with a plough with multiple mouldboards at a depth of 15-20 cm, resulting in soil inversion and a very rough surface
Harrowed Rough	HR	Operation performed normally with a tine harrow to break soil clods and provide a smoother surface suitable for seeding
Harrowed Smooth	HS	In cases where the first harrowing did not smoothen sufficiently the surface a second harrowing is applied
Planted Unmodified*	PU*	Seeding operation performed with conventional sowing machinery, normally seed drills
Planted Compacted	PC	Planted operation followed by a compacting roller
Planted Modified	PM	Planted soils modified by the action of the precipitation during 4 months (~250 mm)

* Planted Unmodified (PU) class was referred as Planted (P) in chapters 4 and 5.

2.1.2. Experimental fields at the School of Agricultural Engineers (chapter 6)

This study area is part of the Public University of Navarre's Arrosadia Campus in Pamplona (Navarre, Spain) (Fig. 2.1). The climate is humid sub-Mediterranean with a mean annual temperature of ~13 ºC and an average precipitation of ~675 mm distributed over 95 days. Soils have a silty-clay-loam texture (13.7% sand, 48.3% silt and 38% clay). In this place three experimental plots (5x5 meters) were created using different tillage operations and obtaining different roughness classes (Table 2.3). Measurements were carried out on three days, November 25-27 2013, where no precipitation was recorded, with the aim of evaluating different roughness measurement techniques.

Table 2.3. Description of the different roughness classes analyzed in chapter 6.

Tillage class	Acronym	Description
Mouldboard Plough	MP	Primary tillage operation performed with a plough with multiple mouldboards (15-20 cm depth) that break and turn over the soil
Chisel	CH	Primary tillage operation that breaks and shatters the soil leaving it rough with residue in the surface
Harrowed Compacted	HS	MP operation followed by a secondary operation using a spike harrow and a compacting roller

2.2. Surface roughness measurement techniques

In this thesis, three different techniques were used to obtain the data for the different analyses. On the one hand, the laser profilometer was used for measuring soil surface roughness consistently in all the studies presented in this thesis (chapters 3 to 6). On the other hand, Terrestrial Laser Scanner (TLS) and Structure from Motion (SfM) techniques were evaluated for quantifying surface roughness in agricultural soils (chapter 6).

2.2.1. Laser profilometer (chapter 3, 4, 5 and 6)

A laser profilometer was used to measure soil surface roughness in all the analyses presented in this thesis, thus it is described in chapters 3 to 6. The profilometer was originally designed for roughness measurements by our research group (Álvarez-

Mozos et al., 2005). This instrument incorporates a laser sensor (SICK DME 2000) (Fig 2.2) that measures the vertical distance from a reference aluminum bar (fixed to two tripods) to the soil surface (Fig. 2.2). The profilometer has a total measurement range of 5 m, a sampling interval set to 5 mm and a vertical accuracy of 1.25 mm. The surface roughness data obtained by the laser profilometer were processed as follows (Fig. 2.3): (1) correction of the bending of the aluminum bar due to its weight and that of the sensor carriage, (2) filtering of outliers (points with height differences higher than 10 cm with the previous and next high records) and (3) the correction of the terrain slope (thorough the subtraction of the linear trend along the profile). For more details about this technique, please see section 3.2.2 of the thesis.

Fig. 2.2. SICK DME 2000 laser sensor (left) of the profilometer (right) used for data taking.

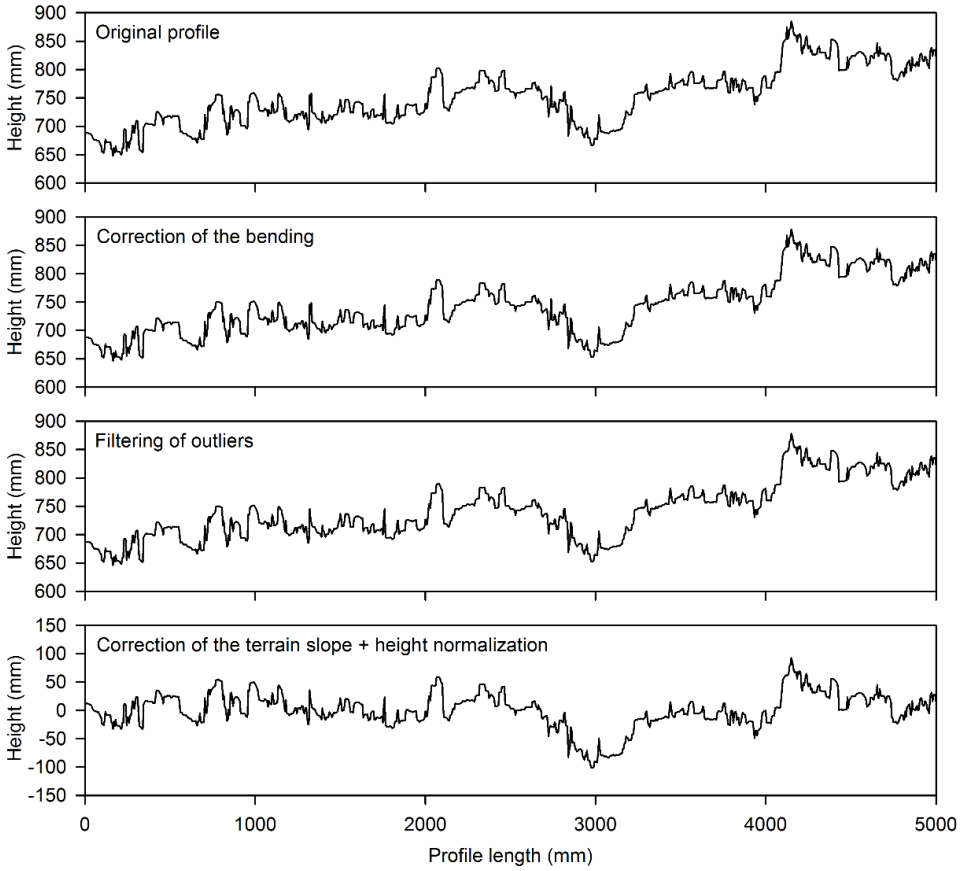

Fig. 2.3. Different steps of the profile processing.

2.2.2. Terrestrial Laser Scanner (chapter 6)

Terrestrial Laser Scanner (TLS) technique is used in chapter 6. The TLS instrument employed in this thesis was the FARO Focus 3D (Fig. 2.4). Four scans were obtained per experimental plot from a tripod ~ 1.75 m high, which were co-registered using five references spheres deployed around the plots (Fig. 2.4). The FARO Focus 3D has a specific ranging accuracy of 0.3 mm and the vertical and horizontal resolution was set to 0.0018º. Terrestrial Laser Scanner (TLS) data processing consisted of: (1) filtering each scan to exclude mixed pixels (using a self-implemented algorithm based on the signal intensity as a function of the incidence angle), and (2) co-registration of the scans using the ICP (iterative closest point) algorithm implemented in the OPALS

(Orientation and Processing of Airborne Laser Scanning) software developed by TU Wien (Otepka et al., 2013; Pfeifer et al., 2014). For more details about this technique, please see section 6.2.3.2 of the thesis.

Fig. 2.4. FARO focus 3D (left) and the scanning setup (right) used for data acquisition.

2.2.3. Structure from Motion (chapter 6)

Structure from Motion (SfM) is a close range photogrammetric technique evaluated in chapter 6. The camera used in this thesis was the Canon EOS 5D Mark II (Fig. 2.5). For each experimental plot 24 photos of 20 megapixels resolution were acquired from a lifting platform (Fig. 2.5). For more details about SfM measurement technique, please see section 6.2.3.2 of the thesis. SfM data processing consisted in: (1) geo-referencing each photo using eight control points measured with a total station and (2) generating the dense point clouds in "ultra-high quality" mode using Agisoft Photoscan software. For more details about this technique, please see section 6.2.3.3 of the thesis.

Fig. 2.5. Canon EOS 5D Mark II camera (left) and the lifting platform (right) used for data acquisition.

2.3. Radar data (chapters 4 and 5)

ENVISAT/ASAR images were used in this thesis for the analysis of soil surface roughness on radar applications. ENVISAT was an Environmental Satellite operated by the European Space Agency (ESA) whose activity period ranged from March 2002 to April 2012. One of the instruments carried by the satellite was the Advanced Synthetic Aperture Radar (ASAR) that operated in C band, with a spatial resolution of 30 m and a selectable polarization configuration (VV was used in this thesis). ENVISAT/ASAR scenes were: (1) orthorectified using a 5 m resolution DEM, (2) calibrated using the local incidence angle, and (3) speckle filtered using a gamma MAP filter with a 5 x 5 window. Then, mean backscattering coefficient (σ^0) values were calculated for each field per date. Further details are given in chapters 4 and 5, where a total of 10 ENVISAR/ASAR scenes acquired over La Tejería watershed were analyzed.

2.4. Soil moisture data (chapters 4 and 5)

In chapters 4 and 5, radar backscatter models were used to evaluate the influence of roughness scale on radar observations. For this, surface soil moisture (SM) data were needed, and thus, SM on La Tejería catchment was measured using a calibrated Time Domain Reflectometry (TDR) probe. For each agricultural field, five spatially distributed locations were monitored per date, so as to obtain a representative average on the fields' SM content at a depth of 5 cm. SM measurements were taken on dates where SAR observations were acquired. However, in some dates no field campaigns could be conducted and therefore SM was modeled using a land-surface model TOPLATS calibrated with the available in-situ measurements. Further details are given in chapters 4 and 5.

2.5. Data analysis

In this section, a brief description of each of the analysis performed during the thesis is made.

2.5.1. Surface roughness parameters analysis

In this thesis, a total of 21 surface roughness parameters were analyzed (Table 2.4). These parameters can be grouped in four categories depending on the roughness properties they quantify. In chapter 3, all the 21 parameters were assessed, whereas in the remaining chapters a lower number was considered. In particular, in chapter 4 eight parameters were analyzed, in chapter 5 just two, and in chapter 6 six. These differences were due to the different objectives and scope of each chapter. For more information about roughness parameters definition, please see section 3.2.3 of the thesis.

Table 2.4. Roughness parameters used in the thesis.

Type	Parameter	Chapter 3	Chapter 4	Chapter 5	Chapter 6
Vertical	*s (cm)*	✓	✓	✓	✓
	LD (cm)	✓			
	Sill (cm^2)	✓			
	MI (cm)	✓	✓		
Horizontal	l_{ACF} *(cm)**	✓	✓	✓	✓
	ρ'(0)	✓	✓		✓
	LS	✓			
	Range (cm)	✓			
	F (cm^{-1})	✓	✓		✓
Combined	Z_S *(cm)*	✓			
	Q ($cm^{1/2}$)	✓			
	MIF	✓	✓		
	MUD (cm)	✓			
	T_S	✓	✓		✓
Fractals	D_{SMV} **	✓	✓		✓
	D_{RMS}	✓			
	D_{BC}	✓			
	D_{PS}	✓			
	D_{RS}	✓			
	l_{SMV} *(cm)*	✓			
	l_{RMS} *(cm)*	✓			

* referred to as *l* in chapters 4, 5 and 6.
** referred to as *D* in chapters 4 and 6.

2.5.2. Separability analysis (chapter 3)

In chapter 3 the ability of each roughness parameter to discriminate different roughness types was evaluated. For that, the Jeffries-Matusita Distance (D_{JM}) was calculated for each roughness parameter and pair of roughness classes analyzed:

$$D_{JM} = \int \left[\left(\sqrt{f(x)} - \sqrt{g(x)} \right)^2 \right] dx \qquad (2.1)$$

where D_{JM} is the distance between classes $f(x)$ and $g(x)$ measured by the parameter x. For more detail about Jeffries-Matusita Distance (D_{JM}), please see section 3.2.4.2.

2.5.3. Surface roughness scale analysis (chapters 4 and 5)

In chapter 4 three different scaling issues on the surface roughness characterization were assessed: (1) the influence of measurement range (profile length) by dividing the original profile into 2 to 10 profiles, (2) the influence of low-frequency roughness components by smoothening the original profiles with an increasing window size (Fig. 4.2 in chapter 4), and (3) the influence of high-frequency roughness components by subtracting the smoothened profiles from the original ones (Fig. 4.2 in chapter 4).

On the other hand, the analysis presented in chapter 5 studied the influence of sample size (number of profiles) on the surface roughness characterization. Here, an increasing number of 1-m-long profiles (from 1 to 20) were considered for roughness parameters estimation. For each plot and date, four original 5-m-long profiles were divided into 20 1-m-long profiles. Further details are given in section 5.2.5 of this thesis.

2.5.4. Correlation analysis (chapters 3, 4 and 5)

In chapter 3 a correlation analysis was performed to study the relationship between the 21 roughness parameters evaluated. A correlation analysis was also used in chapters 4 and 5 to evaluate the correlation between backscatter and different roughness parameters and roughness scales. For this purpose, the Spearman correlation coefficient (R) was obtained. R measures the strength and direction of the monotonic relationship between two variables, since it is not limited to the linear case

it is considered to be the non-parametric version of the more common Pearson correlation coefficient. The Spearman coefficient was selected due to the non-linear shape of some of the relationship explored.

2.5.5. Goodness-of-fit of backscatter models (chapters 4 and 5)

In this thesis, the physically based Integral Equation Model (IEM) (Fung et al., 1992) and Geometrical Optics Model (GOM) (Ulaby et al., 1982), and the empirical model of Oh (Oh et al., 1992) were used. On the one hand, Oh model was selected in chapters 4 and 5 because of its rather large validity domain including both rough and smooth roughness conditions. On the other hand, due to their different nature and validity range, IEM and GOM were considered only in chapter 5 (IEM for the smooth classes P and PC and GOM for the rough classes MP, HR and HS). Finally, models' goodness-of-fit was evaluated by computing the root mean square error (RMSE) between simulated and observed average backscatter values per field.

It must be clarified that, in chapter 5, some fields were slightly out of the validity range of the IEM and GOM models (Fig. 2.6), yet they were included in the analysis since their results were considered not significantly different from the rest of the fields of their classes. Not so in chapter 4, that when considering profile lengths and when performing the filtering of the low and high frequency roughness component, the values of the roughness parameters were further compromised with respect to the range of validity.

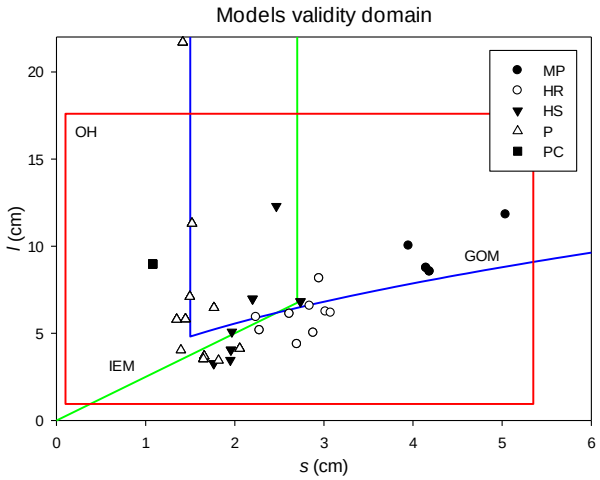

Fig. 2.6. Validity domain of the backscatter models considered in the thesis (IEM, GOM and Oh) and the mean s and l parameters values of the agricultural fields studied in chapters 4 and 5.

2.5.6. Surface roughness measurement techniques (chapter 6)

For the analysis of the measurement techniques, the surface elevation data obtained from the different techniques needed to be processed to be comparable. First, the point clouds obtained with TLS and SfM were co-registered using again the ICP algorithm. Then, profiles were extracted from the point-clouds coinciding with the location of the profiles measured with the profilometer (Fig. 2.7). Further details about this process are given in section 6.2.5.

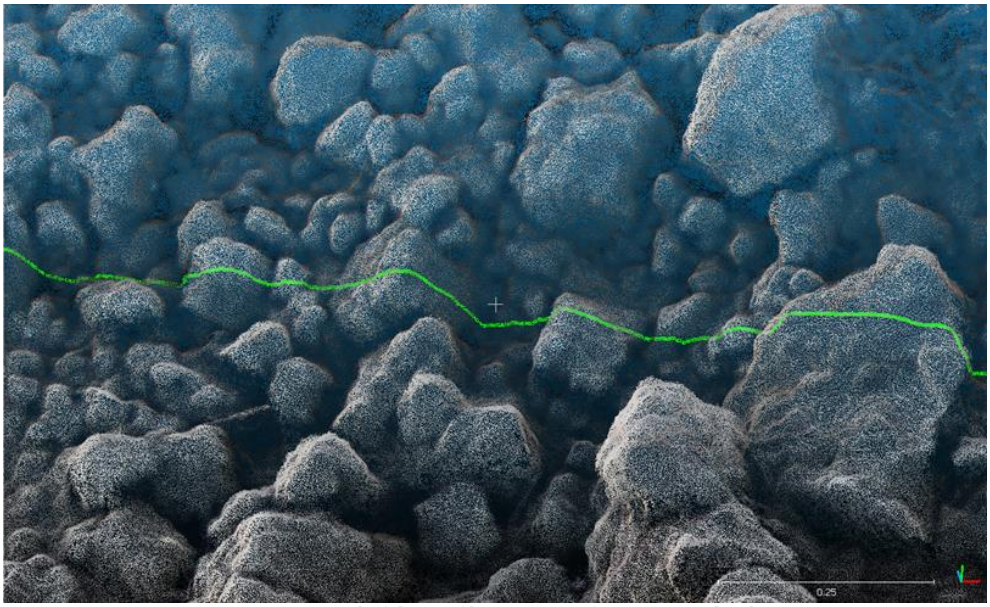

Fig. 2.7. Detail of the profile extraction from a point cloud.

Roughness measurement techniques evaluation was done, first, using 2D measurements, i.e., profiles. Profiles acquired with different techniques were compared first through a visual analysis, and next, with an analytical comparison consisting of scatterplots representation, regression analysis and RMSE calculation between the different techniques. To do this, three scatterplots were analyzed for each roughness class and measurement direction (in parallel and in perpendicular to the tillage direction); (1) Laser profilometer vs. TLS, (2) Laser profilometer vs. SfM and (3) TLS vs. SfM. Finally, an evaluation of the roughness parameter values obtained from the profiles with the three different techniques was performed.

After the 2D analysis, the 3D information contained on TLS and SfM datasets was evaluated. On the one hand, a multidirectional analysis was performed to evaluate the directionality (or anisotropy) of roughness by using polar plots representing roughness parameter values obtained from profiles extracted every 15º azimuth. On the other hand, 5 x 5 mm resolution DEMs were obtained with the two techniques and then subtracted to visualize their differences. Further details about this analysis are given in section 6.2.5.

CHAPTER 3

EVALUATION OF SURFACE ROUGHNESS PARAMETERS

Published in: Martinez-Agirre, A., Álvarez-Mozos, J., Giménez, R., 2016. Evaluation of surface roughness parameters in agricultural soils with different tillage conditions using a laser profile meter. Soil and Tillage Research. 161, 19-30.

Abstract

Surface roughness crucially affects the hydrological and erosive behaviours of soils. In agricultural areas surface roughness is directly related to tillage, whose action strongly affects the key physical properties of soils and determines the occurrence and fate of several processes (e.g., surface storage, infiltration, etc.). The characterisation of surface roughness as a result of tillage operations is not straightforward, and numerous parameters and indices have been proposed for quantifying it. In this article, a database of 164 profiles (each 5 m long), measured in 5 different roughness classes, was analysed. Four roughness classes corresponded to typical tillage operations (i.e., mouldboard, harrow, seedbed, etc.), and the fifth represented a seedbed soil that was subject to rainfall. The aim of the research was to evaluate and select the surface roughness parameters that best characterised and quantified the surface roughness caused by typical tillage operations. In total, 21 roughness parameters (divided into 4 categories) were assessed. The parameters that best separated and characterised the different roughness classes were the limiting elevation difference (*LD)* and the Mean Upslope Depression index (*MUD*); however, the parameters most sensitive to rainfall action on seedbed soils were limiting slope (*LS*) and the crossover lengths measured with the semivariogram method *(l_{SMV})* and the root mean square method (l_{RMS}). Many parameters had high degrees of correlation with each other, and therefore gave almost identical information. The results of this study may contribute to the understanding of the surface roughness phenomenon and its parameterisation in agricultural soils.

Keywords: surface roughness, roughness parameters, agricultural soils, tillage

3.1. Introduction

Surface roughness is a key element in the hydrological and erosive behaviour of soils (Helming at al., 1998), and as a soil-atmosphere frontier, plays an important role in many processes, such as infiltration, runoff, the detachment of soil due to water or wind, gas exchange, evaporation and heat fluxes (Huang and Bradford, 1992).

Depending on the order of magnitude of the soil surface elevation variations, and on the spatial arrangement of its microforms, surface roughness can be classified into different categories (Römkens and Wang, 1986): (1) Variations in the soil`s microrelief due to its individual particles and/or microaggregates (variations of the order of 1 mm, but up to 2 mm). (2) Variations in the surface generated by soil clods caused by agricultural practices (variations of the order of 100 mm, but up to 200 mm); these two roughness types are considered random and isotropic (i.e., uniform in all directions). (3) Roughness due to the systematic differences in elevation (i.e., rows or furrows) caused by tillage implements (variations between 100 and 200 mm); these forms are one-directional and this component is, therefore, oriented or anisotropic. (4) Roughness due to the macroforms of the terrain (of the order of several meters), which together define the topography of the landscape; these elevation variations are usually non-directional. Although the classification of Römkens and Wang (1986) associated the effect of tillage with an oriented type of roughness (category 3), it is understood that random roughness (categories 1 and 2) is also affected, to a greater or lesser extent, by tillage.

The order of magnitude in the elevation variations of the two (or three) first roughness types is lower than the spatial resolution of the digital elevation models that are conventionally used (Govers et al., 2000; Mushkin and Gillespie, 2005). Hence, in order to quantitatively characterise those microforms, it is necessary to take complementary measurements *in situ*, which permit the calculation of different surface roughness parameters or indices.

The parameterisation of the random surface roughness caused by tillage (the first two categories cited above) is not straightforward. Each tillage practices (or implements) causes, in theory, a particular type of microrelief under identical soil conditions (in terms of texture, moisture, density, etc.). Considering the wide range of possible soil

conditions, a huge variety of roughness types could be found in agricultural soils immediately after tilling. In addition, soil physical properties, particularly surface roughness, can also be highly variable in space. To further complicate its characterisation, surface roughness also shows a multi-scale nature making any roughness measurement scale-dependent (Zhixiong et al., 2005; Verhoest et al., 2008; Álvarez-Mozos et al., 2011). Finally, the microrelief generated by the different tillage practices is more or less susceptible to change throughout time due to the action of meteorological agents, e.g., precipitation (Dalla Rosa et al., 2012), wind and temperature changes in the low atmosphere (Pardini, 2003), or even animal activity.

Although there are many parameters and indices for quantifying surface roughness (e.g., Helming et al., 1993; Magunda et al., 1997; Kamphorst et al., 2000; Vermang et al., 2013), none work universally and interested scientists/technicians find it difficult to select the most appropriate one for their particular case. The random roughness parameters that are most commonly used in the literature, described in section 2.3, were considered in this study; these parameters can be divided into four groups, following a criterion similar to that of Smith (2014): (1) parameters measuring the vertical dimension of roughness or the magnitude of the elevation variations of the points at the soil surface (vertical parameters), (2) parameters measuring the horizontal dimension of roughness or the relation between the height of a point and that of its neighbours (horizontal parameters), (3) parameters combining both dimensions (combined parameters), and (4) parameters based on fractal theory, which measure self-affinity or the balance between height variations at different spatial scales (fractal parameters).

In light of the above, the aim of this research was to evaluate and select the most appropriate surface roughness parameters to characterise and quantify the surface roughness caused by typical tillage operations.

3.2. Material and methods

3.2.1. Test site

Roughness data were taken in 10 agricultural fields, with an extension ranging from 3 ha to 7.3 ha. Fields were located in the experimental hydrological watershed of La Tejería (N42º44'10.6'' and W1º56'57.2'') in Navarre (Spain), which has been used in different research works in the past (e.g., Casalí et al., 2008; Álvarez-Mozos et al., 2009; Álvarez-Mozos et al., 2011). Each of the fields was subjected to different tillage operations (see Fig. 3.1. A-E and Table 3.1) following the conventional soil preparation calendar in the area. Thus, during the months of September and October, 2004, the obtained data corresponded to soils subjected to primary tillage, i.e., classes Mouldboard Plough (MP), Harrowed Rough (HR), and Harrowed Smooth (HS). In the month of November 2004, soils were sown with cereal crops, representing typical seedbed conditions; this class was referred to as Planted Unmodified (PU). Finally, a final measurement was carried out in March 2005. By this time, seedbed soils had been modified by the action of the rainfall that had occurred since sowing (~250 mm); this class was referred to as Planted Modified (PM). In total, 164 profiles were taken (see Table 3.1). Profiles were measured in parallel to tillage rows, to reflect the random roughness component.

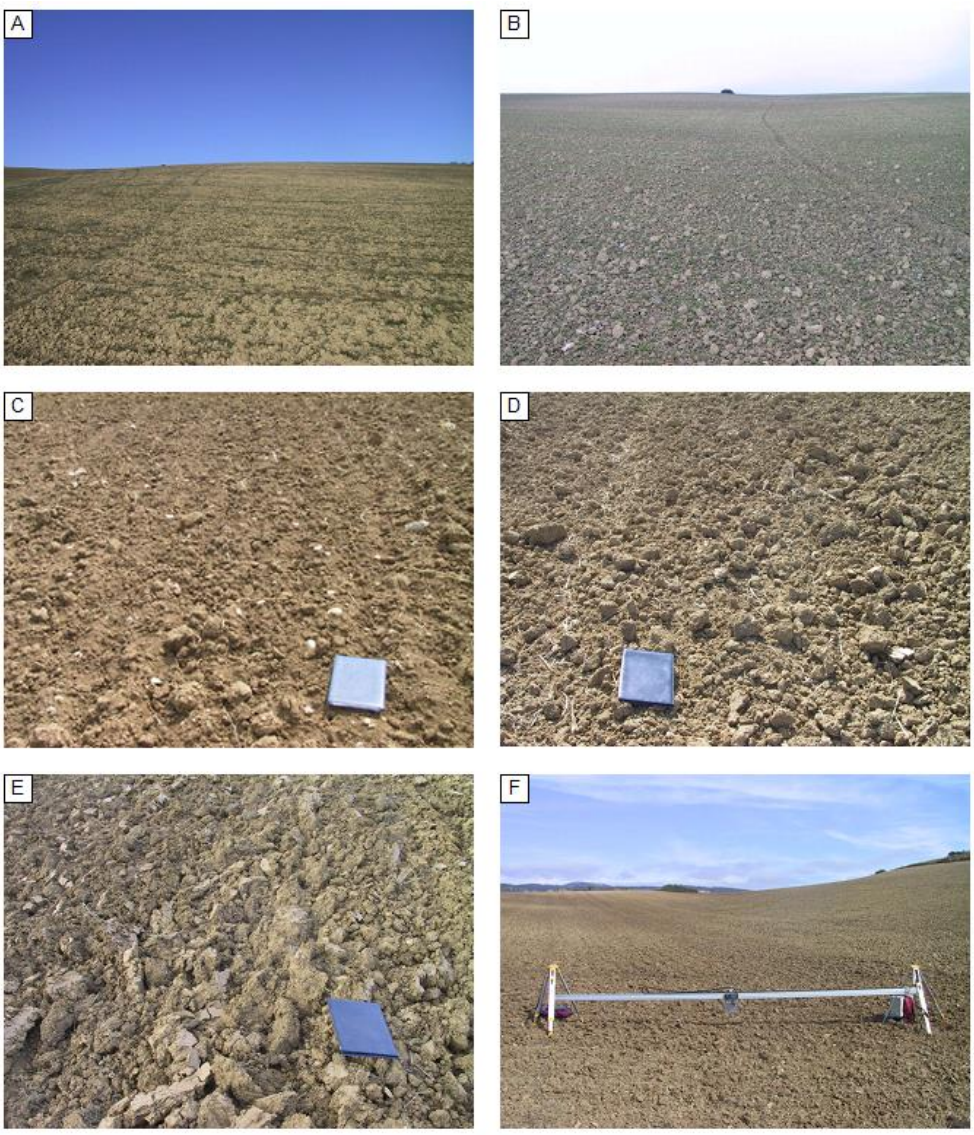

Fig. 3.1. Examples of surface roughness triggered by agricultural treatments; (A) planted modified by rainfall, (B) planted unmodified, (C) harrowed smooth, (D) harrowed rough and (E) mouldboard plough; and (F) profilometer used for data taking. As a reference, the notebook in C, D, and E is 30 cm long; and 5 m the length of the profilometer bar in F.

Table 3.1. Description of the different roughness classes triggered by agricultural treatments.

Tillage class	Acronym	Profiles	Description
Mouldboard Plough	MP	20	Tillage operation performed with a plough with multiple mouldboards at a depth of 15-20 cm, resulting in soil inversion and a very rough surface
Harrowed Rough	HR	43	Operation performed normally with a tine harrow to break soil clods and provide a smoother surface suitable for seeding
Harrowed Smooth	HS	29	In cases where the first harrowing did not smoothen sufficiently the surface a second harrowing is applied
Planted Unmodified	PU	44	Seeding operation performed with conventional sowing machinery, normally seed drills
Planted Modified	PM	28	Planted soils modified by the action of the precipitation during 4 months (~250 mm)

3.2.2. Profile measurements

Profiles were taken with a profilometer designed *ad hoc* for roughness measurement (Álvarez-Mozos et al., 2005). This instrument incorporates a laser sensor that measures the vertical distance from a reference bar down to the surface. The laser profilometer (see Fig. 3.1. F) consists of an aluminium bar with its ends fixed to two tripods. The laser distance meter is located inside a case that moves along the aluminium bar, propelled by a small electric motor. The laser profilometer has a vertical accuracy of 1.25 mm and a measurement interval of 5 mm. The total length of profiles was 5 m, so that in each one there are 1000 height records.

Profiles were processed using a code developed *ad hoc,* consisting of: (1) the correction of the buckling effect on the aluminium bar by detrending profiles with a parabolic curve obtained from a perfect horizontal reference surface, (2) the application of a filter to eliminate the outliers eventually detected in the height records (e.g., plant material) by deleting and interpolating records with height differences larger than 10 cm with the previous and next records, and (3) the correction of terrain slope (i.e., profile detrending) through the subtraction of the linear trend observed in the data (Xingming et al., 2014). Once this process had been carried out, the profiles were ready for the calculation of the different roughness parameters.

It should be noticed that the data analysed in this study are 2D profiles and that inferences about 3D phenomena (e.g., depression storage) should be made with caution.

3.2.3. Calculation of roughness parameters

In total, 21 surface roughness parameters were analysed (Table 3.2); these parameters could be classified into vertical, horizontal, combined, and fractal parameters, as explained in the introduction. Next, each parameter is briefly described; parameter names are highlighted in bold for clarity.

Table 3.2. Summary of roughness parameters analszed.

Type	Parameter	Description	Reference
Vertical	*s (cm)*	Standard deviation of the heights	Allmaras et al., 1966
	LD (cm)	Limiting elevation difference	Linden and Van Doren, 1986
	Sill (cm^2)	Sill of the semivariogram	Croft et al., 2013
	MI (cm)	Microrelief index	Römkens and Wang, 1986
Horizontal	l_{ACF} *(cm)*	Correlation length	Ulaby et al., 1982
	$\rho'(0)$	Initial slope of the auto-correlation function	Ulaby et al., 1982
	LS	Limiting slope	Linden and Van Doren, 1986
	Range (cm)	Range of the semivariogram	Croft et al., 2013
	F (cm^{-1})	Peak frequency	Römkens and Wang, 1986
Combined	Z_S *(cm)*	Combined parameter	Zribi and Dechambre, 2003
	Q ($cm^{1/2}$)	Combined parameter	Linden et al., 1988
	MIF	Combined parameter	Römkens and Wang, 1986
	MUD (cm)	Mean Upslope Depression index	Hansen et al., 1999
	T_S	Tortuosity	Saleh et al., 1993
Fractals	D_{SMV}	Fractal dimension ("semivariogram" method)	Vidal Vázquez et al., 2005
	D_{RMS}	Fractal dimension ("root mean square" method)	Vidal Vázquez et al., 2005
	D_{BC}	Fractal dimension ("box counting" method)	Gneiting et al., 2012
	D_{PS}	Fractal dimension ("power spectrum" method)	Gneiting et al., 2012
	D_{RS}	Fractal dimension ("rescaled range" method)	Liu and Molz, 1996
	l_{SMV} *(cm)*	Crossover length ("semivariogram" method)	Vidal Vázquez et al., 2005
	l_{RMS} *(cm)*	Crossover length ("root mean square" method)	Vidal Vázquez et al., 2005

Random roughness, one of the indices most frequently used to describe surface roughness, was proposed by Allmaras et al. (1966) as the standard deviation of heights after the elevations were transformed to natural logarithms and corrected for slope and tillage tool marks. After Currence and Lovely (1970) showed that the

parameter was more sensitive without any logarithmic transformation, most authors (e.g., Bertuzzi et al., 1990; Hansen et al., 1999; Kamphorst et al., 2000) calculate random roughness as the **standard deviation of heights** *(s)* (eq. 3.1):

$$s = \sqrt{\frac{\sum_{i=1}^{N}(z_i{}^2 - \bar{z}^2)}{N-1}} \tag{3.1}$$

where N is the number of height records, z_i is the height corresponding to record i, and $\bar{z}$ is the mean height of all the records.

The **correlation length** (l_{ACF}) represents the horizontal component of roughness, i.e., it describes the relative location of heights or the way in which the heights vary along the surface (Ogilvy and Foster, 1989). The correlation length was calculated from the autocorrelation function (eq. 3.2) (Ulaby et al., 1982):

$$\rho(h) = \frac{\sum_{i=1}^{N(h)} z_i z_{i+h}}{\sum_{i=1}^{N} z_i{}^2} \tag{3.2}$$

where $\rho(h)$ is the autocorrelation function, which represents the correlation existing between height z of the point i (z_i) and that of another point located at a lag distance h from it (z_{i+h}), and $N(h)$ is the number of pairs considered in each lag h. The correlation length (l_{ACF}) is then defined arbitrarily as the distance at which the heights of two points on the surface are considered independent; i.e., $\rho(h)$ is equal to $1/e$, so that $\rho(l) = 1/e$. Another parameter extracted from the autocorrelation function is its **initial slope** ($\rho'(0)$), which also provides a measure of the horizontal roughness (Borgeaud et al., 1995), but in this case at a more local scale, i.e., focusing on the height variations of a point with its nearest neighbours. Zribi and Dechambre (2003) proposed **parameter Z_S** as a combination of s and l_{ACF} (eq. 3.3), and thus accounted for both vertical and horizontal roughness components:

$$Z_s = s^2 / l_{ACF} \tag{3.3}$$

The concepts of the **limiting elevation difference** (*LD*) and the **limiting slope** (*LS*) were developed to include the spatial aspect of roughness (Linden and Van Doren, 1986). Parameter *LD* supplies information on the characteristics of roughness at long

distances, whereas *LS* is used to characterise roughness at short distances (Bertuzzi et al., 1990). The mean absolute-elevation-difference is defined as (eq. 3.4):

$$\Delta z_h = \sum_{i=1}^{N(h)} \frac{|z_i - z_{i+h}|}{N(h)} \quad (3.4)$$

The relationship between Δz_h and the lag distance h was obtained from a hyperbolic linear model defined by (eq. 3.5):

$$1/\Delta z_h = a + b(1/h) \quad (3.5)$$

where a and b are the fitting parameters obtained for an arbitrary horizontal distance. After testing different values, and following the recommendation of Linden and Van Doren (1986), this distance was set to 20 cm. Parameter *LD* (eq. 3.6) determines the shape of the variogram, assumed to follow a hyperbolic function:

$$LD = 1/a \quad (3.6)$$

Parameter *LS* (eq. 3.7) is the original variogram slope (Kamphorst et al. 2000), given by:

$$LS = 1/b \quad (3.7)$$

Linden et al. (1988) proposed a third parameter that was obtained as a combination of parameters *LD* and *LS*, called **parameter *Q*** (eq. 3.8). This parameter can be considered a combined roughness parameter.

$$Q = (LD \cdot LS)^{1/2} \quad (3.8)$$

The semivariogram represents how height data are related to distance. The semivariance function depending on the lag h can be calculated as:

$$\gamma(h) = \frac{1}{2N(h)} \sum_{i=1}^{N(h)} [z_{i+h} - z_i]^2 \quad (3.9)$$

Once the experimental semivariogram was calculated, a spherical model was fitted to it (Vázquez et al., 2009; Croft et al., 2013):

$$\gamma(h) = \begin{cases} c_1 \left[1.5\frac{h}{h_a} - 0.5\left(\frac{h}{h_a}\right)^3\right] + c_0 \; ; h \leq h_a \\ c_1 + c_0 \qquad\qquad\qquad\qquad ; h > h_a \end{cases} \tag{3.10}$$

where h_a is the Range, c_1 is the Sill, and c_0 is the Nugget. After testing different values, 100 cm of maximum lag distance was deemed sufficient to accurately fit the spherical model to the experimental semivariogram. ***Sill*** represents the value of $\gamma(h)$ where the fitted model reaches the plateau, and ***Range*** is the distance at which the *Sill* is found. No nugget effect was taken into account (Vermang et al., 2013). Both *Sill* and *Range* have been frequently used as soil surface roughness indices (e.g., Helming et al., 1993; Vázquez et al., 2009; Croft et al., 2009, Croft et al., 2013; Vermang et al., 2013).

Parameter *MIF* (eq. 3.11) was formulated by Römkens and Wang (1986) with the aim of quantitatively describing surface roughness. This dimensionless parameter represents the integrated effect of the **peak frequency** (*F*) and the **microrelief index** (*MI*), and it is defined arbitrarily as:

$$MIF = MI \cdot F \tag{3.11}$$

where *MI* represents the area per unit of length between the measured surface profile and the regression line of least squares through all measured elevations on a transect (Römkens and Wang, 1986), and *F* is the number of peaks (i.e., points with higher elevations than their neighbours on both sides) per unit of length of the profile. Parameters *MI* and *F* (eq. 3.11) are evaluated separately as descriptive parameters of vertical and horizontal roughness, respectively.

The **Mean Upslope Depression index** (*MUD*) (eq. 3.12) was specifically developed to predict surface storage capacity (Hansen et al., 1999). The *MUD* is based on the elevation differences ($z_i - z_{i+h}$) between a reference point *i* and another *i+h* on a line segment positioned upslope from the reference point. Within each line segment, the calculation procedure is iterated for a number of sub-segments, each time taking a new upslope point as the reference point (Hansen et al., 1999):

$$MUD = \sum_{i=1}^{m}\left(\sum_{j=1}^{n}\frac{\Delta z}{n}\right)/m \begin{cases} \Delta z = z_i - z_{i+h} \; ; z_i \geq z_{i+h} \\ \Delta z = 0 \qquad\qquad ; z_i < z_{i+h} \end{cases} \tag{3.12}$$

where *n* is the number of points in a line sub-segment and *m* is the number of line sub-segments. In Hansen et al. (1999), no particular segment length was recommended, but they considered a 30-cm length for their conditions. In our case, after testing different values, a segment length of 20 cm was selected.

Tortuosity is a roughness index based on the ratio of the surface profile perimeter length (L_1) and its horizontal projection (L_0). Although variants do exist (e.g., Boiffin, 1984; Planchon et al., 1998), the present study used the tortuosity index of Saleh (T_S) (eq. 3.13) (Saleh et al., 1993):

$$T_S = 100 \cdot \frac{(L_1 - L_0)}{L_1} \tag{3.13}$$

Different methods have been used to calculate the **fractal dimension** (and in some cases the **crossover length**), which characterises the self-affinity of surface roughness profiles. The **semivariogram method** (SMV) was introduced to study the variability of soil properties and subsequently used to quantify roughness (Burrough, 1983a,b; Armstrong, 1986; Huang and Bradford, 1992; Vidal Vázquez et al., 2005; Chi et al., 2012; Vermang et al., 2013). The first step in the estimation of the fractal dimension is the calculation of the experimental semivariogram (eq. 9) (Vidal Vázquez et al., 2005). Assuming a fractal Brownian motion (*fBm*) model, the experimental semivariogram can be described as a function of the lag (Eq. 14):

$$\gamma(h) = l^{1-H} h^H \tag{3.14}$$

where l is the crossover length and H is the Hurst coefficient. After a log-log transformation of eq. 14, H can be estimated as the slope of the semivariance versus the lag distance. When applied to surface roughness profiles, the logarithmic transformation normally yields a curved trend rather than a line, thus revealing a multi-fractal nature (Vidal Vázquez et al., 2005; Moreno et al., 2008). In this study, only the fractality of the first stretch (where the linear assumption holds) was measured. For that purpose, a maximum lag distance of 10 cm was considered because it provided a good fit to the linear trend in all the profiles. Afterward, the Hurst coefficient was related to the fractal dimension as follows (Smith, 2014) (eq. 3.15):

$$D_{SMV} = 1 + d - H = 2 - H \quad (3.15)$$

where d is the Euclidean dimension of the system (i.e., 1 for profiles, 2 for surfaces, etc.). Further, the crossover length (l_{SMV}) (eq. 3.16) can be calculated as follows (Huang and Bradford, 1992):

$$l_{SMV} = exp\left[\frac{a_{SMV}}{(2-2H)}\right] \quad (3.16)$$

where a_{SMV} is the intercept of the linear trend fitted to the first stretch of the semivariogram.

The **root mean square method** (RMS) is based on the evaluation of the root mean square deviation of elevation values for increasing lag distances, and it has been used in different studies (Malinverno, 1990; Gallant et al., 1994; Moreira et al., 1994; Vidal Vázquez et al., 2005). The average RMS values for increasing lag distances (h) are calculated as (Vidal Vázquez et al., 2005):

$$\bar{W}(h) = \frac{1}{n_h}\sum_{u=1}^{n_h}\left\{\frac{1}{n}\sum_{i\in h}[z_i - \bar{z}_h]^2\right\}^{1/2} \quad (3.17)$$

where n_h is the total number of lags of size h and $\bar{z}_h$ represents the average elevation values for all points of each lag. As in the semivariogram method, the slope of the logarithmic transformation of $\bar{W}(h)$ gives an estimation of the Hurst coefficient, which enables the calculation of the fractal dimension (D_{RMS}) and the crossover length (l_{RMS}) (eq. 15 and 16).

The estimation of the fractal dimension by the **box counting method** (BC) is motivated by the scale law defined by Mandelbrot (1977):

$$D(r) = \frac{\log(N_r)}{\log(1/r)} \quad (3.18)$$

where N_r stands for the minimum number of boxes of a width r that can cover the object (i.e., surface profile). The basic idea is simple since the profile to be studied is initially covered by a single box. That box is divided into 4 quadrants, and the number of quadrants required to cover the profile are counted. Then, each quadrant is divided

into another four sub-quadrants, and this division goes on until the width of the boxes reaches the resolution of the data, counting the number of cells required to cover the profile in each step (Gneiting et al., 2012). Function $D(r)$ is transformed into logarithms and fitted to a regression line, from whose slope (α) the fractal dimension D_{BC} (eq. 3.19) (Liang et al., 2012) is obtained:

$$D_{BC} = -\alpha \tag{3.19}$$

A further technique used to determine the Hurst coefficient, and hence the fractal dimension, is the **power spectrum method** (PS) (Gneiting et al., 2012). This estimator is based on the spectral density function $S(v)$ for a stationary stochastic process, obtained by the fast Fourier transform (FFT), which depicts how the roughness is distributed in components of different frequencies (v). The Hurst coefficient is obtained through the regression line of the logarithmic transformation of function $S(v)$, and thereafter the fractal dimension (D_{PS}) (eq. 3.15).

Finally, the **rescaled range method** (RS) (Liu and Molz, 1996; Liang et. al, 2012) was also used, which is based on calculating the fitted range R in terms of the lag distance h:

$$R(h) = R_a/s(h) \tag{3.20}$$

where R_a is the sum of the absolute values of the largest positive and negative deviations of lag points from its trend line, and $s(h)$ is the standard deviation of each lag. As in the previous cases, to obtain the Hurst coefficient, a linear regression of the logarithmic transformation of $R(h)$ is made, from which the fractal dimension (D_{RS}) (eq. 3.15) is obtained.

3.2.4. Parameter evaluation

3.2.4.1. Descriptive analysis

To assess the different parameters, first, the different roughness classes were visually analysed. The box plots generated by each of the parameters per roughness class were also visually analysed.

3.2.4.2. Separability analysis

The evaluated roughness parameters did not necessarily follow Gaussian probability distribution functions, since they might have asymmetric distributions. Furthermore, the different roughness classes did not necessarily have comparable variances. Hence, the comparison of parameters and classes could not rely on classic statistical tools, such as the analysis of variance (requiring Normality and homoscedasticity), and thus the separability analysis was used to select the most suitable parameters for the characterisation of different roughness classes. Separability, or dissimilarity, is a statistical metric that quantifies how different two sets of data are; it can be evaluated by computing different statistical distance measures (e.g., Divergence, Bhattacharyya distance, etc.). In this study, the Jeffries-Matusita Distance (D_{JM}) (Swain and King, 1973) was used, which was calculated for each parameter and pair of roughness classes. D_{JM} (eq. 3.21) has been frequently used to analyse similarity and feature selection processes, and a good number of studies recommend its use (e.g., Bruzzone et al., 1995; D'Urso and Menenti, 1996):

$$D_{JM} = \int \left[\left(\sqrt{f(x)} - \sqrt{g(x)} \right)^2 \right] dx \qquad (3.21)$$

where D_{JM} is the distance between classes $f(x)$ and $g(x)$ measured by the parameter x. D_{JM} has a range of variability between 0 and 2, i.e., 0 means $f(x)$ and $g(x)$ completely overlap and 2 means they are completely separable. Values below 1 can be considered of poor separability, whereas values from 1-1.5 corresponds to moderate separability, and 1.5-2 to high separability (Skriver, 2007). By using this analysis, we aimed to quantify the ability of the different parameters to discriminate between different roughness classes.

3.2.4.3. Correlation analysis

A correlation analysis was performed to study the relationships between the different roughness parameters. For this purpose, the Spearman correlation coefficient (R) was calculated, which is particularly indicated for detecting any type of monotonic relationship.

3.3. Results

3.3.1. Descriptive analysis

Roughness class MP presented a higher range of variation in its profile elevations (i.e., vertical roughness) as a result of the presence of soil clods of up to 10 cm in size, with no clear spatial pattern or arrangement (Fig. 3.2). Visually, classes HR and HS did not exhibit such a large vertical roughness (which was smaller in HS than in HR), but their horizontal roughness seemed greater than in MP, i.e., displaying more serrated profiles. Classes PU and PM showed an even smaller range of vertical variation, and although PU had a high horizontal roughness, the smoothing effect of the rain, which translated into a lesser horizontal roughness, could be clearly seen in PM. In this first visual analysis, they could be ranked –as we understand– in an increasing order of roughness, as follows: PM<PU<HS<HR<MP.

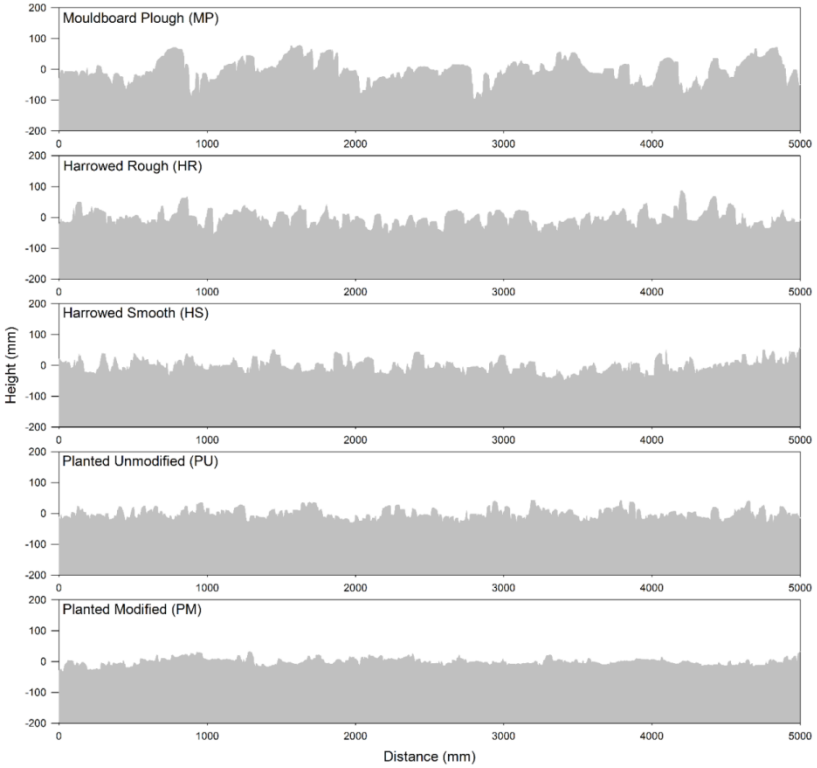

Fig. 3.2. Examples of height profiles of each of the roughness classes studied.

3.3.2. Parameters per roughness class

The behaviour of the different parameters in terms of the roughness classes were analysed using boxplots (Fig. 3.3). In the vertical parameters the mean class values increased with the roughness, which could be visually observed (Fig. 3.2). Furthermore, the variability of each class increased as its roughness did, with a minimum variability for classes PM and PU, followed by HS and HR, and with a maximum variability for MP. All in all, different types of tillage (i.e., classes PU, HS, HR, and MP) could be differentiated with relative clarity. The effect of rainfall lowered class PM's values, compared to PU, in most vertical parameters, but their differences were rather small and both classes overlapped to a certain degree.

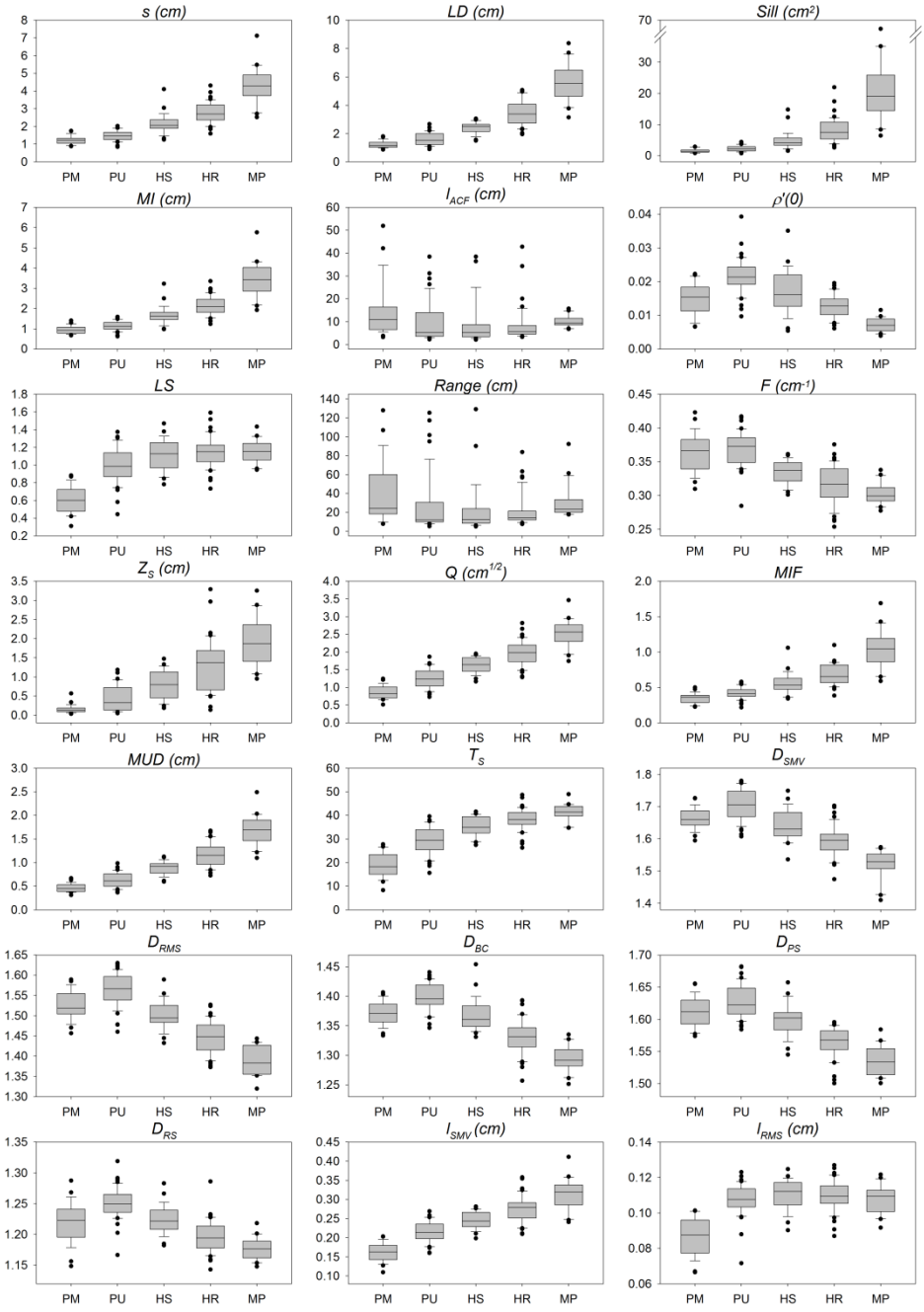

Fig. 3.3. Box diagrams per roughness classes of the estimated values of the different parameters.

Horizontal parameters did not exhibit the same trend as the vertical ones (Fig. 3.3). Regarding the variability per class, different patterns were observed for the different parameters, although MP was less variable than the other classes in all parameters. Parameters l_{ACF} and *Range* behaved similarly, with comparable values for the different classes and many outliers especially in the least rough classes (i.e., PM and PU). Parameters $\rho'(0)$ and F followed a similar trend, showing a moderate differentiation between classes PU, HS, HR, and MP; however, the action of precipitation modified that trend and made class PM take lower $\rho'(0)$ and F values than PU, indicating a higher correlation between the surface elevations. Finally, parameter *LS* took increasing values for increasing roughness conditions (i.e., PU, HS, HR, and MP), but there was a high overlap between classes; nevertheless, this parameter seemed to clearly differentiate PM from the other classes.

The combined parameters followed a trend similar to the vertical parameters (Fig. 3.3), i.e., their values increased with increasing roughness, but the combine parameters did not have the same marked difference in parameter variability than the vertical parameters did, at least not in all cases (see parameters Q and T_S in Fig. 3.3). Parameters *MIF* and *MUD*, and to a lesser extent Z_S, did behave very similarly to the vertical ones, with increases in variability as roughness increased; however, parameter Q did not follow this behaviour, as it had a very similar variability in all the classes. Finally, parameter T_S followed a completely different pattern, with a good separation between classes PM and PU but minor differences between the rest.

Regarding fractal parameters, the D values calculated with different techniques behaved similarly, although their absolute values differed slightly (Fig. 3.3); their performance resembled that of parameter $\rho'(0)$. This pattern indicates a more self-affine behaviour as tillage classes increased in roughness, although the precipitation effect modified that tendency. The variability of the fractal dimensions was rather homogeneous for all the classes, but the crossover lengths behaved completely differently. Parameter l_{SMV} followed a very similar trend to the mixed parameters Q and *MUD*, with incrementing values for roughness classes, and a very homogeneous variability for all of them. Meanwhile, parameter l_{RMS} was similar to the horizontal parameter *LS*, with similar values for most tillage classes, but with a clear differentiation of class PM.

3.3.3. Separability between roughness classes

The vertical parameters and the combined parameters *MUD* and *Q* showed better mean separability with D_{JM} values >1 (Table 3.3). More precisely, parameters *LD* and *MUD* were those with a higher mean separability (D_{JM}~1.25). The rest of the combined parameters (*MIF*, Z_S and T_S) offered moderate separabilities (D_{JM}~0.9). The horizontal parameters displayed somewhat lower mean separabilities, with D_{JM} values of 0.6-0.7, but in the case of l_{ACF} and *Range*, D_{JM} did not reach 0.3. Lastly, the fractal dimensions calculated with different techniques followed similar patterns, although their mean separabilities varied significantly, from 0.92 (D_{RMS}) to 0.52 (D_{RS}), though the crossover lengths behaved differently. Parameter l_{SMV} ended up reaching a higher separability than 1, while parameter l_{RMS} hardly exceeded the mean separability of 0.4.

Table 3.3. Separability (D_{JM}) of the parameters per pairs of roughness classes. The parameter with the highest separability is in dark grey, and the other two parameters with a high separability for each pair of classes in pale grey.

Parameter	Separability between classes										
	PM-PU	PM-HS	PM-HR	PM-MP	PU-HS	PU-HR	PU-MP	HS-HR	HS-MP	HR-MP	Mean
s (cm)	0.23	1.03	1.61	1.84	0.64	1.33	1.75	0.28	1.24	0.80	1.07
LD (cm)	0.40	1.61	1.67	1.92	0.72	1.25	1.81	0.73	1.64	0.80	1.26
Sill (cm²)	0.27	1.07	1.45	1.68	0.73	1.25	1.59	0.27	1.16	0.87	1.03
MI (cm)	0.20	0.99	1.58	1.82	0.60	1.29	1.73	0.27	1.23	0.81	1.05
l_{ACF} *(cm)*	0.09	0.08	0.17	0.73	0.01	0.02	0.52	0.03	0.58	0.46	0.27
$\rho'(0)_{ACF}$	0.40	0.09	0.11	1.00	0.15	0.82	1.66	0.34	1.11	0.83	0.65
LS	0.90	1.38	1.47	1.70	0.11	0.16	0.29	0.01	0.06	0.04	0.61
Range (cm)	0.05	0.08	0.27	0.17	0.01	0.16	0.13	0.12	0.11	0.08	0.12
F (cm⁻¹)	0.02	0.43	0.59	1.19	0.58	0.78	1.41	0.28	0.76	0.21	0.62
Z_S *(cm)*	0.69	1.26	1.44	1.83	0.24	0.71	1.39	0.37	0.98	0.21	0.91
Q (cm$^{1/2}$)	0.65	1.67	1.75	1.97	0.50	0.96	1.69	0.40	1.36	0.51	1.15
MIF	0.22	0.81	1.37	1.73	0.43	0.98	1.60	0.17	1.06	0.75	0.91
MUD (cm)	0.49	1.65	1.74	1.96	0.64	1.19	1.83	0.58	1.59	0.73	1.24
T_S	0.74	1.58	1.72	1.92	0.38	0.63	1.14	0.10	0.50	0.17	0.89
D_{SMV}	0.34	0.11	0.65	1.59	0.41	1.04	1.74	0.27	1.15	0.50	0.78
D_{RMS}	0.24	0.12	0.90	1.72	0.56	1.30	1.85	0.51	1.47	0.50	0.92
D_{BC}	0.38	0.04	0.59	1.62	0.37	1.11	1.86	0.37	1.35	0.47	0.82
D_{PS}	0.12	0.06	0.75	1.42	0.30	1.12	1.65	0.46	1.16	0.33	0.74
D_{RS}	0.28	0.06	0.15	0.66	0.27	0.81	1.50	0.27	0.95	0.25	0.52
l_{SMV} *(cm)*	0.82	1.61	1.70	1.87	0.38	0.82	1.35	0.35	0.96	0.25	1.01
l_{RMS} *(cm)*	0.85	1.10	1.03	0.93	0.04	0.02	0.01	0.00	0.04	0.02	0.40

The vertical parameters had the highest separability values between classes PU, HS, HR, and MP, especially parameter *LD*, but none of the vertical parameters was particularly successful at detecting rainfall smoothening, i.e., separating PM and PU, since in no case did D_{JM} reach values above 0.4 for these two classes. Separability values between neighbouring tillage classes (i.e., PU vs. HS, HS vs. HR, and HR vs. MP) were not high for any of the vertical parameters; *Sill* and *LD* functioned best in these cases. For horizontal parameters, separability between class pairs was generally lower than for vertical parameters. Nevertheless, the highest D_{JM} value between classes PM and PU was obtained by parameter *LS* with a value ~0.9. The behaviour of the combined parameters, once more, was similar to the vertical ones, offering separabilities comparable to those, especially for parameters *MUD* and *Q*. Regarding the separation between classes PM and PU, better separabilities were obtained than with the vertical parameters (especially for T_S, Z_S, and *Q*), although still lower than those of *LS*. In addition, parameters *Q*, *MUD*, and T_S offered the highest separabilities between PM and classes HS, HR, and MP. Lastly, regarding fractal parameters, although the different dimensions did not generally exhibit high separabilities, D_{RMS} had some of the highest separabilities between PU and classes HR and MP and between HS and HR and MP, and D_{BC} had the highest separability between classes PU and MP. Regarding the crossover lengths, although the separability between the different tillage types (PU, HS, HR, and MP) was not high, the good separability obtained between class PM and the rest was highly noteworthy (especially for l_{SMV}).

3.3.4. Parameter correlation

With regard to the correlations between parameters of one type, the vertical parameters were highly correlated with each other, with R~0.9 (Fig. 3.4); however, the horizontal parameters showed more heterogeneous behaviour with different R values. Parameters l_{ACF} and *Range* had a good correlation (R~0.85), as did $\rho'(0)$ with *F*, l_{ACF}, and *Range* (although slightly lower, R~0.6), but the other parameters had relatively low correlations. Parameter *LS,* in general, had low correlations with the rest of the horizontal parameters. On the other hand, mixed parameters showed quite homogeneous behaviour with high correlations (R~0.9) with each other, but a little lower for Z_S and *MIF* (R~0.75). Finally, the different fractal dimensions showed high correlations between each other (R≥0.8), except for parameter D_{RS} (R~0.6). The crossover lengths (l_{SMV} and l_{RMS}) were only moderately correlated (R~0.6).

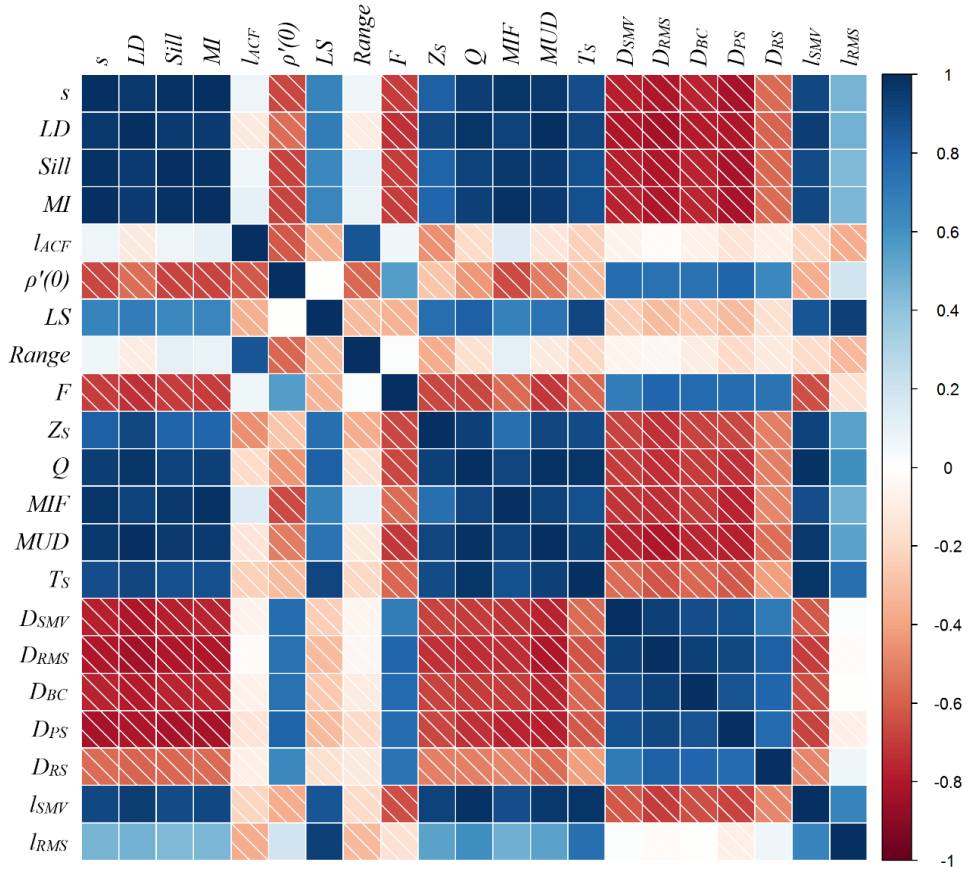

Fig. 3.4. Spearman correlation matrix of the roughness parameters (n=164).

Overall, vertical parameters correlated well with mixed ones (R≥0.8), except for Z_S and T_S, which had somewhat lower correlations (R~0.6). A negative correlation was found between the vertical parameters and fractal dimensions, although they measure different phenomena; this would indicate that the greater the vertical roughness, the more self-affine a surface is. The crossover lengths (l_{SMV} and l_{RMS}) presented a disparate behaviour. Although l_{SMV} had a good correlation with the different fractal dimensions (negative correlation), F (negative correlation), and most vertical and combined parameters, l_{RMS} had no correlations with the different fractal dimensions and lower correlations than l_{SMV} with the vertical and combined parameters. In both

cases, the correlation with parameter *LS* was high, especially in the case of l_{RMS} (R≥0.9).

3.4. Discussion

3.4.1. Differentiation between tillage types

The values of *s* and *LD* obtained for the different classes are comparable to those reported in the literature for similar conditions (e.g., Zobeck and Onstad, 1987; Helming et al., 1993; Arvidsson and Bolenius, 2006; Bauer et al., 2015). In the absence of significant changes caused by the rainfall, *s* and *LD* have been successfully related to the size of soil clods and then proposed as good indices for distinguishing different tillage types (Helming et al., 1993; Eltz and Norton, 1997; Magunda et al., 1997; Kamphorst et al., 2000; Vermang et al.. 2013; Bauer et al., 2015). The values of *Sill* obtained here were considerably higher (although within the range of variation) than those reported by Helming et al. (1993) and Vermang et al. (2013), partly because their experiments were carried out using artificial roughness and because of the measurement scale.

Regarding the horizontal parameters, there is no agreement in the literature. For instance, several authors reported increasing values of l_{ACF} for increasing roughness conditions (Davidson et al., 2003; Baghdadi et al., 2008b), while others observed more similar behaviour to that obtained here, with no clear differences between roughness classes (Álvarez-Mozos et al., 2005; Verhoest et al., 2008). The *Range* values obtained in this study were, in general, higher (although within the range of variation) than those reported by other authors (Helming et al., 1993; Vermang et al., 2013), but with an important overlap between classes and frequent outliers. Parameters l_{ACF} and *Range* were obtained using different techniques but represent analogous concepts (Vidal Vázquez et al., 2005), and this is corroborated by the results presented here. Parameters $\rho'(0)$ and *F* were the horizontal parameters that best differentiated tillage classes; this is due to the geometry of the microforms presented in the smooth classes and the macroforms presented in the roughest classes, since the smaller the size of the clods, the more parameter *F* increased (Bertuzzi et al., 1990). This same phenomenon explains that the reason that $\rho'(0)$ took lower values in the roughest classes was due

to the presence of macroforms, which made the autocorrelation function descend more gently in these classes, whereas it did so more abruptly in smoother tillage classes with greater microform presence.

On the other hand, the combined parameters have been rarely used as an approach to separate tillage types. Baghdadi et al. (2008b) mentioned that parameter Z_S took on values of <0.1 cm for smooth soils and >0.1 cm for ploughed ones, but did not investigate different tillage practices in greater detail. Zribi and Dechambre (2003) found a direct correlation between the values of Z_S and the clod's size; they reported a variation range of Z_S between 0.07 cm and 1.93 cm for agricultural soils. This trend agrees with our results, although we observed considerable overlapping between similar tillage classes and a slightly narrower range of values. On the other hand, *MIF* appeared to be good parameter to separate different tillage classes (Lehrsch et al., 1988; Bertuzzi et al., 1990).

In fractal parameters, although some authors found that the values of fractal dimensions and their respective crossover lengths (calculated with different techniques) should be relatively similar (Vidal Vázquez et al., 2005; Vivas Miranda et al., 2002), there is not always an agreement between the values shown in different works. For instance, some authors (e.g., Gallant et al., 1994) found substantial variations between methods. In our case, despite the differences in magnitude, we observed that the behaviour was very similar in the different procedures used. This is in accord (except for the case of l_{RMS}) with Chi et al. (2012), who concluded that, generally, the fractal dimension (parameter *D*) decreased and the crossover length (parameter *l*) increased with the increment of soil clods. Vermang et al. (2013) also reported that the rougher the surface, the lower parameter *D* was.

For all the above, parameter *LD* is recommended to separate the different types of tillage studied in terms of the vertical roughness, parameter $\rho'(0)$ in terms of the horizontal roughness, parameter *MUD* in terms of both properties, and parameter D_{RMS} in terms of its self-affinity.

3.4.2. Effect of rainfall on the different roughness parameters

Although the values of all the vertical parameters changed after successive rainfalls, those changes were not significant enough to clearly differentiate the precipitation effect (Huang and Bradford, 1992; Vermang et al., 2013). In this sense, Bertuzzi et al. (1990) and Magunda et al. (1997) found that parameters representing the roughness' vertical component were good indicators of roughness at higher scales (and then useful to differentiate tillage types), whereas the horizontal parameters were appropriate at lower scales (and hence suitable to evaluate changes in roughness due to rainfall).

As opposed to the vertical parameters, in Vermang et al. (2013), the values of *Range* and l_{ACF} increased after rainfall events (applied with a rain simulator). Helming et al. (1993) and Croft et al. (2009) also observed an increase in parameter *Range* after rain, which Helming et al. (1993) attributed to the smoothing and broadening of the largest soil clods, and Croft et al. (2009) indicated a higher spatial correlation. From a semivariogram analysis, Helming et al. (1993) and Vermang et al. (2013) observed that, on surfaces with small roughness, rain events gave rise to more erratic *Range* patterns. Our results are in agreement with these trends, since the rainfall led to a reduction in vertical parameter values and increases in the *Range* and l_{ACF} values.

There were other parameters that displayed a greater sensitivity to the effect of rain. Parameter *LS* was the most sensitive to the changes in roughness caused by precipitation, followed by l_{RMS} and l_{SMV} or T_S. Taconet and Ciarletti (2007) concluded that T_S was a more suitable parameter than *s* to detect soil smoothing due to rain. With regard to the fractal dimensions, in contrast to what was observed here, Vermang et al. (2013) reported that parameter *D* increased after rain events in the soils with small roughness, while it decreased in very rough soils. Eltz and Norton (1997) also observed an increase in parameter *D* and a reduction in *l* after precipitation. Further, Vidal Vázquez et al. (2007) and Paz-Ferreiro (2008) found similar behaviour to that seen here, with reductions both in *D* and in *l* after rain.

Some of these variations can be, to some extent, explained if we take into account that rain can either smoothen the roughness, if the sealing processes in the soil are dominant, or increase roughness, if rills or gullies are developed (Vermang et al.,

2013). The soils studied here had a single tillage treatment modified by the precipitation (roughness class PM), so that in order to confirm these trends, it would be necessary to carry out similar experiments in all the other treatments.

3.4.3. Correlation between parameters

Most of our findings are in agreement with previous investigations. We observed a strong correlations between the vertical parameters, such as: *s* and *LD* (Linden and Van Doren, 1986; Bertuzzi et al., 1990; Magunda et al., 1997); *s* and *Sill* (Croft et al., 2013); *LS* and T_S (Bertuzzi et al., 1990); l_{ACF} and *Range* (Vidal Vázquez et al., 2005); and *s* and D_{SMV} (negative correlation) (Chi et al., 2012). However, some of our results partly disagreed with previous findings, e.g., the lack of correlation between *MIF* and other parameters, such as *s* or T_S (Bertuzzi et al., 1990), or the high correlation between *s and LS* (Magunda et al., 1997).

3.5. Conclusions

In this study, the most widely used roughness parameters in earth sciences were selected and their ability to discriminate between the different soil roughness classes created by typical tillage operations was evaluated.

Vertical and combined parameters took higher values as tillage became rougher. Horizontal parameters did not show such a clear pattern, with some parameters being rather insensitive to tillage (l_{ACF} and *Range*), and other increasing (*LS*) and some others decreasing ($\rho'(0)$ and *F*) as tillage became rougher. On the contrary, the different fractal dimensions that were tested showed a consistent behaviour, with values decreasing (more auto-affine behaviour) as tillage became rougher. All in all, the best parameters for differentiating and characterising different tillage types were *LD* and *MUD*.

The effect of rainfall was apparent in most parameters. The ones most sensitive to rainfall action were the horizontal parameter *LS*, the crossover lengths (l_{SMV} and l_{RMS}), and, to a lesser extent, the combined parameter T_S.

Many of the evaluated parameters were highly correlated with each other (all the vertical parameters or the combined parameters Q and MUD) and therefore provided almost identical information. For these, our recommendation is to select the simplest ones (i.e., s or MUD); however, some parameters showed low correlation values with the rest, since they offered complementary information (i.e., l_{SMV}, LS, or l_{ACF}). These parameters could be interesting depending on the particular application pursued.

It is expected that the results of this study could contribute to the understanding of the surface roughness phenomenon and to its parameterisation in agricultural soils; however, more research is needed to better characterise roughness dynamics due to the action of rainfall.

Acknowledgements

The authors are grateful to the Spanish Minister of Economy and Competitiveness for partly founding this research throw scholarship BES-2012-054521 and project CGL2011-24336.

upna
Universidad Pública de Navarra
Nafarroako Unibertsitate Publikoa

CHAPTER 4

SURFACE ROUGHNESS MEASUREMENT SCALE INFLUENCE ON RADAR BACKSCATTERING

Published in: Martinez-Agirre, A., Álvarez-Mozos, J., Lievens, H., Verhoest, N.E.C., 2017. Influence of Surface Roughness Measurement Scale on Radar Backscattering in Different Agricultural Soils. IEEE Transactions on Geoscience and Remote Sensing. 55 (10), 5925-5936.

Abstract

Soil surface roughness strongly affects the scattering of microwaves on the soil surface and determines the backscattering coefficient (σ^0) observed by radar sensors. Previous studies have shown important scale issues that compromise the measurement and parameterization of roughness especially in agricultural soils. The objective of this study was to determine the roughness scales involved in the backscattering process over agricultural soils. With this aim, a database of 132 5-m profiles taken on agricultural soils with different tillage conditions was used. These measurements were acquired coinciding with a series of ENVISAT/ASAR observations. Roughness profiles were processed considering three different scaling issues: (1) influence of measurement range, (2) influence of low frequency roughness components and (3) influence of high frequency roughness components. For each of these issues, eight different roughness parameters were computed and the following aspects were evaluated: (a) roughness parameters values, (b) correlation with σ^0 and (c) goodness-of-fit of the Oh model. Most parameters had a significant correlation with σ^0 especially the fractal dimension, the peak frequency and the initial slope of the auto-correlation function. These had higher correlations than classical parameters such as the standard deviation of surface heights or the correlation length. Very small differences were observed when profiles longer than 1 m were used as well as when small-scale roughness components (<5 cm) or large-scale roughness components (>100 cm) were disregarded. In conclusion, the medium frequency roughness components (scale of 5-100 cm) seem to be the most influential scales in the radar backscattering process on agricultural soils.

Keywords: agriculture, rough surfaces, scattering, soil, synthetic aperture radar (SAR)

4.1. Introduction

Soil surface roughness (SSR) is a variable that represents the microtopographic variations of soil surface elevations. As such, SSR greatly influences different processes at the soil-atmosphere interface including the partition of precipitation into infiltration or runoff (Govers et al., 2000; Zhao et al., 2013), the heat and energy balance at the soil surface (Matthisas et al., 2000; Cierniewsky et al., 2015), the occurrence of wind and water driven soil erosion (Helming et al., 1998; Vermang et al., 2015), etc. As a result, SSR has been approached from different fields of science, addressing different research questions and using different instruments, parameters and analysis techniques (Smith, 2014).

SSR-measuring instruments can be grouped into contact and non-contact devices (Verhoest et al., 2008). Non-contact devices have developed rapidly in the last years and offer a cost-effective way to survey the soil surface with unprecedented resolution and data (Marzahn et al., 2012a; Milenkovic et al., 2015). However, while different instruments have large differences in performance, versatility, comfort, etc. the resulting data can be considered very similar in terms of applications (Thomsen et al., 2015).

Different parameters have been proposed for measuring SSR ranging from very simple indices to more complex ones (Martinez-Agirre et al., 2016). The simplest ones characterize the height variations of the surface elevation records in a dataset (i.e., profile, point-cloud or Digital Elevation Model) and are normally referred to as vertical parameters. Some other parameters measure the spatial arrangement of surface heights, i.e., whether height variations occur in short or long horizontal distances, these can be referred to as horizontal parameters. To combine both properties, hybrid or combined parameters have been proposed, normally as a ratio or product of two parameters, one of each category. Finally, parameters based on fractal geometry have also been used in the context of SSR to measure the self-similarity or self-affinity of soil surface elevations.

In Synthetic Aperture Radar (SAR) remote sensing, the backscattered signal over bare soils, as measured through the backscattering coefficient (σ^0), is influenced by a combination of factors including sensor configurations (frequency and polarization),

surface characteristics (soil moisture and surface roughness) and the incidence angle of the incoming microwave pulse (Fung, 1994; Ulaby et al., 1996). The ability to obtain accurate soil moisture estimations from SAR observations has received much interest from researchers across different disciplines (Wagner et al., 2007; Dobriyal et al., 2012; Kornelsen and Coulibaly, 2013). However, for current space-borne systems, the main sources of retrieval errors were due to issues related to surface roughness parameterization (Verhoest et al., 2008; Bryant et al., 2007; Lievens et al., 2009).

Therefore, many research efforts in SSR parameterization have focused on how to isolate its effect on soil moisture retrieval techniques (Verhoest et al., 2008). Early studies (e.g., Ulaby et al., 1982), based on field radiometers and scatterometers, were conducted in different experiments to understand the role of SSR in backscatter. These datasets were also used to develop or to evaluate mathematical models (physically based or empirical based) describing the scattering of microwave pulses at the soil surface (Fung et al., 1992; Oh et al., 1992; Fung, 1994; Dubois et al., 1995). These models were later numerically inverted to retrieve a variable of interest (mostly soil moisture) from σ^0 observations, based on the previous knowledge of the other intervening variables (i.e., SSR parameters) or by making simplifying assumptions.

When backscatter models were applied to observations obtained from space-borne platforms (SAR sensors), a problem arose related to the scale of observation (spatial resolution and wavelength) and the required roughness measurement scale (Verhoest et al., 2008). Roughness parameters especially the correlation length were found to have multi-scale properties, and their values appeared very sensitive to the measurement range (i.e., profile length) (Oh and Kay, 1998; Mattia et al., 2003). Callens et al. (2006) observed that some parameters reached equilibrium with increasing profile lengths. Other studies (Oh and Kay, 1998; Davidson et al., 2000; Manninen, 2003) defended the need for long profiles to include all roughness components present on the antenna-illuminated area (i.e., one pixel). However, this recommendation can be very difficult (if not impossible) to follow in practice because the spatial resolutions of SAR sensors ranges from ~1 m to ~1000 m depending on the sensors' beam modes (European Spatial Agency, 2016).

The spatial sampling of SSR measurements is also a key element. In general, it has been related to the wavelength of the SAR sensors. For example, Ulaby et al. (1982) recommended a sampling interval of ~1/10 the wavelength of observations. Barber et al. (2016) evaluated the influence of sampling interval on the SSR statistics over agricultural soils and observed that class differences were reduced as the measurement interval increased. They also recommended intervals of 15 and 5 mm for L- and C-bands, respectively.

These issues in SSR characterization caused some authors to use effective or optimum roughness parameters rather than real or measured ones (Su et al., 1997; Baghdadi et al., 2006a). The effective roughness parameters are those obtained by optimization or inversion of backscatter models (depending on whether soil moisture measurements are used or not). As such, they provide a good model fit without necessarily producing realistic values of roughness parameters (i.e., not comparable to field measurements). In recent years, several studies successfully implemented the effective roughness approach (Joseph et al., 2008; Lievens et al., 2011; Dong et al., 2013; Baghdadi et al., 2015; Bai et al., 2016).

Recently, Fung (2015) proposed that many natural surfaces (e.g., agricultural surfaces and sea surfaces) have multi-scale roughness properties, but not all their roughness scales contributed to backscatter. He proposed that only one specific roughness spectral component, $\kappa = (4\pi/\lambda)\sin\theta$, was responsible for microwave backscatter, where λ is the incident wavelength and θ is the incidence angle. Therefore, at centimeter wavelengths (typical of existing SAR sensors), meter-size roughness components should not play a role in backscatter from multiscale surfaces (Fung, 2015).

The aim of this research was to analyze the influence of surface roughness measurement scale on radar backscattering across different agricultural soils. The objective was to determine the roughness scales, which contribute to backscatter from agricultural soils and to provide some guidelines on how roughness should be characterized in these applications.

4.2. Materials

4.2.1. Test site

The data acquisition was carried out on the experimental watershed of La Tejería (N42º44'10.6'' and W1º56'57.2'') in the Spanish region of Navarre (Fig. 4.1). This watershed is part of the Experimental Agricultural Watershed Network of Navarre, created by the local Government of Navarre in 1993. The watershed is used to study the impact of agriculture on hydrological resources (Casalí et al., 2008). The total area of the watershed is about 169 ha with homogenous slopes of ~12% and an altitude range from 496 to 649 m. Its climate is humid sub-Mediterranean with a mean annual temperature of 13º C and an average annual precipitation of ~700 mm distributed over 105 days. Ten agricultural fields were monitored (Fig. 4.1), and their sizes ranged from 3.0 ha to 7.3 ha.

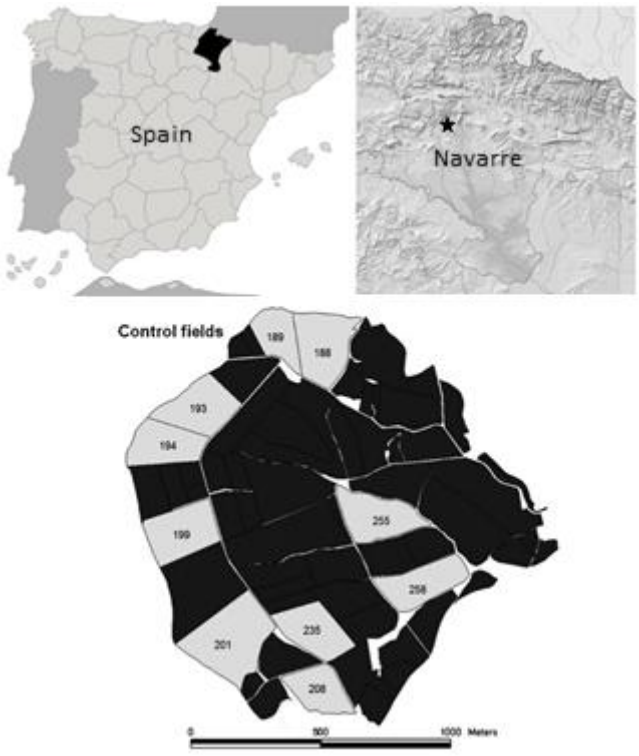

Fig. 4.1. Location of La Tejería experimental watershed and distribution of control fields (fields in black were not used in this study).

Soils have a Silty-Clay texture (approximately 43% clay, 5% sand, 52% silt) and are relatively shallow (0.5-1.0 m deep) except for swales where deeper soils can be found. The monitored fields were cultivated with rain-fed winter cereal crops (wheat, barley or oats) sown at the end of October and harvested at the end of June. Soil preparation operations were performed sequentially during September and October. The different tillage operations (considered as different roughness classes) were Mouldboard Plough (MP), Harrowed Rough (HR), Harrowed Smooth (HS), Planted (P) and Planted Compacted (PC) (Table 4.1).

Table 4.1. Description of the different roughness classes caused by agricultural treatments.

Tillage class	Acronym	Fields	Profiles	Description
Mouldboard Plough	MP	04	16	Tillage operation performed with a plough with multiple mouldboards at a depth of 15-20 cm, resulting in soil inversion and a very rough surface
Harrowed Rough	HR	09	39	Operation performed normally with a tine harrow to break soil clods and provide a smoother surface suitable for seeding
Harrowed Smooth	HS	07	29	In cases where the first harrowing did not smoothen sufficiently the surface a second harrowing was applied
Planted	P	11	44	Seeding operation performed with conventional sowing machinery, normally seed drills
Planted Compacted	PC	01	04	In few cases farmers compacted the soil surface with a roller after sowing

4.2.2. Surface roughness data

Surface roughness was measured using a laser profilometer with a total measurement range (profile length) of 5 m, a resolution (sampling interval) of 5 mm and a vertical accuracy of 1.25 mm (Martinez-Agirre et al., 2016; Álvarez-Mozos et al., 2009). Profiles (n=132) were measured under bare soil conditions in parallel to the tillage direction and spatially distributed over each field, so as to obtain field average roughness parameters representative of the spatial variability within the field; in most cases 4 profiles were acquired per field and date of study (Table 4.2). For 6 satellite acquisition dates (Table 4.3), the surface roughness measurements were not available and the roughness data of the previous date were considered under the assumption of no roughness change between dates. This assumption was deemed plausible because roughness smoothening due to rainfall can be considered relevant only during the first precipitation events after tillage (Zobeck and Onstad, 1987; Gilley and Kootwitz, 1995), which was not the case. For the time this assumption was applied a cumulative

rainfall of 103.3 mm had already been recorded since tillage, and besides subsequent precipitation events were weak (intensity <2 mm/h).

Table 4.2. Roughness classes corresponding to each field and measurement date. Four roughness profiles were acquired per field, expect where indicated.

Field ID.	22/09/2004	08/10/2004	24/10/2004	17/12/2004
188	HR*	HR	-	P
189	HR*	HR	HS	P
193	HR*	HR	P	P
194	-	HR	HR	P
199	MP*	MP	MP	P
201	HS*	HS	-	P
208	MP**	-	-	PC
235	HS	HS	P	P
255	HS	HS	-	P
258	HR	-	-	P

- Fields not monitored on that particular day
* Fields with 5 profiles measured
** Fields with 3 profiles measured

Profiles were processed using a code developed *ad hoc*, with following steps: (1) correction of the buckling effect on the aluminum bar using a parabolic calibration function, (2) filtering the outliers corresponding to plant material or small holes eventually present in the soil, by deleting and linearly interpolating any records with height differences larger than a certain threshold (i.e., 2 cm) with the previous and subsequent records, and (3) linear correction for the terrain slope. Further information on profile processing can be found in (Martinez-Agirre et al., 2016).

4.2.3. Soil moisture data

The soil moisture (SM) of the top 10 cm of the soil was measured using a commercial Time Domain Reflectometry (TDR) instrument (TRIME FM-3, IMKO GmbH) connected to a portable three-rod probe. On each field, five SM measurement locations were monitored per date, and these were spatially distributed to cover the entire field. On each location 3 TDR readings were taken. The TDR probe was calibrated with *in situ* soil moisture data measured with the thermogravimetric method. Here, soil samples with a known volume (necessary for the calculation of the bulk density) were also collected regularly. For four satellite acquisition dates (Table 4.3) the TDR measurements were not available and modelled SM values were used instead. For SM modelling TOPLATS was used (Famiglietti and Wood, 1994; Pauwels et al., 2001) to

calibrate and validate the surface SM per field using the available TDR measurements; this offered a RMSE of ~0.02 cm^3cm^{-3}.

4.2.4. SAR data

During the study period, 10 ENVISAT/ASAR scenes (C-band) were acquired over La Tejería watershed (Table 4.3). Scenes were ordered as VV polarization Precision Image products in swath IS2 (incidence angles around 19º-26º), multilooked (4 looks), except for one scene (22/09/2004) that was acquired in swath IS1 and Alternate Polarization (HH-VV) mode with 2 looks. In the latter, only the VV channel was used for consistency with the rest of the dataset. Half of the scenes were obtained in ascending pass, and the other half in descending pass. In all cases, the resolution was 30 m x 30 m. Scenes were: (1) orthorectified (with an error <1 pixel), (2) calibrated (using the local incidence angle) and (3) speckle-filtered (Gamma MAP filter with a window of 5x5). The DEM used for preprocessing was obtained by photogrammetric techniques with a spatial resolution of 5 m. Mean backscatter coefficient values (σ^0) were calculated for each field per date.

Table 4.3. Summary of SAR data.

Date	SAR data	θ_{LOC} (º)	Pass	Fields	Roughness	SM data
22/09/2004	ENVISAT/ASAR*	7.2-16.2	Descending	9	Profilometer	TDR
08/10/2004	ENVISAT/ASAR	11.6-20.9	Descending	8	Profilometer	TDR
11/10/2004	ENVISAT/ASAR	20.9-31.4	Ascending	8	=	TOPLATS
24/10/2004	ENVISAT/ASAR	15.7-24.9	Descending	5	Profilometer	TDR
27/10/2004	ENVISAT/ASAR	16.9-27.2	Ascending	5	=	TOPLATS
17/12/2004	ENVISAT/ASAR	11.6-20.9	Descending	10	Profilometer	TDR
20/12/2004	ENVISAT/ASAR	20.8-31.2	Ascending	10	=	TOPLATS
02/01/2005	ENVISAT/ASAR	15.8-24.5	Descending	10	=	TDR
05/01/2005	ENVISAT/ASAR	16.8-26.9	Ascending	10	=	TDR
24/01/2005	ENVISAT/ASAR	20.9-31.3	Ascending	10	=	TOPLATS

* Scene acquired in Alternative Polarization (HH-VV) Mode with 2 looks in swath IS1

4.3. Methods

The analysis presented here focused on the influence of surface roughness scale on backscatter. Roughness was characterized through different parameters (explained in section 4.3.1) that were measured considering different scales. Here, three scaling issues were investigated: (1) the influence of measurement range (profile length), (2)

the influence of low frequency roughness components and (3) the influence of high frequency roughness components.

To study the influence of the measurement range, each roughness parameter was calculated with decreasing profile lengths by dividing the original profile into 2, 3, …, 10 profiles of equal length, leading to profiles of 2.5 m, 1.66 m,…, 0.5 m length. Next, to study the low frequency components, profiles were smoothened using moving median filters of increasing window size; 1 cm, 2 cm, 5 cm, 10 cm, 20 cm, 50 cm, 100 cm and 200 cm. This way, the high frequency components of increasing wavelengths were masked from the profiles. Finally, to study the influence of high frequency components, the smoothened profiles obtained for increasing filter sizes were subtracted from their corresponding original profiles such that only the high frequency components remained (Fig. 4.2).

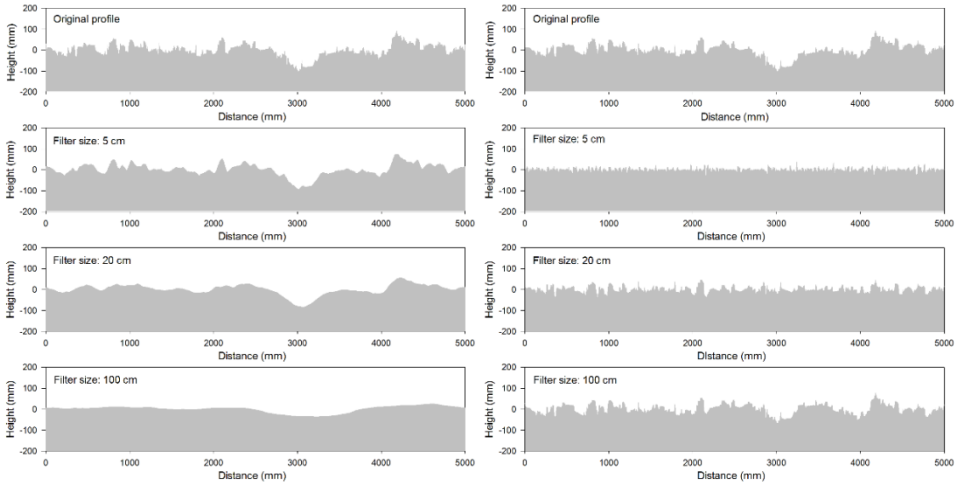

Fig. 4.2. Example of profile filtering. Original profile (above), low frequency roughness components (left column) and high frequency roughness components (right column) for increasing filter sizes.

For each of these three scaling issues, the following analyses were carried out: (1) assessment of the behavior of roughness parameters for the different scales investigated, (2) correlation of SAR backscatter with roughness parameters obtained at different scales and (3) evaluation of the goodness-of-fit of a backscatter model parameterized with roughness parameters obtained from different scales.

4.3.1. Behavior of roughness parameters

In total, 8 roughness parameters were analyzed (Table 4.4). These parameters were selected after a detailed analysis (Martinez-Agirre et al., 2016), where their ability to discriminate different tillage classes was assessed. Some of these parameters were descriptors of the vertical roughness component (vertical parameters), i.e. the standard deviation of surface heights (s) (Allmaras et al., 1966) and the microrelief index (MI) (Römkens and Wang, 1986). Others parameters measured the horizontal component (horizontal parameters), i.e. the correlation length (l) (Ulaby et al., 1982), the initial slope of the autocorrelation function ($\rho'(0)$) (Ulaby et al., 1982) and the peak frequency (F) (Römkens and Wang, 1986). Some parameters combined both components (combined parameters), i.e. parameter MIF (Römkens and Wang, 1986) and the tortuosity index of Saleh (T_S) (Saleh, 1993). Finally, fractal dimension (D) (Vidal Vázquez et al., 2005) was also considered. The behavior of the different roughness parameters was evaluated by comparing the average and standard deviation of each roughness parameter per class for the different scales under study.

Table 4.4. Summary of the roughness parameters analyzed.

Type	Parameter	Description	Equations
Vertical	s (cm)	Standard deviation of surface heights	$s = \sqrt{\frac{\sum_{i=1}^{N}(z_i{}^2 - \bar{z}^2)}{N-1}}$
	MI (cm)	Microrelief index	---
Horizontal	l (cm)	Correlation length	$\rho(h) = \frac{\sum_{i=1}^{N(h)} z_i z_{i+h}}{\sum_{i=1}^{N} z_i{}^2}$
	$\rho'(0)$	Initial slope of the auto-correlation function	---
	F (cm^{-1})	Peak frequency	---
Combined	MIF	Combined parameter	$MIF = MI \cdot F$
	T_S	Tortuosity	$T_S = 100 \cdot \frac{(L_1 - L_0)}{L_1}$
Fractal	D	Fractal dimension (semivariogram method)	$\gamma(h) = l^{1-H}h^H;\ D = 2 - H$

s is the standard deviation of heights where N is the number of height records, z_i is the height of record i, and $\bar{z}$ is the mean height of all records. $\rho(h)$ is the autocorrelation function, the correlation length l is then defined arbitrarily as the distance at which the heights of two points are considered independent; i.e., $\rho(h)$

is equal to 1/e, so that $\rho(l) = 1/e$. Another parameter extracted from the autocorrelation function is its initial slope $\rho'(0)$. *MIF* is a combined parameter where *MI* represents the area per unit length between the measured surface profile and the regression line obtained through least squares, and *F* is the number of peaks per unit length. Tortuosity is a roughness index based on the ratio of the surface profile perimeter length (L_1) and its horizontal projection (L_0). Assuming a fractal Brownian motion (*fBm*) model, the experimental semivariogram can be described as a function of the lag, where *l* is the crossover length and *H* is the Hurst coefficient. Afterward, *H* was related to the fractal dimension as $D = 2 - H$.

4.3.2. Correlation of backscatter with roughness parameters

To analyze the correlation between backscatter signal and roughness parameters, a two stage backscatter data normalization was applied to remove the influence of factors other than roughness on σ^0 values. First, the σ^0 values were normalized toward a reference incidence angle based on the generalized Lambert's law (Abdel-Messeh and Quegan, 2000):

$$\sigma^0_{\theta_{ref}} = \sigma^0 \frac{cos^n \theta_{ref}}{cos^n \theta} \tag{4.1}$$

with σ^0 being the linear backscatter observation at the incidence angle θ, and $\sigma^0_{\theta_{ref}}$ being the linear backscatter normalized to a reference incidence angle θ_{ref} set to 20º (which corresponds to the average value of the observations). The exponent *n* represents the degree of Lambertianity of the target and was therefore optimized for each roughness class minimizing the correlation between $\sigma^0_{\theta_{ref}}$ and the incidence angle (*n* values between 2 and 8 were obtained for the different roughness classes). A second normalization was performed to compensate σ^0 variations due to SM fluctuations. With this aim, a linear relation was assumed between $\sigma^0_{\theta_{ref}}$ and SM for fields of different roughness classes observed on dates with contrasting SM conditions. The resulting linear function was used to detrend $\sigma^0_{\theta_{ref}}$ leading to σ^0_{norm}. The linear regression approach has offered good results in the past (e.g., Hegarat-Mascle et al., 2002; Thoma et al., 2006). To assess the correlation between backscatter signal and roughness parameters, the Spearman R coefficient was computed between the field average σ^0_{norm} and the roughness parameters obtained for each field and date.

4.3.3. Goodness-of-fit of backscatter model

In the last part, the empirical backscatter model of Oh et al. (1992) was considered. The Oh model was selected because of its ample validity range including both rough

and smooth conditions and its adequate simulation of the co-polarized backscatter (Baghdadi and Zribi, 2006b; Panciera et al., 2014). Other models (i.e. Integral Equation Model (IEM) (Fung et al., 1992), Geometrical Optic Model (GOM) and Small Perturbation Model (SPM) (Beckmann and Spizzichino, 1987) were discarded because a significant part of the measured fields were outside their validity range. Model goodness-of-fit was evaluated by computing the RMSE between simulated and observed σ^0 values (without backscatter data normalization). It must be mentioned that the Oh model was empirically built based on in situ data with some particular roughness conditions (s values between 0.32 cm and 3.02 cm) and measurement techniques (1-m long profiles with 0.25 cm sampling interval), and this fact might have influenced the results obtained here.

4.4. Results

4.4.1. Roughness measurements using original profiles

Prior to roughness scale analysis, the results obtained with the original profiles (5 m length, 5 mm sampling interval) were analyzed. The behavior of the different roughness parameters per roughness class is shown in the boxplots (Fig. 4.3). The vertical parameters s and MI and the combined parameter MIF presented a very similar behavior. The mean class values and class variability decreased from the roughest to the smoothest class (MP and PC, respectively). The combined parameter T_S also showed decreasing mean class values but with similar variability in all classes. On the other hand, horizontal parameters $\rho'(0)$ and F and fractal parameter D had increasing mean class values and similar variability. Finally, the horizontal parameter l, i.e. the correlation length, behaved completely different with no clear trends and overlapping values for the different classes.

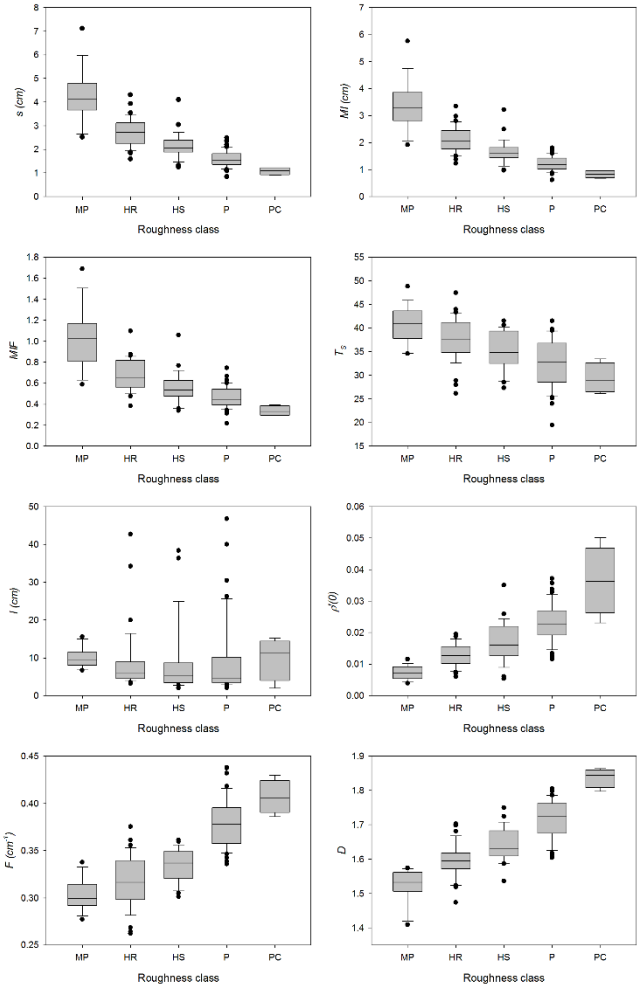

Fig. 4.3. Box plots of the different roughness parameter values per roughness classes.

The correlation of the normalized backscatter coefficient (σ^0_{norm}) with the roughness parameters varied markedly depending on the parameter under study (Fig. 4.4). The fractal parameter *D* (R=−0.651) and the horizontal parameters *F* (R=−0.641) and *ρ'(0)* (R=−0.617) showed the highest correlations followed by the vertical parameters *MI* (R=0.585) and *s* (R=0.584). The combined parameters *MIF* (R=0.528) and especially T_S (R=0.433) had a lower correlation. On the other hand, the horizontal parameter *l* had the lowest correlation (R=0.064).

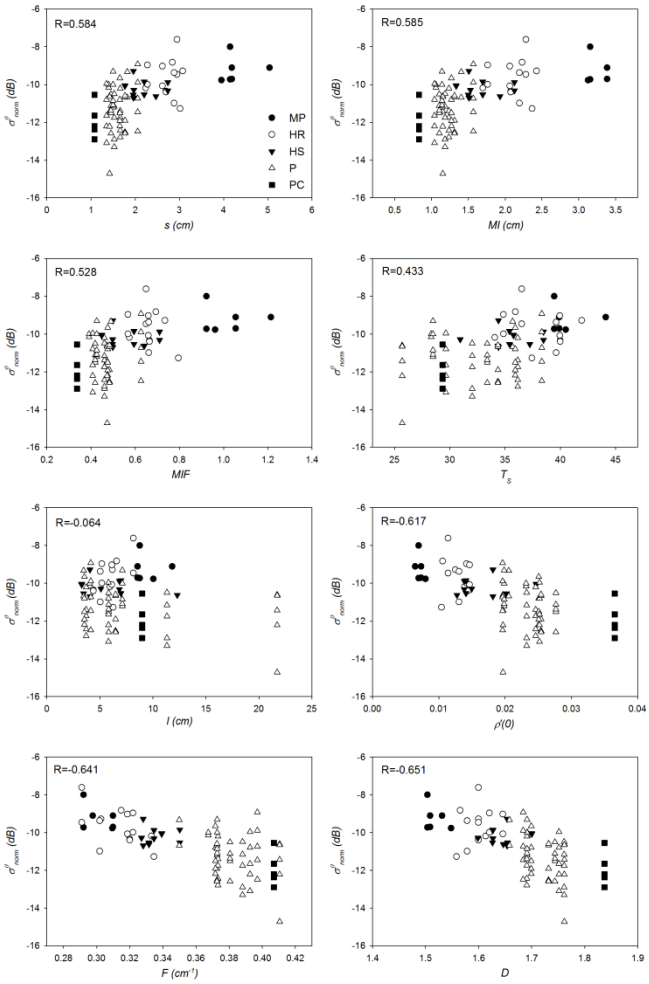

Fig. 4.4. Scatterplots between $\boldsymbol{\sigma^0_{norm}}$ and the different roughness parameters by field. The Spearman correlation coefficient (R) is also given.

Regarding the goodness-of-fit of the Oh model (Fig. 4.5), the mean RMSE value between the simulated and the observed backscatter was 1.323 dB. The fitting for the HS roughness class (RMSE < 1 dB) was very good. For the P, HR and MP roughness classes, the RMSE values ranged from 1 to 1.5 dB. Finally, for the PC roughness class (only one field at different dates) the RMSE value was close to 2 dB.

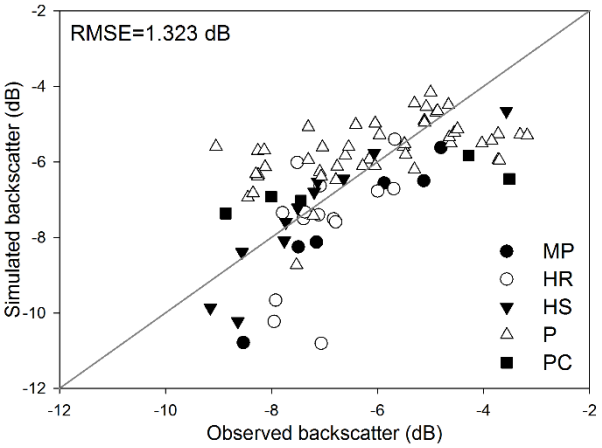

Fig. 4.5. Goodness-of-fit between simulated and observed backscatter coefficients per field.

4.4.2. Influence of profile length

Fig. 4.6 depicts the behavior of the different roughness parameters per class depending on the profile length. Vertical parameters (*s* and *MI*) increased with increasing profile lengths especially for rough classes (e.g., MP). The variability per class (error-bars in Fig. 4.6) of the vertical parameters normally decreased with increasing profile lengths. Horizontal parameters did not exhibit a consistent trend, and different patterns were observed for the different parameters. For instance, parameters *ρ'(0)* and *F* followed a generally decreasing trend, steeper in the shortest profile lengths and gentler at longer lengths. There were some exceptions, particularly in the MP class. Furthermore, the *ρ'(0)* and *F* values were quite different for the different classes regardless of the profile length. The variability per class of *ρ'(0)* and *F* parameters normally decreased with increasing profile lengths, with the variability of *ρ'(0)* being lower than that of *F*. The parameter *l* had a different pattern and a growing trend for increasing profile lengths, although values at short profile lengths were quite erratic and variable. In this case, the variability per class seemed to increase for longer profiles. The combined parameters (*MIF* and *TS*) had a similar trend as the vertical ones with slightly increasing values and decreasing class variabilities for increasing profile lengths. Finally, the fractal parameter *D* had a trend very similar to *ρ'(0)* except for the MP class.

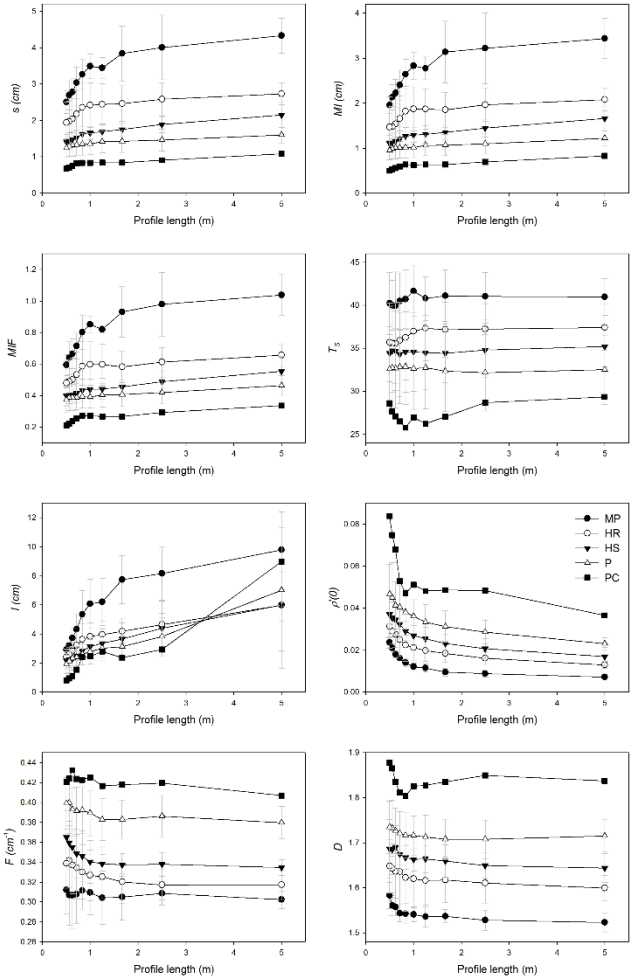

Fig. 4.6. Influence of profile length on roughness parameters. Mean values of roughness parameters and standard deviation (error bars) for the different roughness classes depending on the profile length.

The correlation of σ^0_{norm} with the different roughness parameters depending on profile length is presented in Fig. 4.7. Spearman correlation values are given (R) for a more straightforward interpretation of results. Vertical parameters showed a very similar correlation trend with R values ranging from 0.5 to 0.6. These increased at short profile lengths (from 0.5 to 1 m) and then stabilized for longer profiles (from 1 m to 5 m). Horizontal parameters did not show a consistent pattern. On one hand, *ρ'(0)* and *F* behaved similar to the vertical parameters (inverse correlation) with R values increasing for longer profile lengths. The R values achieved by these two

parameters, especially *F*, was very high (~−0.6). This was even higher than those for vertical parameters regardless of the profile length. In contrast, *l* had maximum R values of ~0.4 with short profile lengths and very low correlations with longer profiles. The combined parameters also behaved very similar to the vertical ones, but with slightly lower correlation values. Parameter *D* also showed an increasing trend with high R values (<−0.6) for profiles longer than 2-3 m and values dropping to ~−0.5 for lengths below 1 m.

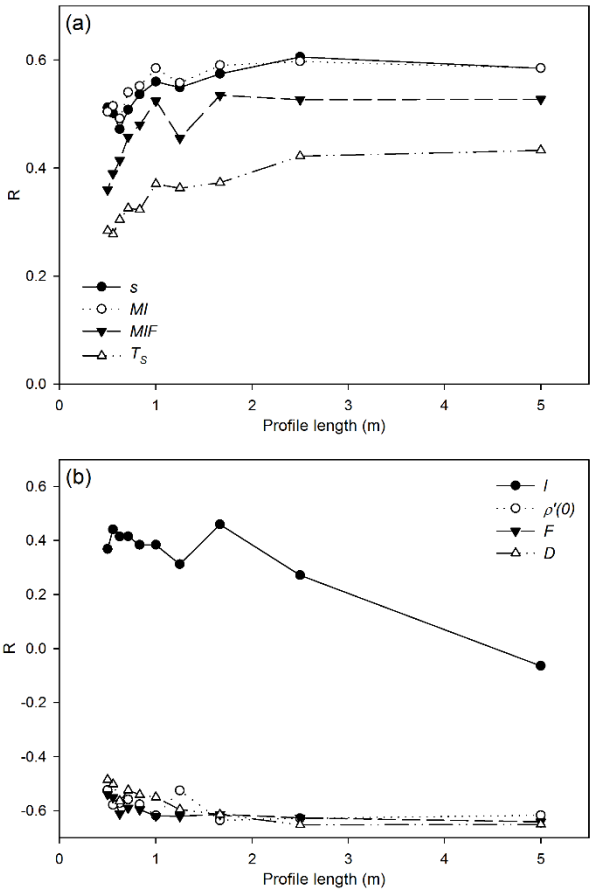

Fig. 4.7. Spearman correlation coefficients (R) between σ^0_{norm} and the different roughness parameters depending on the profile length. (a) represents vertical and combined parameters and (b) horizontal and fractal ones.

The Oh model showed a consistent trend of decreasing RMSE values for increasing profile lengths. This was true across all of the different roughness classes (Fig. 4.8) with RMSE values decreasing mostly between 0.5 and 1 m profile lengths and then stabilizing for longer profiles. With short profiles, the errors were particularly large for class PC (the smoothest class and with only one field observed on different dates). On the other hand, the MP class showed a rather insensitive behavior with profile lengths.

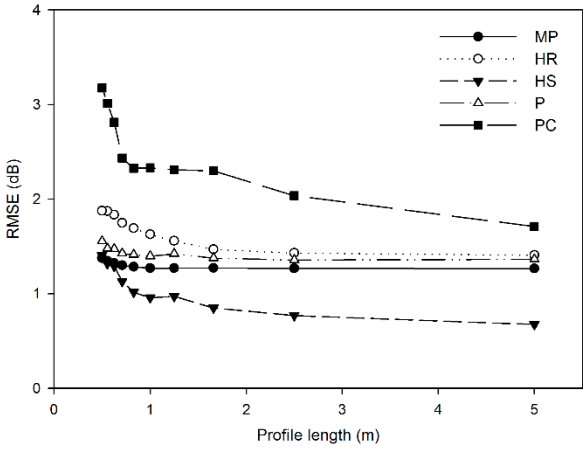

Fig. 4.8. Roughness class average Root Mean Square Error (RMSE) between simulated (Oh model) and observed field backscatter values depending on the profile length.

The higher RMSE values observed for shorter profile lengths might be partly explained by the fact that the short profiles survey a much smaller soil surface sample than longer ones. That is, the field average roughness parameters computed using four 1-m profiles (with a sampling interval of 5 mm) are based on 800 surface height records, whereas four 5-m profiles are based on 4000 records. This sampling effect might hide the influence of different roughness scale components in Fig. 4.8. Therefore, Fig. 4.9 shows the same results but obtained by increasing the number of profiles at shorter lengths to the maximum allowed by the original 5 m length (i.e., one 5-m profile, two 2.5-m profiles, four 1.25-m profiles, etc.). This way, different profile lengths correspond to the same soil surface sample (same number of height records) and differences are only due to the influence of different roughness scale components. This time, the influence of profile length on the Oh model fit is much lower (Fig. 4.9). There were only slight increases in the RMSE values for profiles shorter than 1 m.

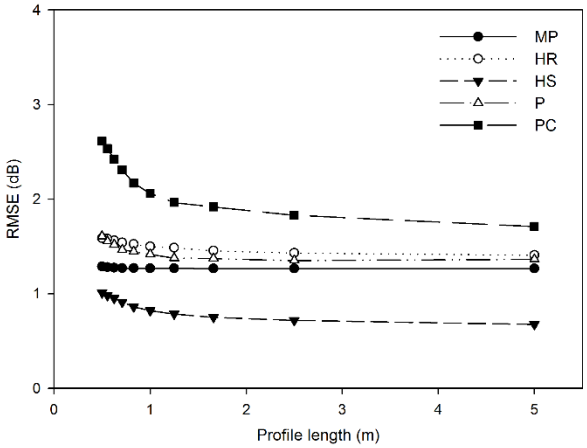

Fig. 4.9. Roughness class average Root Mean Square Error (RMSE) between simulated (Oh model) and observed field backscatter values depending on the profile length. The number of shorter profiles was increased so that the same soil surface sample was surveyed than for longer profiles.

4.4.3. Influence of low frequency roughness components

Most parameters (except *l*) had decreasing values for all roughness classes (Fig. 4.10) as profiles were smoothened (i.e. short frequency components discarded). However, this the decreasing trend varied. Vertical parameters *s* and *MI* decreased gently at the beginning but were steeper after a filter size of 10 cm (expect for PC). This indicates a higher sensitivity to larger scale components. Most horizontal, combined and fractal parameters had an opposite trend with a strong decrease at small filter sizes and a stabilization for larger ones. This illustrates the higher influence of small-scale components on their values. The parameter *l* showed a very unique trend (among horizontal parameters) of steady growth as the filter size increased. But then took higher increasing rates for filter size between 20 cm to 100 cm. Therefore, it seems that *l* is more strongly influenced by larger scale components than the other horizontal parameters.

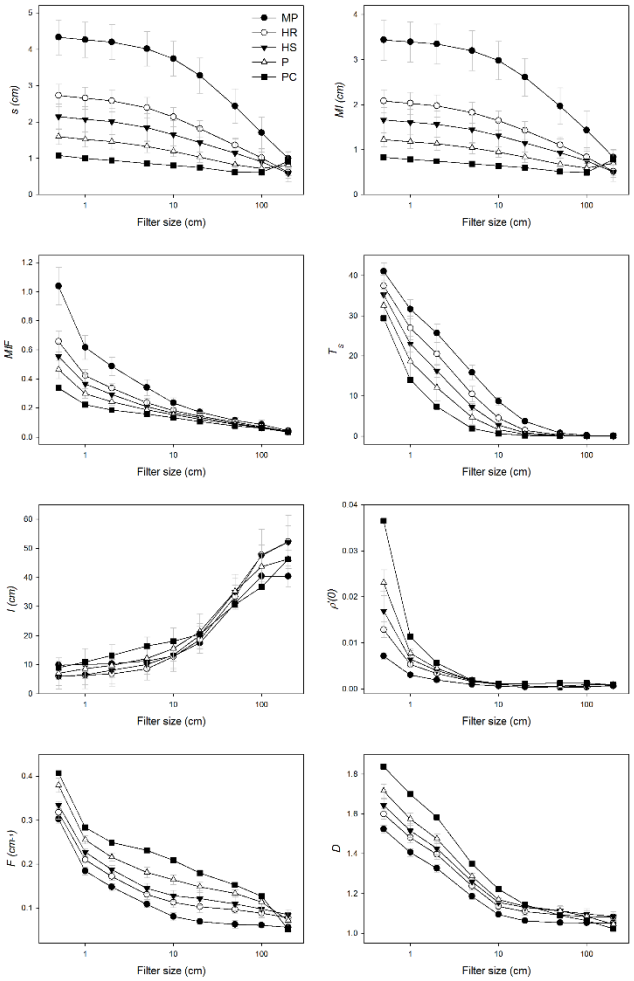

Fig. 4.10. Influence of profile smoothening on roughness parameters. Mean values of roughness parameters and standard deviation (error bars) for the different roughness classes for increasing filter size. Filter size of 0.5 cm corresponds to original profiles.

Correlation values of vertical parameters (s and MI) with σ^0_{norm} slightly decreased as the profiles were smoothened until a window size of 50 cm. It then sharply decreased until 200 cm (Fig. 4.11). Horizontal parameters did not show a unique behavior. Parameter l increased in correlation as the finest roughness components (until 5 cm window size) were discarded. It then peaked at R~−0.35 and took the opposite trend with R values ~0 for window sizes longer than 50 cm. On the contrary, $\rho'(0)$ had a strongly decreasing correlation as the finest components (<5 cm) were filtered out but

then increased again with filter sizes of 50-100 cm (R~−0.55). Parameter *F* showed high correlation values (R~−0.6) that were insensitive to the removal of high frequency components until a filter size of 10 cm. After this point, correlation decreased as filter sizes increased. The combined parameter *MIF* quickly decreased in correlation for increasing filter sizes. In contrast, T_S showed a rather insensitive behavior as long as the roughness components below 50 cm were maintained with maximum correlation values of R~0.65 for a filter size of 10 cm. Finally, *D* had a similar pattern to *F* with maximum correlation values for profiles that maintained the small scale roughness components (filter size below 2 cm).

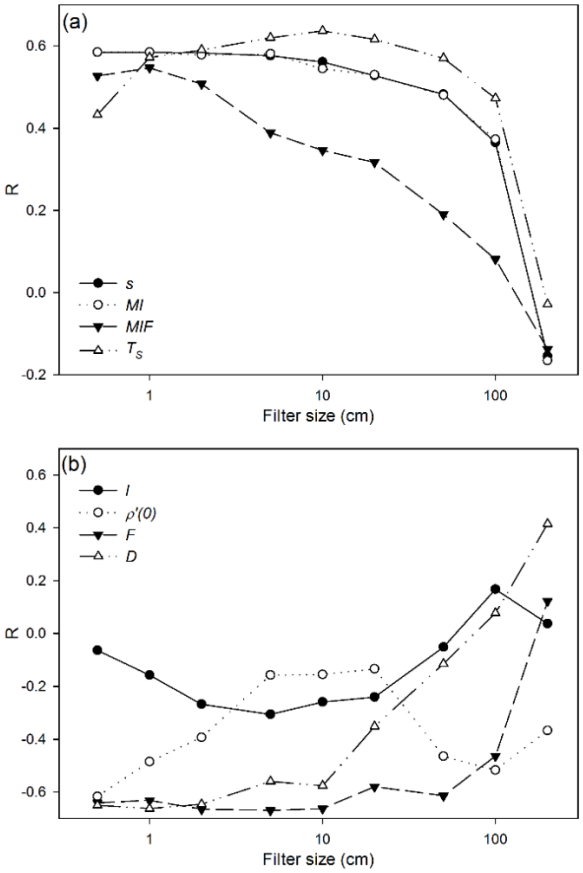

Fig. 4.11. Influence of profile smoothening on the correlation between $\boldsymbol{\sigma^0_{norm}}$ and the different roughness parameters. Spearman correlation coefficients (R) are represented for increasing filter sizes. Filter size of 0.5 cm corresponds to original profiles. (a) represents vertical and combined parameters and (b) horizontal and fractal ones.

The results obtained with the Oh model confirmed the observations above with RMSE values increasing consistently as high frequency roughness components were removed from the original profiles (i.e., window size increasing in Fig. 12). Smooth classes (i.e., PC and P) were more sensitive than medium or rough classes, and RMSE values increased faster on the first. Rough classes (in particular MP) were more insensitive and had similar RMSE values until filter sizes of 20-50 cm.

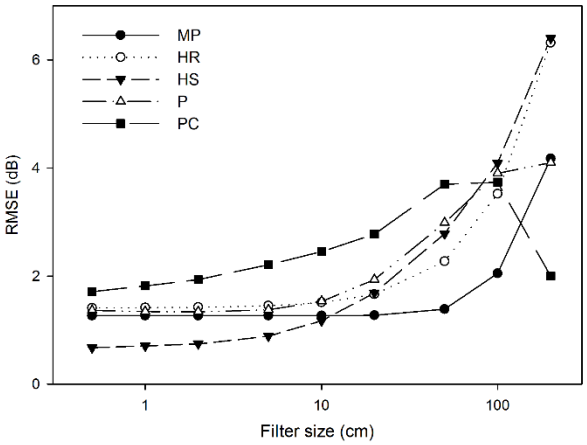

Fig. 4.12. Roughness class average Root Mean Square Error (RMSE) between simulated (Oh model) and observed backscatter values depending on profile smoothening (filter size). Filter size of 0.5 cm corresponds to original profiles.

4.4.4. Influence of high frequency roughness components

Most roughness parameters clearly varied when low frequency components were subtracted from the roughness profiles. This variation was small when only roughness scale components larger than 1 m were subtracted (Fig. 4.13). In turn, when only the shortest components were left (filter window sizes below 10 cm) most parameters changed strongly, and the differences between tillage classes were reduced. Parameters *s*, *MI* and *MIF* also had some sensitivity to the removal of the longer roughness components. They showed a linear decay as the frequencies were discarded. The others were quite stable at least until a filter size of 50 cm (for $\rho'(0)$ and *D*) or 20 cm (for *F*) was achieved. The T_S was quite exceptional, and its values only changed when roughness components shorter than 5 cm were removed. Finally, *l* had a decaying trend taking lower values when longer frequency components were

discarded. However, this general pattern was altered by outliers particularly in smooth classes (PC and P).

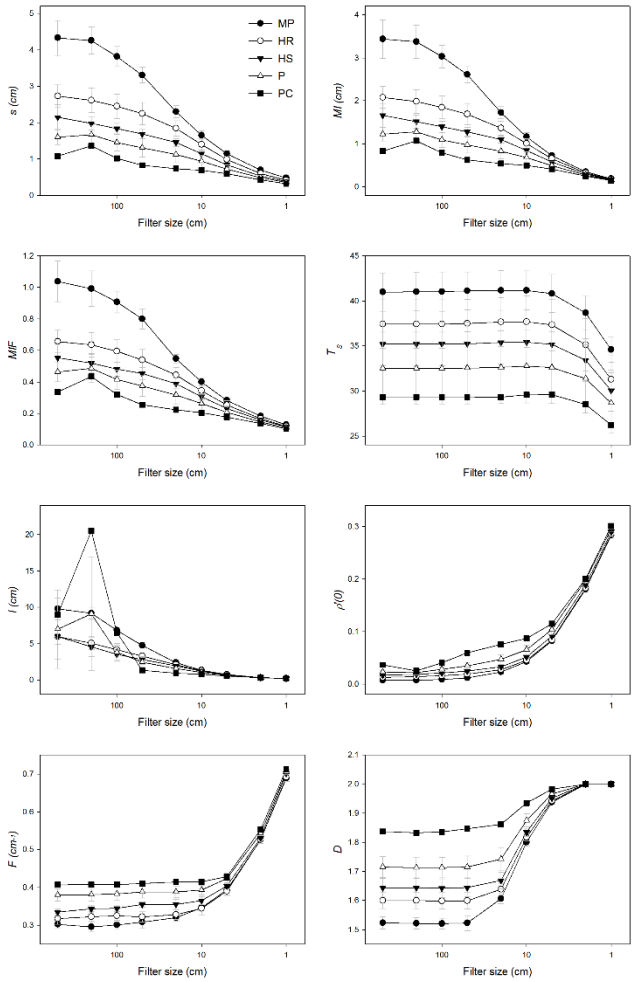

Fig. 4.13. Influence of high frequency roughness components on parameter values and standard deviation (error bars) for the different roughness classes for increasing filter size. Parameter values are computed from profiles obtained as a subtraction of smoothened profiles for increasing filter sizes from the original profiles. Filter size of 500 cm corresponds to original profiles without filtering.

Correlation values of vertical parameters with σ^0_{norm} decreased when lower frequency roughness components were subtracted (i.e., shorter filter window size) (Fig. 4.14). However, the decrease was only noticeable when the filter size was smaller than ~50

cm. Thus, the inclusion of roughness frequencies longer than this value did not result in additional enhancements in correlation with σ^0_{norm}. Parameters *ρ'(0)*, *F* and *D* showed a low dependence on the removal of low frequency components with correlation values decreasing when only scale components smaller than 1 cm remained. On the other hand, *l* showed a high sensitivity to roughness components longer than ~50 cm with correlation values dropping abruptly after this value. It is remarkable that when roughness components longer than 50 cm were discarded, *l* had R values ~0.6, which is similar to those of other horizontal roughness parameters (i.e., *F* or *ρ'(0)*).

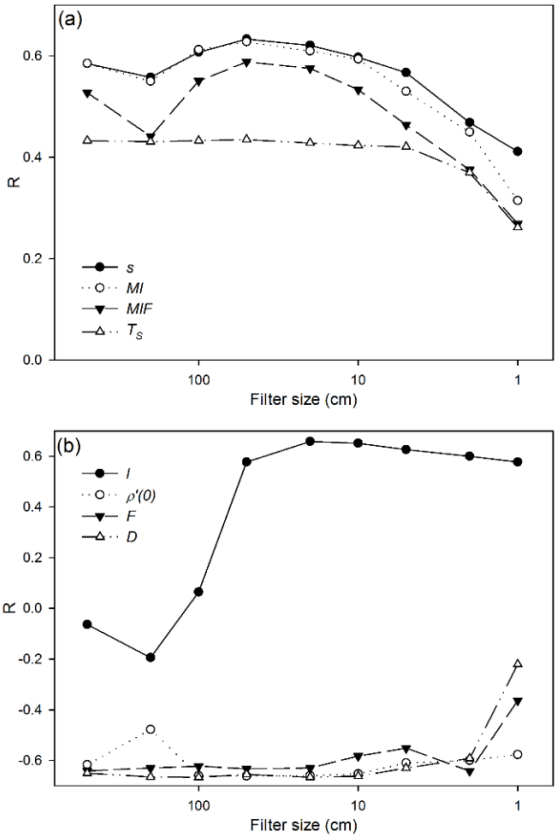

Fig. 4.14. Influence of high frequency components on the correlation between $\boldsymbol{\sigma^0_{norm}}$ and the different roughness parameters. Parameter values are computed from profiles obtained as a subtraction of smoothened profiles for increasing filter size from the original profile. Spearman correlation coefficients (R) are represented for increasing filter size. Filter size of 500 cm corresponds to original profiles without filtering. (a) represents vertical and combined parameters and (b) horizontal and fractal ones.

The Oh model simulations had a very clear pattern of increasing RMSE when roughness scales below 50 cm were subtracted (Fig. 4.15). They rose as high as 8-9 dB when only components smaller than 1 cm remained. However, for most classes the inclusion of roughness components longer than 20 or 50 cm did not result in additional improvements in RMSE. Only the smoothest class (PC) seemed to further improve when wavelengths of 100 cm or longer were included.

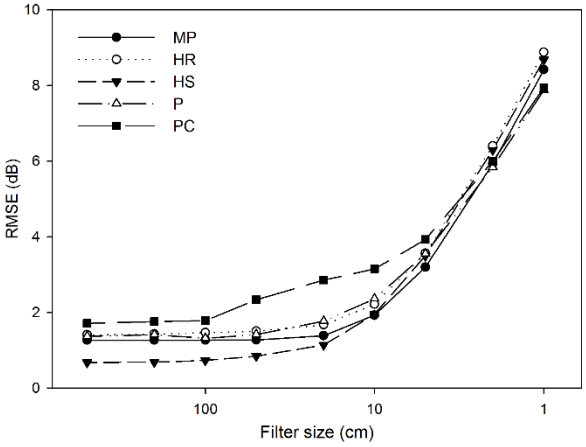

Fig. 4.15. Influence of high frequency roughness components on Oh model fit. Roughness class average Root Mean Square Error (RMSE) between simulated and observed backscatter values are represented for increasing filter size. s values are computed from profiles obtained as a subtraction of smoothened profiles for increasing filter sizes from the original profile. Filter size of 500 cm corresponds to original profiles without filtering.

4.5. Discussion and conclusions

The results confirm the clear dependency between roughness measurement scales (i.e., profile lengths) and parameter values. They demonstrate the multiscale behavior of surface roughness, as also observed in the literature (Oh and Kay, 1998; Mattia et al., 2003; Zhixiong et al., 2005; Callens et al., 2006; Verhoest et al., 2008; Snapir et al., 2014). Thus, it is necessary to determine which roughness scales are relevant in the backscattering of microwaves over bare soils. Regarding the influence of small-scale components, the results demonstrate that eliminating these small-scale roughness components from the profiles caused a strong variation in the values of horizontal parameters, while vertical ones were more insensitive. This is in agreement with

Barber et al. (2016) who observed that when the sampling interval increased, *s* decreased slightly and *l* increased causing the separability between different roughness classes to decrease. The results also confirm that *l* values did not stabilize with long profiles, but showed rather an increase in their variability (Callens et al., 2006; Lievens et al., 2009). However, the correlation of most parameters with σ^0_{norm} and the results obtained with the Oh model did not show great sensitivity to the elimination of these short roughness components until a scale of 2 or 5 cm.

Regarding the influence of large-scale roughness components, previous studies defended the need for long profiles so as to reflect all the roughness components present on a pixel (Davidson et al., 2000; Manninen, 2003) or for a statistically robust estimation of roughness parameters (Oh and Kay, 1998). However, this idea is not in agreement with the rather successful results obtained in studies based on short profiles, i.e., 1-2 m, (Baghdadi et al., 2006a; Davidson et al., 2003) or in some studies where best results were obtained when roughness parameters were computed after de-trending the underlying topographic trend, i.e., removing large-scale roughness (Bryant et al., 2007). Fung (2015) also proposed that meter size roughness scales did not influence the backscattering process at centimeter scale wavelengths. The results obtained here illustrate that incorporating roughness scales larger than 1-2 m to the measurements did not significantly improve the correlation with σ^0_{norm} or in the goodness-of-fit of Oh model simulations. These results support the idea that the low frequency roughness components do not play an important role in backscattering and also distort different parameter values (especially *l*).

Based on these results, it can be suggested that roughness scales between 5 and 50 cm are the most relevant for C-band backscatter. When the high frequency roughness components (scales below 5 cm) were smoothened, most roughness parameters only slightly decreased their correlation with observed backscatter. Similarly, few differences were observed in the Oh model results when profiles were smoothened up to a filter size of 5-10 cm. Roughness scales larger than 1-2 m might not be relevant in the backscattering of microwaves at C-band. The inclusion of these components in the profile did not provide additional enhancement to the correlation of roughness parameters with backscatter nor in the goodness-of-fit of the Oh model. In addition, large-scale roughness components had a distorting effect in some roughness parameters especially *l*. Whit regard to this, it is remarkable that some roughness

parameters (i.e., D, F and $\rho'(0)$) were more stable and showed a better correlation with backscatter. This could open new possibilities in backscatter modelling. It is important to note that this analysis was based solely on C-band SAR data, and any extrapolation of these results to other frequencies would require new data and analyses.

Acknowledgments

The authors are grateful to the Spanish Ministry of Economy and Competitiveness for partly funding this research through scholarship BES-2012-054521 and projects CGL2011-24336, CGL2015-64284-C2-1-R and CGL2016-75217-R (MINECO/FEDER, EU). Hans Lievens is a postdoctoral research fellow of the Research Foundation Flanders (FWO). The authors thank V.R.N. Pauwels for his collaboration for modelling field soil moisture values with TOPLATS.

CHAPTER 5

SURFACE ROUGHNESS SAMPLE SIZE INFLUENCE ON RADAR BACKSCATTERING

Published in: Martinez-Agirre, A., Álvarez-Mozos, J., Lievens, H., Verhoest, N.E.C., Giménez, R., 2017. Influence of surface roughness sample size for C-band SAR backscattering applications on agricultural soils. IEEE Geoscience and Remote Sensing Letters. Available on-line. DOI: 10.1109/LGRS.2017.2762434.

Abstract

Soil surface roughness determines the backscatter coefficient observed by radar sensors. The objective of this study was to determine the surface roughness sample size required in SAR applications and to provide some guidelines on roughness characterization in agricultural soils for these applications. With this aim, a dataset consisting of ten ENVISAT/ASAR observations acquired coinciding with soil moisture and surface roughness surveys have been processed. The analysis consisted of (1) assessing the accuracy of roughness parameters *s* and *l* depending on the number of 1-m long profiles measured per field, (2) computing the correlation of field average roughness parameters with backscatter observations and (3) evaluating the goodness-of-fit of three widely used backscatter models, i.e., Integral Equation Model (IEM), Geometrical Optics Model (GOM) and Oh model. The results obtained illustrate a different behavior of the two roughness parameters. A minimum of 10-15 profiles can be considered sufficient for an accurate determination of *s*, while 20 profiles might still be not enough for accurately estimating *l*. The correlation analysis revealed a clear sensitivity of backscatter to surface roughness. For sample sizes >15 profiles R values were as high as 0.6 for *s* and ~0.35 for *l*, while for smaller sample sizes R values dropped significantly. Similar results were obtained when applying the backscatter models, with enhanced model precision for larger sample sizes. However, IEM and GOM results were poorer than those obtained with the Oh model and more affected by lower sample sizes, probably due to larger uncertainly of *l*.

Keywords: agricultural soils, backscatter models, surface roughness, synthetic aperture radar (SAR)

5.1. Introduction

Synthetic Aperture Radar (SAR) sensors measure the backscatter of observed targets and offer valuable information for the identification of terrain covers and for the retrieval of bio-geophysical parameters of interest, such as soil moisture (SM), vegetation phenology and biomass. Among other terrain parameters, soil surface roughness (SSR) strongly affects the scattering of microwaves, and hence largely determines the backscatter coefficient (σ^0) observed by radar sensors, complicating the interpretation and analysis of SAR data (Verhoest et al., 2008). In the SAR literature, SSR has been mostly parameterized by the standard deviation of the heights (*s*), the correlation length (*l*) and the shape of the autocorrelation function (Ulaby et al., 1982), generally assumed exponential for agricultural soils. Several backscatter models exist that use these parameters as input for simulating σ^0. If backscatter observations are available, models can be inverted for retrieving a certain terrain parameter of interest (normally SM). An accurate estimation of roughness parameters is a prerequisite for this. Yet, their spatial variability and also the multi-scalar nature of roughness makes it difficult to determine *s* and *l* values with the required accuracy for obtaining useful inversions (Ulaby et al., 1982).

Surface roughness is known to be a multi-scalar phenomenon, causing instruments with different measuring range (i.e., profile length or surveying area) yield parameter values that are not comparable with each other (Ulaby et al., 1982). In particular, the presence of long wavelength roughness components (i.e., several meters) on a soil surface or profile can strongly affect the shape of the obtained autocorrelation functions, introducing uncertainty in the determination of *l* (Mattia et al., 2003). On the other hand, recent research has evidenced that these long wavelength components might not play a significant role in the scattering of microwaves at the frequencies used by Earth Observation satellites (Fung, 1994; Martinez-Agirre et al., 2017a). This is in line with previous studies that used profile lengths of 1-2 m for surface roughness characterization with good results (Davidson et al., 2003; Baghdadi et al., 2006a).

However, due to the spatial variability of surface roughness, a minimum amount of samples might be required for accurately characterizing roughness parameters for a particular agricultural field or roughness class. Bryant et al. (2007) observed that at least 20 profiles were required to accurately determine *s*. Similarly, Baghdadi et al.

(2008a) reported a ±10% accuracy for parameter *s* and ±20% for *l* when 10 roughness profiles were used. Yet, it is necessary to assess not only how the roughness sample size (i.e., number of profiles measured) affects the accuracy of the computed parameters, but also to evaluate how it influences the accuracy of backscatter simulations using observed σ^0 data.

The aim of this research was to evaluate the influence of surface roughness sample size on SAR backscattering in different agricultural soils. The objective was to determine the minimum number of 1-m long profiles required in SAR applications and to provide same guidelines on how roughness should be characterized for these applications. With this aim, a dataset consisting of ENVISAT/ASAR observations acquired coinciding with some ground surveys have been processed. The analysis consisted of (1) assessing the accuracy of *s* and *l* depending on the number of profiles measured per field, (2) computing the correlation of field average roughness parameters with backscatter and (3) evaluating the goodness-of-fit of backscatter models depending on the roughness sample size considered.

5.2. Material and methods

5.2.1. Test site

The experimental data acquisition was carried out on the watershed of La Tejería (N42º44'10.6'' and W1º56'57.2'') in Navarre (Spain) (Casalí et al., 2008). The climate is humid sub-Mediterranean with a mean annual temperature of 13 ºC and an average annual precipitation of ~700 mm. Soils have a silty-clay texture and are relatively shallow (0.5-1.0 m deep). Ten agricultural fields were studied with an area ranging between 3 and 7.3 ha.

Soil preparation operations were performed sequentially during September and October 2004 for cultivating winter cereal. Five different tillage treatments were observed from September to December 2004 (Table 5.1): Mouldboard Plough (MP), Harrowed Rough (HR), Harrowed Smooth (HS), Planted (P) and Planted Compacted (PC).

Table 5.1. Roughness classes corresponding to each field and measurement date. Four 5-m long roughness profiles were acquired per field

Field ID.	22/09/2004	08/10/2004	24/10/2004	17/12/2004
188	HR	HR	-	P
189	HR	HR	HS	P
193	HR	HR	P	P
194	-	HR	HR	P
199	MP	MP	MP	P
201	HS	HS	-	P
208	MP	-	-	PC
235	HS	HS	P	P
255	HS	HS	-	P
258	HR	-	-	P

- Fields not monitored on that particular day

5.2.2. Surface roughness data

Surface roughness was measured using a 5-m long laser profile meter with a resolution of 5 mm and a vertical accuracy of 1.25 mm (Martinez-Agirre et al., 2016). On each monitored field four 5-m long profiles were measured per date (except for field 208 in 22/09/2004) spatially distributed throughout the field and in parallel to the tillage direction. Each acquired profile was subdivided into five 1-m long profiles, and these were detrended using a linear function to subtract the terrain slope. Thus, twenty 1-m long profiles (i.e., independent samples) were obtained per field, making a total of 635 1-m long profiles.

Two standard surface roughness parameters were analyzed: the standard deviation of surface heights (s) and the correlation length (l) obtained considering an exponential autocorrelation function [2]. Further details on the processing of profiles and roughness parameters are available in (Martinez-Agirre et al., 2016).

5.2.3. Soil moisture data

Soil moisture (SM) was measured using a commercial Time Domain Reflectometry (TDR) instrument. On each field, five spatially distributed measurement locations were monitored per date. Soil samples were used to calibrate the TDR probe. Also, TOPLATS (Famigliatti and Wood, 1994) modelled SM values were used for 4 satellite acquisition dates (Table 5.2) in which the TDR measurements were not available.

Table 5.2. Summary of SAR data

Date	SAR data	θ_{LOC} (º)*	Pass	Fields	Roughness	SM data
22/09/2004	ENVISAT/ASAR	7.2-16.2	Descending	9	Profilometer	TDR
08/10/2004	ENVISAT/ASAR	11.6-20.9	Descending	8	Profilometer	TDR
11/10/2004	ENVISAT/ASAR	20.9-31.4	Ascending	8	=	TOPLATS
24/10/2004	ENVISAT/ASAR	15.7-24.9	Descending	5	Profilometer	TDR
27/10/2004	ENVISAT/ASAR	16.9-27.2	Ascending	5	=	TOPLATS
17/12/2004	ENVISAT/ASAR	11.6-20.9	Descending	10	Profilometer	TDR
20/12/2004	ENVISAT/ASAR	20.8-31.2	Ascending	10	=	TOPLATS
02/01/2005	ENVISAT/ASAR	15.8-24.5	Descending	10	=	TDR
05/01/2005	ENVISAT/ASAR	16.8-26.9	Ascending	10	=	TDR
24/01/2005	ENVISAT/ASAR	20.9-31.3	Ascending	10	=	TOPLATS

*Local incidence angle

5.2.4. SAR data

Ten ENVISAT/ASAR scenes were acquired over La Tejería watershed during the study period (Table 5.2). Scenes were acquired as VV Single-Pol Image Mode Precision Image products in swath IS2 (except for 22/09/2004 that was HH-VV Alternate Pol in IS1), half of them in ascending pass and the other half in descending. In all cases, the resolution was 30 m x 30 m. Scenes were: (1) orthorectified (with an error < 1 pixel), (2) calibrated (using the local incidence angle) and (3) speckle-filtered (Gamma MAP filter with a window of 5x5). Mean backscatter coefficient values σ^0 were calculated for each field per date.

5.2.5. Data analysis

The analysis presented here focused on the influence of sample size on the characterization of surface roughness for SAR applications. For this, an increasing number of 1-m long roughness profiles (from 1 to 20) was considered for each field, and the following analyses were carried out: (1) assessment of the behavior of roughness parameters, (2) evaluation of the correlation between normalized σ^0 with roughness parameters and (3) evaluation of the goodness-of-fit of different backscatter models.

The behavior of roughness parameters was evaluated by comparing the average and standard deviation of *s* and *l* per class as computed considering an increasing sample size (i.e. number of profiles). For the correlation analysis, field average σ^0 values were normalized for incidence angle and soil moisture variations, so as to remove the

influence of factors other than surface roughness on σ^0 values (Martinez-Agirre et al., 2017a). Further details on the normalization can be found in (Martinez-Agirre et al., 2017a). The Spearman R coefficient was computed between the σ^0_{norm} (normalized σ^0) series and field average *s* and *l* values as computed considering an increasing sample size. Finally, the goodness-of-fit of three backscatter models was evaluated by computing the RMSE between observed σ^0 values and simulated ones, the latter were obtained using field average *s* and *l* values for an increasing sample size. Due to their different nature and validity range, three backscatter models were considered: the physically-based Integral Equation Model (IEM) (Fung et al., 1992) and Geometrical Optics Model (GOM) (Ulaby et al., 1982) for the smooth (P and PC) and rough classes (MP, HR and HS), respectively; and the semi-empirical Oh model (Oh et al., 1992) that was applicable to all classes.

5.3. Results

5.3.1. Behavior of roughness parameters

Mean *s* values did not change significantly for increasing sample sizes, except for some minor variations when only 1-4 profiles were used (Fig. 5.1). However, class variability decreased as the sample size increased, stabilizing for a certain sample size that depended on the particular roughness class. The behavior of *l* was rather different (Fig. 5.1), with strongly variable mean values for small sample sizes, which only stabilized after 10 profiles. In this case the reduction of class variability with sample size was slower than in *s*, being still high for the largest sample sizes analyzed.

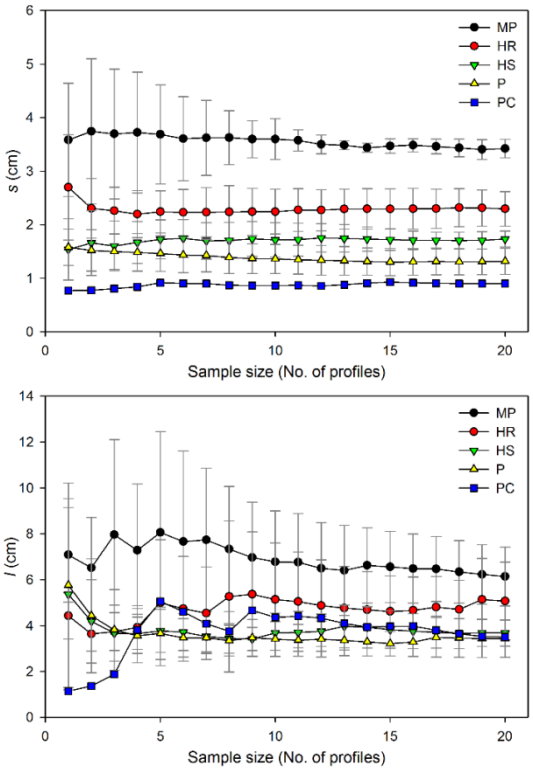

Fig. 5.1. Mean values of s (top) and l (bottom) and their standard deviation (error bars) for the different roughness classes depending on the sample size.

Increasing sample sizes resulted in more clustered roughness classes in the *s*–*l* space and also in an increase in the correlation between *s* and *l* (results not shown). With twenty profiles, a correlation of R=0.640 was obtained for the linear function *l=1.89+1.29s* being similar to that found in (Davidson et al., 2003) in comparable conditions.

5.3.2. Roughness correlation with backscatter

The correlation of σ^0_{norm} with both roughness parameters for all the sample sizes investigated is presented in Fig. 5.2. Parameter *s* showed a steady increase of R as sample size increased, reaching values of ~0.6 when the number of profiles was larger than 12. Parameter *l* presented a very low correlation with σ^0_{norm} (R~0.1) when the sample size was smaller than 8 profiles. When the number of profiles ranged between

8 and 15, it showed a constant increase of correlation, and for greater sample sizes correlation stabilized at R~0.4. Small sample sizes lead to a higher class variability, in particular for *l* and for the planted (P) roughness class, and this was the main cause for R to drop. When a higher number of samples were used, fields were better clustered around the class-mean leading to higher R values.

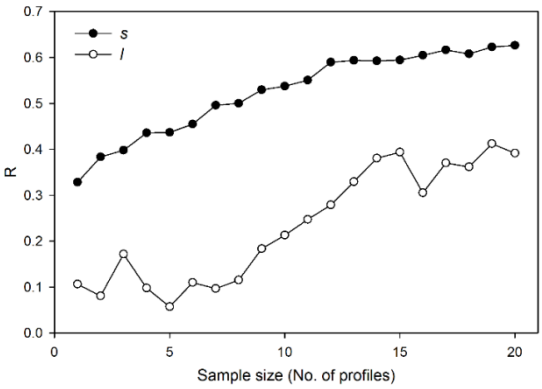

Fig. 5.2. Spearman correlation coefficient (R) between $\boldsymbol{\sigma^0_{norm}}$ and the roughness parameters s and l depending on sample size.

5.3.3. Backscatter modeling

The goodness-of-fit of physically based models (IEM and GOM) improved as the sample size increased (Fig. 5.3a, Fig. 5.4a-c). The improvements were clear when using the GOM for rough classes (MP, HR and HS), with RMSE reductions of ~1.5 dB when passing from 1-5 profiles to 15-20 profiles. Similar RMSE reductions were obtained when applying the IEM to planted fields (P class). In this case RMSE values passed form >4 dB for 1-5 profiles to ~3 dB for 15-20 profiles. On the contrary, the class PC had very stable RMSE values (~2.75 dB), independent of the sample size considered. Considering all the classes, an RMSE of ~2.5 dB was obtained in the best case (Fig. 5.4c), with the largest residuals corresponding to class P. The best RMSE values achieved per class (Fig. 5.3a) were still high, with values of 2-2.75 dB, except for class HS with ~1 dB. These values are too high for a viable retrieval of SM from SAR observations.

The semi-empirical Oh model also showed a mostly decreasing RMSE trend for increasing sample sizes (Fig. 5.3b, Fig. 5.4d-f). However, this decreasing trend was

much weaker (Fig. 5.4d-f) with an overall RMSE reduction of only 0.078 dB when passing from 5 to 20 samples. The decreasing trend was different for each of the classes (Fig. 5.3b). For MP, HR and P the RMSE values (1.2-1.5 dB) were very stable and almost independent of the sample size. Conversely, decreasing RMSE values were observed for HS and PC with some stabilization for sample sizes above 5 profiles for PC (~2 dB) and 12 profiles for HS (~1 dB). The Oh model achieved significantly lower RMSE values than the GOM and IEM, with largest residuals (~1-2 dB) obtained at both the lowest and highest ends (Fig. 5.4f), where σ^0 values were underestimated for some rough and smooth fields, respectively. From the analysis, the Oh model seemed to be less sensitive to the different sample sizes.

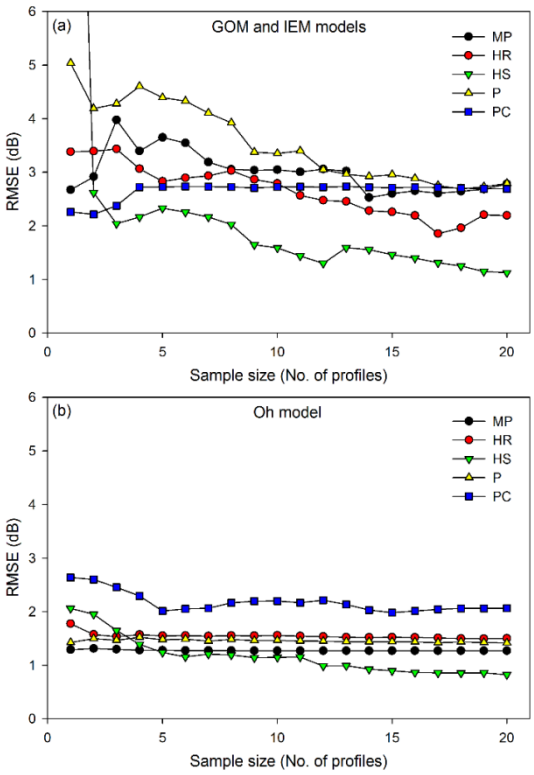

Fig. 5.3. Roughness class Root Mean Square Error (RMSE) between simulated and observed field backscatter values depending on sample size: (a) GOM model for classes MP, HR and HS and IEM model for classes P and PC, and (b) Oh model.

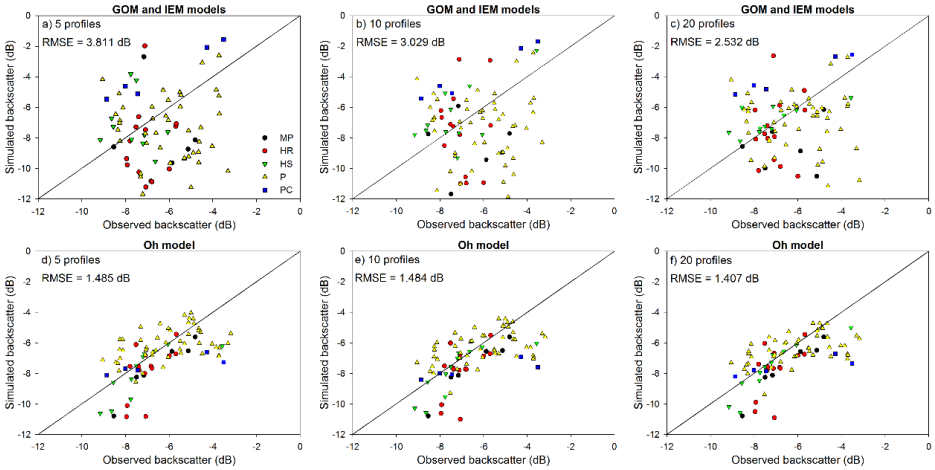

Fig. 5.4. Goodness-of-fit between simulated and observed backscatter coefficients per field for different roughness sample sizes with GOM model for classes MP, HR and HS and IEM model for classes P and PC, and Oh model.

5.4. Discussion and conclusions

The results obtained illustrate a different behavior of the two classical roughness parameters, *s* and *l* (Fig. 5.1). On the one hand, *s* was rather insensitive to the influence of sample size, with quite stable class means, although, as expected, its variability decreased as the sample size increased. A minimum of 10-15 profiles can be considered sufficient for an accurate determination of *s*. On the other hand, class mean *l* values varied more strongly for low sample sizes, and even if its variability also decreased for increasing sample sizes, it was still much higher than that of *s.* In this case, depending on the particular roughness class a sample of 20 profiles might still be insufficient for estimating *l* with the required accuracy. Similarly, Baghdadi et al. (2008a) found that averaging ten profiles (1-m long), resulted in quite accurate *s* estimates (~10% error) but much more variable *l* estimates (~20% error). For larger sample sizes a significant correlation between s and l was observed, similar to (Davidson et al., 2003). The existence of an *l=f(s)* dependence could be used to reduce the number of unknown roughness parameters, which can be important for ill-posed algorithm inversion problems.

The correlation analysis (Fig. 5.2) revealed a clear sensitivity of backscatter to surface roughness, and in particular s, similar to (Zribi et al., 2016). However, when the number of profiles was insufficient for accurately determining the field mean roughness parameters, R values dropped significantly. On the contrary, for sample sizes >15 profiles R values were as high as 0.6 for *s* and ~0.35 for *l*. As the number of samples increased class variability decreased, leading to better clustered field means that positively correlated with backscatter.

Similar results were obtained when applying the backscatter models (Fig. 5.3, Fig. 5.4), with enhanced model precision for larger sample sizes. However, this analysis highlighted the influence of *l* on the physically-based IEM and GOM models. IEM and GOM results were poorer than those obtained with the semi-empirical Oh model, due to the higher uncertainly of *l*. This could be explained by the larger number of samples required for an accurate estimation of *l*, which caused larger errors in IEM and GOM simulations for a given number of profiles than in Oh model.

To conclude, the results obtained evidence the existing relation between C-band SAR backscatter and soil surface roughness for roughness scales shorter than 1 m, as long as a sufficient number of samples is used to accurately characterize roughness. Due to the large spatial variability of roughness parameters a minimum of 10 samples was required for *s* and a value even larger than 20 might be required for *l*. The lower variability of *s* caused a better fit of the semi-empirical Oh model than the physically-based IEM and GOM, which were affected by the higher variability of *l*. Altogether, the relatively small errors obtained with the Oh model (between 1-1.5 dB in most cases) recommend its use for the retrieval of soil moisture, as long as a minimum of 10-15 1-m long roughness profiles are available per field.

Acknowledgments

The authors are grateful to the Spanish Ministry of Economy and Competitiveness for partly funding this research through scholarship BES-2012-054521 and projects CGL2011-24336, CGL2015-64284-C2-1-R and CGL2016-75217-R (MINECO/FEDER, EU). Hans Lievens is a postdoctoral research fellow of the Research Foundation

Flanders (FWO). The authors thank V.R.N. Pauwels for his collaboration for modelling field soil moisture values with TOPLATS.

upna
Universidad Pública de Navarra
Nafarroako Unibertsitate Publikoa

CHAPTER 6

EVALUATION OF SURFACE ROUGHNESS MEASUREMENT TECHNIQUES

Published in: Martinez-Agirre, A., Álvarez-Mozos, J., Milenkovic, M., Pfeifer, N., Giménez, R., Valle Melón, J.M., Rodríguez Miranda, A., 2017. Evaluation of Terrestrial Laser Scanner and Structure from Motion techniques for quantifying soil surface roughness parameters over agricultural soils. ISPRS Journal of Photogrammetry and Remote Sensing. Under Review.

Abstract

Soil surface roughness on agricultural soils is mainly related to the type of tillage performed, typically consisting of an oriented and a random component. Traditionally, soil surface roughness characterization has been difficult, due to its high spatial variability and the sensitivity of roughness parameters to the instruments characteristics, including its measurement scale. Recent advances in surveying have improved spectacularly the resolution, extent and availability of surface elevation datasets. The objective of this paper is to evaluate Terrestrial Laser Scanner (TLS) and Structure from Motion (SfM) techniques, so as to assess their accuracy and suitability for quantifying surface roughness over different agricultural soils. With this aim, an experiment was carried out in three plots (5 x 5 meters) representing different roughness conditions, where TLS and SfM measurements were co-registered with 2D profiles obtained using a laser profilometer. Differences between techniques were evaluated visually and quantitatively using regression analysis and comparing the values of different roughness parameters. TLS and SfM measurements were further compared by evaluating multi-directional roughness parameters behavior and by Digital Elevation Models subtraction. The results obtained demonstrate the ability of both TLS and SfM techniques to measure surface roughness over agricultural soils. However, both techniques (especially SfM) showed a loss of high frequency elevation information that affected the values of some parameters. Altogether, both TLS and SfM provide very powerful 3D information that enables a detailed analysis of surface roughness directionality, which is very relevant for different applications such as those focused in hydrological and soil erosion processes or microwave scattering.

Keywords: soil surface roughness, TLS, SfM, roughness parameters, agricultural soils

6.1. Introduction

Soil Surface Roughness (SSR, also referred to as micro-topography or micro-relief) can be defined as the variation in soil surface elevation at scales smaller than the resolution of typical topographic surveys or Digital Elevation Models (DEMs) (Govers et al., 2000). In agricultural soils, SSR is mainly an anthropic factor determined by the type of tillage and management, typically with an oriented component consisting of pseudo-periodical height variations due to tillage implements and a random component representing soil clods or aggregates. In agricultural soils, SSR is a property with a high spatial variability, since the same type of tillage can result in surfaces with different SSR depending on the physical characteristics of the soil and atmospheric conditions.

SSR is a key element in hydrology and soil erosion processes occurring at the soil-atmosphere interface (Helming et al., 1998), such as infiltration, runoff, the detachment of soil due to water or wind, gas exchange, evaporation and heat fluxes (Huang and Bradford, 1992). Therefore, its knowledge can be useful for understanding and modelling processes relevant for different applications. However, the parameterization of the SSR is not straightforward because of the many different tillage tools that exist, which cause a particular type of micro-relief under identical soil conditions. Furthermore, considering the wide range of possible soil conditions, a huge variety of roughness types could be found in agricultural soils (Martinez-Agirre et al., 2016).

Many different parameters and indices have been proposed for quantifying SSR (e.g. Helming et al., 1993; Magunda et al., 1997; Kamphorst et al., 2000; Taconet and Ciarletti, 2007; Vermang et al., 2013). These can be divided into four groups, following a criterion similar to that of Smith (2014): (1) parameters measuring the vertical dimension of roughness, (2) parameters measuring the horizontal dimension of roughness, (3) parameters combining both dimensions, and (4) parameters based on fractal theory (Martinez-Agirre et al., 2016). The first ones measure the magnitude of elevation differences along a transect or area. On the other hand, horizontal parameters evaluate the spacing at which these elevation differences occur. Combined parameters represent both properties, since they are normally obtained as the product or ratio of a vertical and a horizontal parameter. Finally, fractal parameters

measure the self-affinity of surfaces transect or areas, i.e., whether similar statistical properties can be obtained at different spatial scales along the surface. Although the number of parameters found in the literature is high, many of them measure similar properties and are thus strongly correlated (Martinez-Agirre et al., 2016). Depending on the particular application of interest some parameters have been preferred to others, being the standard deviation of heights (s), also referred to as RMSE of height (when their mean is zero), the most commonly used one.

Recent advances in surveying have improved spectacularly the resolution, extent and availability of surface elevation datasets (Smith, 2014). Surface roughness measurement techniques can be classified according to different criteria: the dimensionality of measure (2D/3D), precision (mm/cm), sensor type, and whether the measure is done with contact to the soil surface or not (Jester and Klik, 2005; Gilliot et al., 2017). However, most of the literature in the topic centered the classification into contact and non-contact techniques (Govers et al., 2000; Verhoest et al., 2008, Aguilar et al., 2009; Thomsen et al., 2015; Nouwakpo et al., 2016). Regarding to this, non-contact devices are preferred because the physical contact between an instrument and the soil surface is associated with measurement biases and disturbances (Jester and Klik, 2005). Laser scanners and image based 3D reconstruction technologies are non-destructive and have been the most commonly used technologies for non-contact micro-topography measurements (Barneveld et al., 2013, Nouwakpo et al., 2016).

Image-based 3D reconstruction technologies can be divided into traditional stereo-photogrammetry and Structure from Motion photogrammetry (SfM) (Nouwakpo et al., 2016). Traditional photogrammetric techniques required specific and expensive cameras, precise camera calibration, and imposed geometric constrains while acquiring photographs (Gilliot et al., 2017). In contrast, SfM relaxes some of these constrains, making image acquisition and processing significantly faster and easier (Castillo et al., 2012; James and Robson, 2012; Woodget et al., 2015; Gomez et al., 2015; Mosbrucker et al., 2017). Nowadays, the interest of scientists across different disciplines of geosciences in this technology as a surface reconstruction tool has expanded since the development of readily available SfM software (Nouwakpo et al., 2016).

Laser-based technologies also known as light detection and ranging (LiDAR) have been used for high resolution soil micro-topography measurements (Perez-Gutierrez et al., 2007; Aguilar et al., 2009; Castillo et al., 2012; Milenkovic et al., 2015; Nouwakpo et al., 2016). Specifically, Terrestrial Laser Scanner (TLS) technique presents accuracies within a range of 0.1-0.5 mm and 0.1-2 mm for vertical and horizontal measurements, respectively (Aguilar et al., 2009). Although, TLS's high hardware acquisition cost and bulky size have limited its widespread use for field measurement campaigns (Nouwakpo et al., 2016), technical improvements in sensor design may improve this in the near future. In the recent years different authors have studied the suitability of TLS for SSR characterization in agricultural soils (e.g. Milenkovic et al, 2015; Thomsen et al., 2015; Rodríguez-Caballero et al., 2016). Yet, the large variety of SSR conditions in agricultural soils recommends further studies.

Although some studies have already attempted to measure SSR with different techniques, there is still a need for further research comparing the accuracy and adequacy of recently developed 3D measuring techniques with conventional ones, in particular on agricultural soils with contrasting roughness conditions. The laser profilometer is a traditionally used technique as a high-resolution non-contact alternative to mechanical profiles (Mattia et al., 2003). Therefore, in this study terrestrial laser scanner (TLS) and Structure from Motion (SfM) 3D measurements were evaluated and compared with laser profilometer 2D measurements obtained on three experimental plots tilled with different tillage implements. The objective of this work was thus to evaluate TLS and SfM techniques, and to assess their accuracy and suitability for quantifying surface roughness in different agricultural soils. With this aim, an experiment was carried out where TLS and SfM surveys were precisely co-registered with 2D profiles obtained using a laser profilometer. Differences between techniques were evaluated visually and analytically using regression analysis, and next by comparing the values of a number of roughness parameters obtained with the techniques evaluated. Then, DEMs obtained with TLS and SfM were compared to detect areas and surface features were a mismatch existed between techniques. Finally, polar plots showing multi-directional roughness parameters were computed and compared between TLS and SfM.

6.2. Materials and methods

6.2.1. Study area

This study was conducted in the experimental fields at the School of Agricultural Engineers of the Public University of Navarre in Pamplona (Navarre, Spain) (42.79º N, 1.63º W). The climate is humid sub-Mediterranean with a mean annual temperature of ~13 ºC and an average annual precipitation of ~675 mm distributed over 95 days. The experimental field is almost horizontal (slope < 2%) and soils have a silty-clay-loam texture (13.7% sand, 48.3% silt and 38% clay).

Three experimental plots (5x5 meters) were created using different tillage implements, so as to represent different surface roughness conditions typical of agricultural soils (Fig. 6.1): Plot 1 corresponds to high roughness conditions (Mouldboard Plough), Plot 2 to medium roughness (Chisel), and Plot 3 to low roughness (Mouldboard Plough + Harrowed Compacted). Mouldboard Plough (MP) is a primary tillage operation performed with a plough with multiple mouldboards (15-20 cm depth) that break and turn over the soil, resulting in very rough surface. Chisel (CH) is also a primary tillage operation that breaks and shatters the soil leaving it rough with residue on the surface, yet not as rough as MP. Mouldboard Plough + Harrowed Compacted (HC) consists of a MP operation followed by a secondary operation using a spike harrow and a compacting roller, leading to a smooth soil.

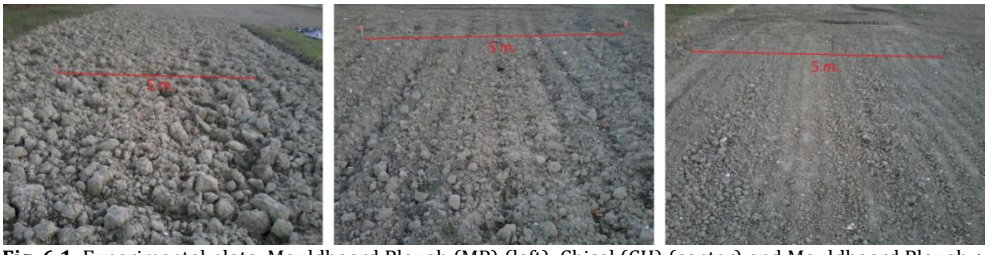

Fig. 6.1. Experimental plots: Mouldboard Plough (MP) (left), Chisel (CH) (center) and Mouldboard Plough + Harrowed Compacted (HC) (right).

6.2.2. Experimental protocol

The data collection was carried out on three days, November 25-27 2013, where no precipitation was recorded. Profilometer measurements (Fig. 6.2) were performed on

November 25 afternoon in plot 2 (CH), and on November 26 afternoon in plot 3 (HC) and plot 1 (MP). On each plot eight profiles were measured, four in parallel to the tillage direction and four in perpendicular. The beginning and end points of each profile were marked with nails and referenced using a total station. The acquisition of photographs for SfM technique was done on November 26 afternoon, so as to avoid the influence of shadows. Twenty four photographs were taken per plot from different points of view using a lifting platform (Fig. 6.2). Eight surveying targets were spatially distributed around the experimental plots for referencing the data. Finally, TLS measurements (Fig. 6.2) were carried out on November 27 morning. Four scans were measured per plot (i.e., one from each side) which were co-registered using five reference spheres deployed around the plots.

Fig. 6.2. Measurement techniques: Laser profilometer (left), Structure for Motion (center) and Terrestrial Laser Scanner (right).

6.2.3. Measuring techniques

Data collection was performed using three different measurement techniques (Fig. 6.2). On the one hand, 2D measurements were performed using a laser profilometer, and on the other hand, 3D measurements were performed using Terrestrial Laser Scanner (TLS) and Structure from Motion (SfM) photogrammetric technique. A description of the three techniques is given below.

6.2.3.1. Laser profilometer

Profiles were taken with a laser profilometer (see Fig. 6.2) designed specifically for measuring roughness (Álvarez-Mozos et al., 2009). The device consists of a laser distance meter located inside a case that moves along an aluminum bar (fixed with two tripods) propelled by a small electric motor. The profilometer measures the vertical distance to the soil surface using a 3 mm wide laser beam with an accuracy of

1.25 mm and a sampling interval of 5 mm. For each experimental plot 8 profiles (4 in parallel to the tillage direction and 4 in perpendicular) were measured with the laser profilometer, making a total of 24 profiles.

Profilometer data pre-processing was carried out following three steps: (1) aluminum bar buckling effect correction using a parabolic function, (2) outlier filtering by deleting and interpolating records larger than a threshold (i.e. 2 cm) with the previous and following records, and (3) terrain slope correction (i.e., profile detrending) subtracting the linear trend observed in the data, if any.

6.2.3.2. Terrestrial Laser Scanning (TLS)

Terrestrial laser scanners (TLS) utilize the light detection and ranging (LiDAR) technique to capture precise and detailed geometric information (point clouds) about natural and artificial objects (Milenkovic et al., 2015). The TLS used in this study was the FARO Focus 3D (see Fig. 6.2). The scans were obtained from tripod ~1.75 m high. The TLS has a specific ranging precision of 0.3 mm (90% reflectivity) and a small beam divergence of 0.16 mrad (0.009º), with a beam diameter of 3.8 mm. The scan vertical and horizontal resolution was set in 0.0018º (20480 3D pixel in 360º), so for a range distance of 6 meters (maximum distance in our measurements) the sampling interval was about 1.8 mm. For each of the three experimental plots four scans (i.e. one from each side of the plot) were measured.

For TLS data processing, raw scans were first filtered to exclude mixed pixels measurements, and then, co-registered and merged into a single point cloud. The filtering of mixed-pixels measurements was performed using a self-implemented algorithm as the existing predefined filters in the manufacturer software did not provide satisfying results for our data. The co-registration of individual TLS scans was done globally and using the ICP (iterative closest point) algorithm implemented in the OPALS software (Otepka et al., 2013; Pfeifer et al., 2014). This ICP algorithm minimizes point-to-plane distances between the corresponding points (Glira et al., 2015), and the standard deviation, based on more than 5000 such residuals, was about 1.1 mm for the CH and HC plots. For the MP plot, the standard deviation was slightly higher, i.e. 2.5 mm. Finally, for each 5x5 meters experimental plot ~30 million

point cloud was obtained by merging the individual co-registered TLS scans per plot (see details in Table 6.1).

Table 6.1. Details of the data after pre-processing.

Plot	Measurement technique	Nº of sampling locations	Nº of readings
MP	Profilometer (PRO)	08	~ 8.000 points
MP	Terrestrial Laser Scanner (TLS)	04	30.447.219 points
MP	Structure from Motion (SfM)	24	17.303.166 points
CH	Profilometer (PRO)	08	~ 8.000 points
CH	Terrestrial Laser Scanner (TLS)	04	26.513.592 points
CH	Structure from Motion (SfM)	24	13.507.994 points
HC	Profilometer (PRO)	08	~ 8.000 points
HC	Terrestrial Laser Scanner (TLS)	04	31.964.773 points
HC	Structure from Motion (SfM)	24	11.548.505 points

6.2.3.3. Structure from Motion (SfM)

Structure from Motion (SfM) technology was based on a set of overlapping photographs acquired from different points of view using a high quality digital camera, which are processed automatically to determine the scene geometry and camera parameters (Favally et al., 2012; Gilliot et al., 2017). For each plot 24 photos of 20 megapixels were acquired with a Canon EOS 5D Mark II camera with a 21 mm objective. Photos were homogenously distributed and obtained from a height of ~8 meters above ground (using a lifting platform) capturing the entire experimental plot from each photo (see Fig. 6.2).

For SfM data processing, eight control points were measured with a total station and used for referencing the photos, obtaining a mean error lower than 2 mm for each plot (1.9 mm for MP class, 1.6 mm for CH and 1.1 for HC). The dense point cloud generation was done in "ultra-high quality" mode using the software Agisoft Photoscan. After this process, final point clouds were obtained with an average point spacing of ~1.7 mm corresponding to a minimum of 10 million points for each experimental plot (see details in Table 6.1).

6.2.4. Roughness parameters

In total, six roughness parameters were analyzed (Table 6.2). These parameters were selected after a previous analysis (Martinez-Agirre et al., 2016), where their correlation and their ability to discriminate different tillage classes were assessed.

Table 6.2. Summary of roughness parameters analyzed.

Parameter	Description	Reference
s (cm)	Standard deviation of the heights	Allmaras et al., 1966
l (cm)	Correlation length	Ulaby et al., 1982
ρ'(0)	Initial slope of the auto-correlation function	Ulaby et al., 1982
F (cm⁻¹)	Peak frequency	Römkens and Wang, 1986
T_S	Tortuosity	Saleh et al., 1993
D	Fractal dimension	Vidal Vázquez et al., 2005

The standard deviation of heights (s) is a descriptor of the vertical roughness component:

$$s = \sqrt{\frac{\sum_{i=1}^{N}(z_i{}^2 - \bar{z}^2)}{N-1}} \tag{6.1}$$

where N is the number of the records registered in the profile, z_i is the height corresponding to record i, and $\bar{z}$ is the mean height of all the records. The correlation length (l) represents the horizontal component of roughness and is defined as the distance at which the heights of two points on the surface are considered independent. The correlation length is obtained from the autocorrelation function (Ulaby et al., 1982):

$$\rho(h) = \frac{\sum_{i=1}^{N(h)} z_i z_{i+h}}{\sum_{i=1}^{N} z_i{}^2} \tag{6.2}$$

where $\rho(h)$ is the autocorrelation function, representing the correlation existing between height of the point i (z_i) and that of another point located at a lag distance h from it (z_{i+h}), and $N(h)$ is the number of pairs considered in each lag h. The correlation length (l) is then defined as the distance at which the heights of two points on the profile are considered independent; i.e., $\rho(h)$ is equal to $1/e$, so that $\rho(l) = 1/e$. The initial slope of the autocorrelation function ($\rho'(0)$) characterizes the horizontal component of roughness focusing on the height variations of a point with its nearest neighbors. The peak frequency (F) describes the horizontal component of roughness

as the number of peaks (i.e., points with higher elevations than their neighbours on both sides) per unit length of the profile (Römkens and Wang, 1986). The tortuosity index of Saleh (T_S) is the ratio of the perimeter length of a profile (L_1) and its projected distance on a horizontal surface taken as reference (L_0) (Saleh et al., 1993):

$$T_S = 100 \cdot \frac{(L_1 - L_0)}{L_1} \quad (6.3)$$

Finally, the fractal dimension (D), obtained by the semivariogram method, represents the self-affinity of surface roughness profiles (Vidal Vázquez et al., 2005). The semivariogram represents how height data are related to distance. The semivariance function depending on the lag h can be calculated as:

$$\gamma(h) = \frac{1}{2N(h)} \sum_{i=1}^{N(h)} [z_{i+h} - z_i]^2 \quad (6.4)$$

Assuming a fractal Brownian motion (*fBm*) model, the experimental semivariogram can be described as a function of the lag:

$$\gamma(h) = l^{1-H} h^H \quad (6.5)$$

where l is the crossover length and H is the Hurst coefficient. After a log-log transformation, H is estimated as the slope of the semivariance versus the lag distance. Afterwards, the fractal dimension is obtained from the Hurst coefficient as $D = 2 - H$ (Smith, 2014).

6.2.5. Data analysis

The analysis presented here focused on the suitability of different measurement techniques for surface roughness parameterization in agricultural soils. For doing so, data needed to be processed so as to ensure that different measurements were comparable. First, the point clouds (for each experimental plot) obtained with TLS and SfM were co-registered to the same reference system using again IPC algorithm implemented in OPLAS. The standard deviation of the point-to-plane residuals (and based on more than 1000 correspondences) was less than 2 mm for the three plots. Then, profiles were extracted from TLS and SfM point clouds coinciding with the location of the profiles measured with the profilometer. To extract these profiles, all

the points of the cloud closer than 3 mm (comparable to the laser beam size of the profilometer) to the profile centerline were selected. Then, these points were (1) filtered to avoid occlusion, (2) binned at bin intervals of 5 mm and (3) interpolated to avoid empty data.

Next, measurement techniques were compared in two steps. First, a comparison based on 2D roughness (i.e., profiles) data was performed both in parallel and in perpendicular to the tillage direction. This comparison was done following three criteria: (1) visual analysis of the profiles obtained with the different techniques, (2) analytical comparison of the profiles using scatterplots, regression analysis and RMSE estimation; and (3) evaluation in terms of the roughness parameters values extracted from the profiles. Secondly, a 3D roughness analysis was carried out using point clouds obtained with TLS and SfM. Here, two elements were compared: (1) multidirectional roughness parameters values (using four profiles obtained in every 15º azimuth); and (2) DEMs comparison (considering a pixel size of 5 mm).

6.3. Results

6.3.1. Visual analysis

A first visual exploration of the same profiles obtained with the three different measurement techniques reveals interesting details (Fig. 6.3). Although, the analyzed profiles showed generally a very similar behavior, some differences were noticed, particularly in the roughest classes. Both TLS and SfM resulted in smoothed profiles when compared to the profilometer, with SfM yielding the smoothest profile (Fig. 6.3). Both techniques were not able to describe accurately sudden elevation changes (both positive and negative) typical at the edges of soil clods and larger aggregates. In the CH and HC classes the agreements were higher but still some slight differences were observed when height variations occurred at small distances. These differences are expected to affect particularly horizontal roughness parameters, such as the peak frequency (F) or those obtained from the autocorrelation function (l and $\rho'(0)$).

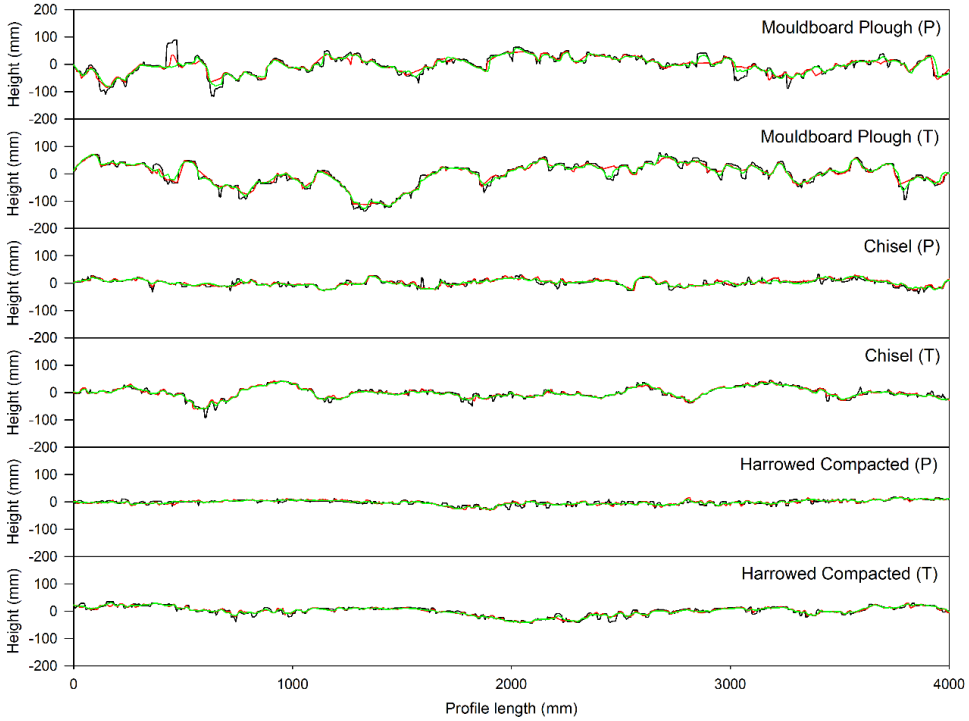

Fig. 6.3. Example profiles of the different roughness classes (Mouldboard Plough (MP), Chisel (CH) and Harrowed Compacted (HC)) in parallel (P) and in perpendicular (T) to the tillage direction with the different measurement techniques analyzed; Laser profilometer (black), Terrestrial Laser Scanner (red) and Structure from Motion photogrammetry (green).

6.3.2. Scatterplot analysis

Scatterplots representing the height of each point of the profiles obtained with the different techniques were represented for each roughness class and direction (parallel and perpendicular to the tillage). For each scatterplot a linear regression was fitted and the agreement between techniques was evaluated by means of the root mean square error (RMSE) and the coefficient of determination (R^2).

In Mouldboard Plough (MP) roughness class (Fig. 6.4) TLS and SfM techniques compared similarly to the profilometer (PRO) in both parallel and perpendicular to the tillage direction. However, they agreed better (higher R^2 and lower RMSE) in perpendicular direction (RMSE ~ 13 mm and R^2 ~ 0.9) than in parallel (RMSE ~ 20 mm and R^2 ~ 0.7). When comparing TLS and SfM, the error decreased and correlation

increased specially in perpendicular direction (R^2 > 0.95). However, in parallel to tillage some outliers appeared in medium-high values of TLS and in medium-low of SfM which could represent interpolated TLS data in shadow regions (occlusions).

In Chisel (CH) roughness class (Fig. 6.5) the errors between TLS and SfM with PRO were lower than in MP class with values of ~ 7 mm in parallel direction and ~ 8 mm in perpendicular. Also, the goodness-of-fit between TLS and SfM techniques was higher with a lower error (RMSE ~ 5 mm) and higher correlation than in MP, especially in perpendicular direction (R^2 ~ 0.95). In this case, the number of outliers was lower than in MP class.

The Harrowed Compacted (HC) roughness class (Fig. 6.6) presented the lowest errors between TLS and SfM with PRO, yielding RMSE values ~ 5 mm in both directions. Also, the values between TLS and SfM presented the best fit with an error ~ 3 mm and high correlation and slope values especially in perpendicular direction (slope and R^2 > 0.95). In this case, the presence of outliers was practically null.

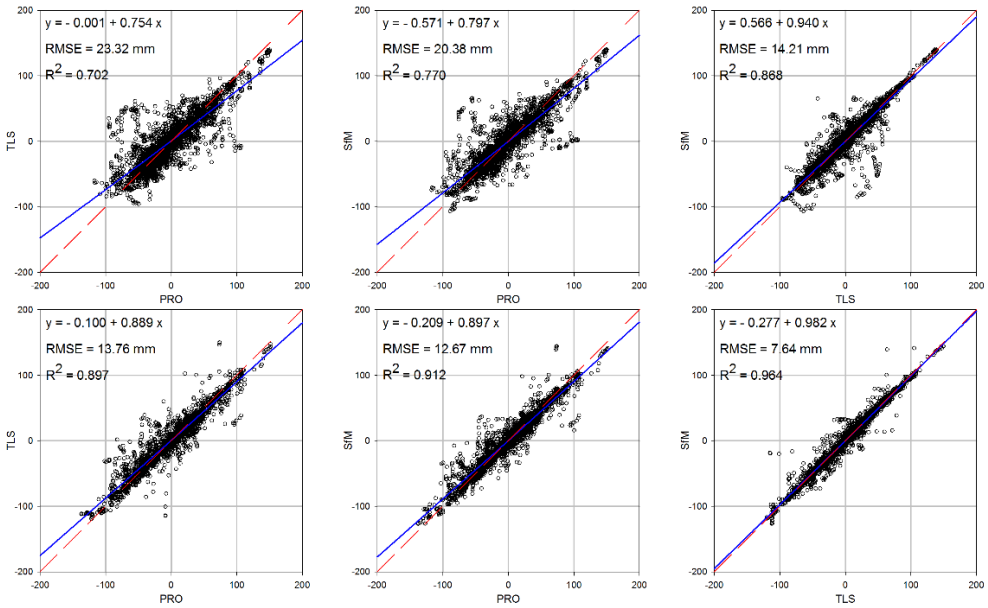

Fig. 6.4. Scatter plot between the different measurement techniques for Mouldboard Plough (MP) class in parallel (top) and in perpendicular (bottom) to the tillage direction.

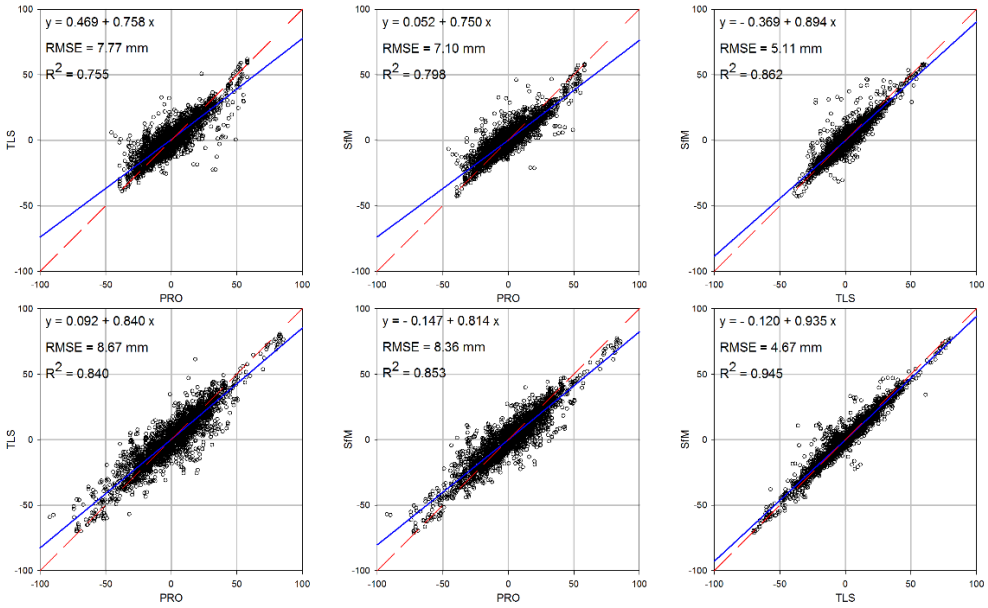

Fig. 6.5. Scatter plot between the different measurement techniques for Chisel (CH) class in parallel (top) and in perpendicular (bottom) to the tillage direction.

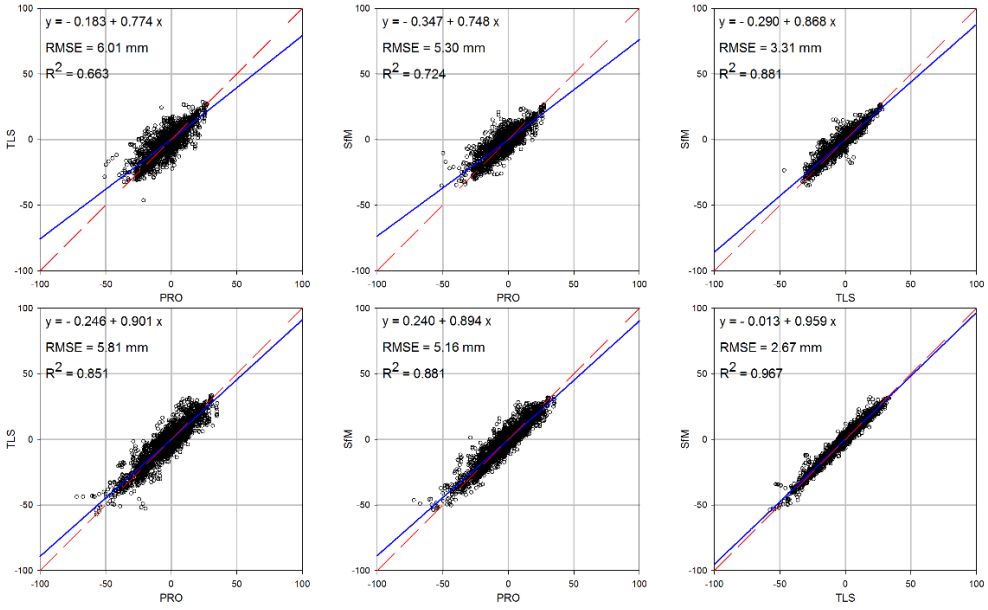

Fig. 6.6. Scatter plot between the different measurement techniques for Harrowed Compacted (HC) class in parallel (top) and in perpendicular (bottom) to the tillage direction.

6.3.3. Roughness parameters analysis

The roughness parameters mean values and standard deviations obtained with the three techniques for each experimental plot and measurement directions are presented in Fig. 6.7. Parameter *s* showed very similar class mean values and standard deviations for the three techniques analyzed. However, PRO presented slightly higher values followed by TLS and SfM. The difference in MP roughness class between TLS and SfM technique was inappreciable. Obviously, MP class presented higher values followed by CH and HC and also the perpendicular direction showed higher values than the parallel one. The correlation length (l) presented a different behavior with lower values (and deviations) for CH class, followed by MP and HC (with higher values and especially larger deviations) and also the perpendicular direction showed higher values than the parallel one. Regarding the different techniques, in general PRO showed the lowest values followed by TLS and SfM. The initial slope of the autocorrelation function ($\rho'(0)$), although being similar to l in concept, presented a very different behavior, with higher values for HC class followed by CH and MP and higher values in parallel than in perpendicular. The differences between the measurement techniques were higher than in any other parameter evaluated with higher values for PRO followed by TLS and SfM.

The tortuosity (T_S) showed higher values for PRO followed by TLS and SfM, and also higher values for MP class followed by CH and HC. However, no remarkable differences were appreciated between parallel and perpendicular directions. The peak frequency (F) took higher values for PRO or TLS depending on the roughness class and lower values for SfM. In general, MP class showed lower values followed by CH and HC (except for PRO technique) and no remarkable differences were observed between parallel and perpendicular directions. The fractal dimension (D) had a similar behavior with higher values for PRO followed by TLS and SfM, lower values for MP roughness class followed by CH and HC, and with no important differences between parallel and perpendicular directions.

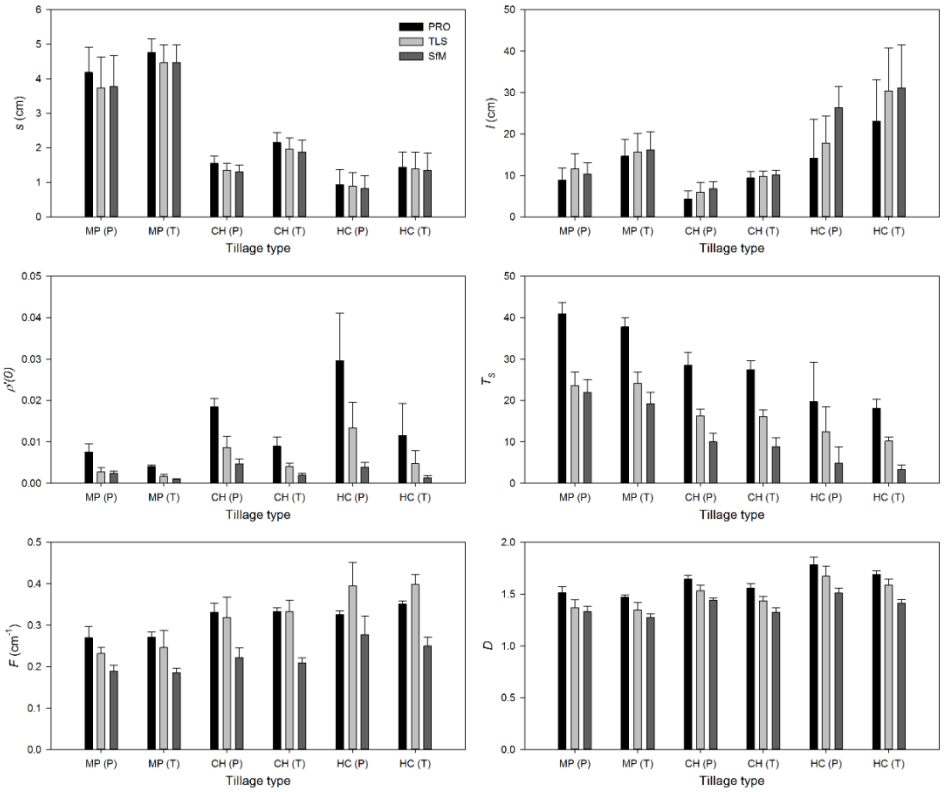

Fig. 6.7. Roughness parameters values for the different measurement techniques and for the different roughness classes analyzed: Mouldboard Plough (MP) in parallel (P) and in perpendicular (T), Chisel (CH) in parallel (P) and in perpendicular (T), and Harrowed Compacted (HC) in parallel (P) and in perpendicular (T).

6.3.4. Multi directional roughness parameter analysis

In order to analyze multidirectional roughness parameters behavior with TLS and SfM techniques, polar plots were used to represent mean values (out of four repetitions) of the roughness parameters. For Mouldboard Plough (MP) roughness class (Fig. 6.8), *s* showed a similar behavior for both techniques (with little exceptions) with higher values at 90º (and 135º) direction. The correlation length (*l*) also presented a similar behavior with both techniques, but no clear directionality was observed. Parameter *ρ'(0)* showed differences between techniques (higher values with TLS) and a notable anisotropic behavior with peak values in 0º direction. On the other hand, tortuosity (T_S) and peak frequency (*F*) presented higher values for TLS technique and no

significant directional behavior. Finally, the fractal dimension (*D*) showed similar values from both techniques and an isotropic behavior.

Regarding Chisel (CH) roughness class (Fig. 6.9), *s* and *l* parameters presented very similar values with both techniques. However, they showed an anisotropic behavior (especially *l*) with low values in 0º direction and higher values in 30º or 105º. Parameter $\rho'(0)$ presented higher values with TLS and a strong anisotropic behavior with higher values in 0º direction. Finally, parameters T_S, *F* and *D* showed clear differences with higher values obtained for TLS (only slight differences in *D*) and no significant directional behavior.

For Harrowed Compacted (HC) roughness class (Fig. 6.10), *s* parameter presented similar values with both techniques and an anisotropic behavior with lower values in 345º, 0º and 15º directions. The parameter *l* showed little differences with higher values for SfM technique (especially in some directions) and a clear anisotropic behavior with lower values in 345º and 0º directions. Parameter $\rho'(0)$ presented clear differences with higher values observed for TLS and a strong directional behavior with highest values in 0º direction. Finally, parameters T_S, *F* and *D* showed large differences with higher values for TLS technique (less differences in *D*) and isotropic behavior (with the exception of tortuosity (T_S) in 0º direction).

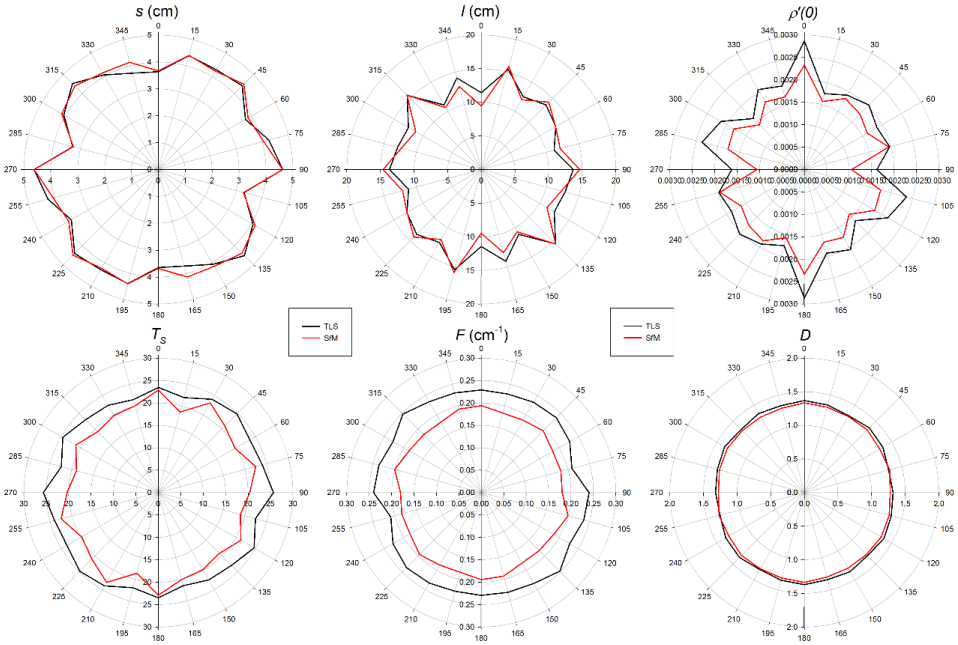

Fig. 6.8. Roughness parameter values from TLS and SfM techniques in MP class.

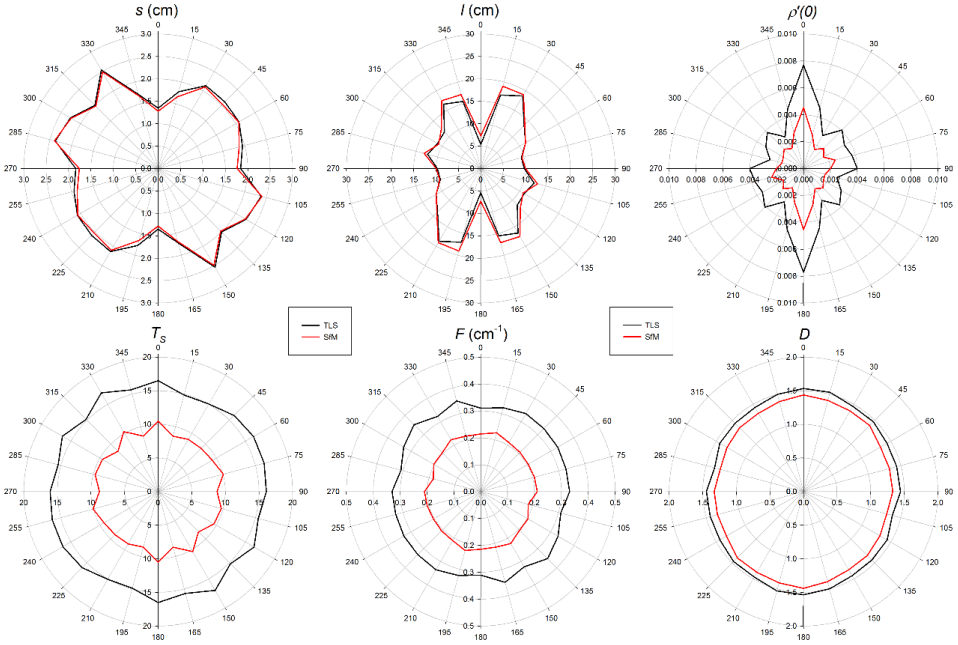

Fig. 6.9. Roughness parameter values from TLS and SfM techniques in CH class.

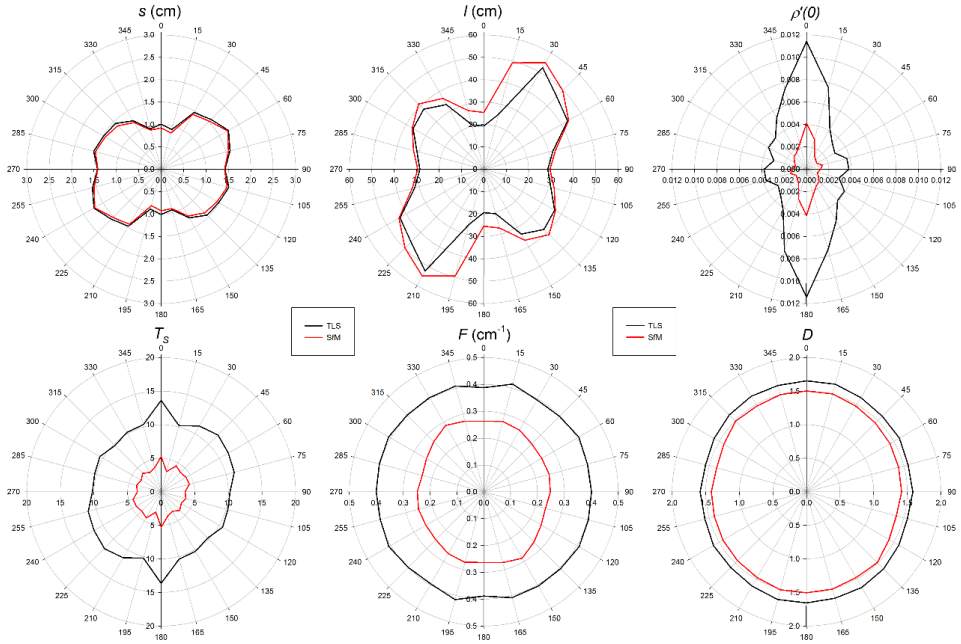

Fig. 6.10. Roughness parameter values from TLS and SfM techniques in HC class.

6.3.5. DEM analysis

The shadowed DEMs obtained with TLS and SfM techniques and their differences are shown in Fig. 6.11. In general, DEMs obtained with TLS seemed to be more detailed than SfM ones. This phenomenon is better appreciated in CH and HC classes where a difference in the higher frequency roughness component is apparent between TLS and SfM.

Regarding the differences between roughness classes, in MP class some dark blue zones (with higher values for TLS) were observed due to interpolated shadow regions for TLS (occlusions). Also little dark red zones (with higher values for SfM) appeared in the lower part of some aggregates because of the smoothening surface behavior of SfM, especially in the border of the plot (due to a higher zenith incidence angle for TLS). In the center of the plot light blue color was predominant (0-5 mm), which could be caused by a higher detailed geometry of the clods (medium and high parts) with TLS, comparing with the surface smoothing behavior with SfM. For CH class, the differences were lower than in MP with just some little red zones (with higher values

for SfM) in the border of the experimental plot caused by the same phenomenon explained for MP class. Finally, the differences observed in HC class were practically null.

It should be noticed that the blue zones appeared in different corners of the three experimental plots were caused by the reference spheres used for the TLS co-registration.

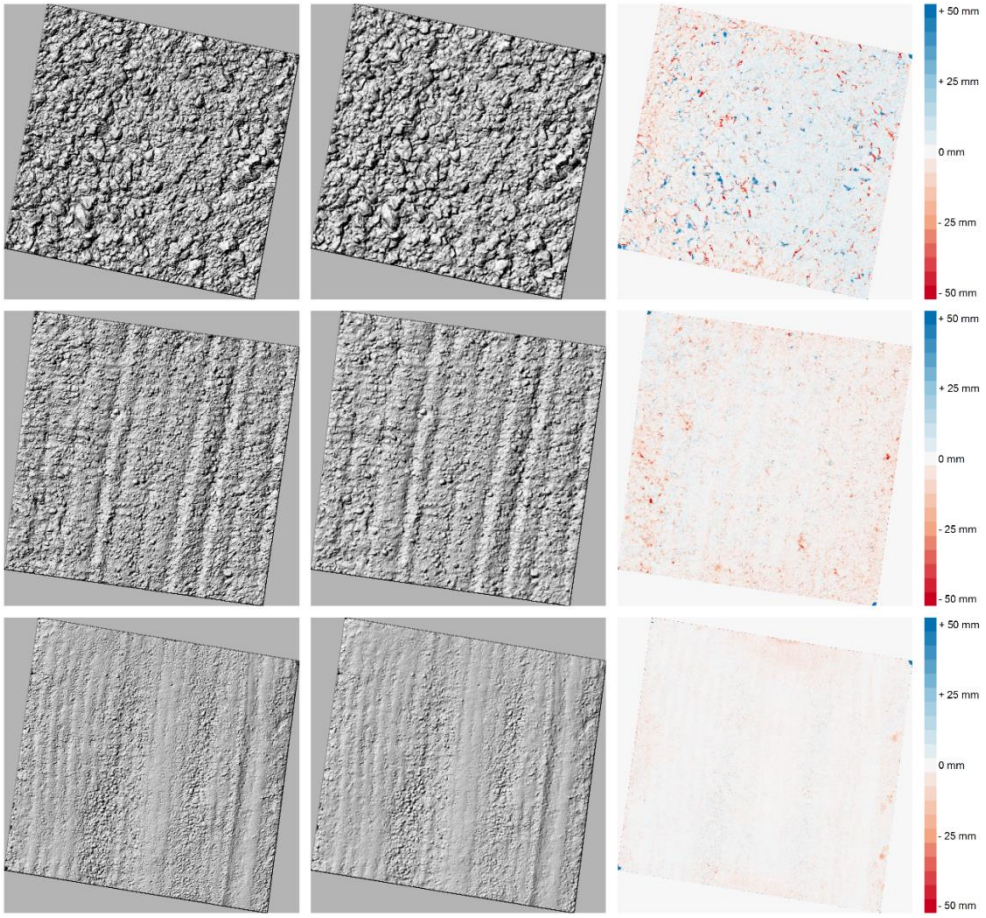

Fig. 6.11. Shadowed 5 mm DEMs obtained using TLS (left) and SfM (center), and their difference (TLS-SfM) (right); for Mouldboard Plough (MP) class (top), Chisel (CH) class (middle) and Harrowed Compacted (HC) class (bottom).

6.4. Discussion

The analysis performed is quite unique since it considers experimental plots with different roughness (i.e., tillage) classes and significantly larger in size than other studies on this topic (e.g. Jester and Klik, 2005; Mirzaei et al., 2012, Marzahn et al., 2012a; Milenkovic et al., 2015; Thomsen et al., 2015, Gilliot el al., 2017), and also because it enables a direct comparison of height profiles obtained with different techniques due to precise co-registration achieved. In this sense, the final point clouds obtained with the TLS and SfM techniques have a very good geometric accuracy. After co-registration, CGP mean errors ranged between 1.1 mm (for HC class) and 1.9 mm (for MP class), these values are comparable to Bretar et al. (2013), Snapir et al. (2014) and Gilliot et al. (2017) who reported errors ~ 1.5 mm. On the other hand, the average distance between the corresponding points among each TLS scan pair was ~ 1 mm (similar to Milenkovic et al., 2015), with the exception of MP (2.5 mm) due to a highly rough terrain that imposed occlusion, and thus, affected the ICP correspondences. Finally, the average distance between point clouds obtained by TLS and SfM techniques was less than 2 mm for all the three plots.

Regarding the bidirectional (parallel and perpendicular to tillage direction) analysis of the different measurement techniques, the visual analysis provided interesting information. The rougher the surface the more evident the smoothing of the profiles obtained by TLS and SfM techniques was with respect to PRO, with SfM yielding the smoothest profiles (Fig. 6.3). An explanation to this phenomenon was addressed by Nouwakpo (Nouwakpo et al., 2016) who affirmed that in SfM technique computed 3D points positions are inherently influenced by loss of detail due to analog to digital conversion in RGB (red, green and blue) value interpolations. This process tends to smooth out irregularities from SfM-derived surfaces. There were also occlusion effects (especially in TLS) due to large aggregates on the soil surface (Heng et al., 2010) that together with TLS incidence angle caused considerable differences in some parts of the profiles, mainly due to interpolated shadow zones. Therefore, the eventual availability of a nadir-looking of TLS acquisition (e.g., installed on a lifting platform or even on board a Remotely Piloted Aerial System) could circumvent this limitation.

Regarding the roughness parameters values obtained with different techniques, the slight differences for parameter *s* observed in the presented work are in agreement

with the harrowed and ploughed surfaces studied in Thomsen et al. (2015). Differences between roughness classes were clear with this parameter, which confirmed the results of different studies where *s* has been proposed for distinguishing different roughness classes (Helming et al., 1993; Magunda et al., 1997; Kamphorst et al., 2000; Vermang et al., 2013; Bauer et al., 2015; Martinez-Agirre et al., 2016). For horizontal parameter *l*, there is no agreement in the literature. Some authors (Davidson et al., 2003; Baghdadi et al., 2008b) reported increasing values for *l* for increasing roughness conditions, while others observed more similar behavior in different roughness classes (Álvarez-Mozos et al., 2005; Verhoest et al., 2008). This parameter has been found to be strongly dependent on the scale of measurement with large values corresponding to larger sampling intervals (Barber et al., 2016) and low frequency roughness components (Martinez-Agirre et al., 2017a). For the rest of the parameters analyzed, the general behavior with SfM and, to a lesser extent, with TLS was the underestimation of the different parameters values when compared to PRO.

In the multi directional analysis, both techniques (TLS and SfM) coincided in the directional behavior of the different roughness parameters analyzed, reveling notable differences in their values as a function of the direction. This phenomenon is especially relevant for $\rho'(0)$, with higher values in parallel to tillage direction and lower values in directions near to the perpendicular, and to a lesser extent for *s* and *l* in CH and HC roughness classes. For these two parameters (especially for *l*), the highest values are obtained in oblique to the tillage direction (15º-75º or 105º-175º), this seems logical in the case of *l*, since the distance between the tillage marks were greater than in perpendicular (90º). This type of information is of great interest in radar remote sensing, since it has been observed that in agricultural soils the backscattering could be greatly affected by the directionality of the soil roughness (Wegmueller et al., 2011; Marzahn et al., 2012b).

Regarding to the DEMs obtained with TLS and SfM, it could be said that both techniques were valid to represent the surface roughness of the typical agricultural soils. Despite this, some limitations must be taken into account. On the one hand, the high accuracy and resolution of TLS was limited by the data acquisition geometry (scans positions) generating shadow regions (occlusions) without data, especially in the roughest soils. On the other hand, in spite of the good geometry of the data acquisition of SfM (from a lifting platform), the generated DEMs (and also the point

clouds) showed a certain smoothing behavior with respect to other techniques, which was particularly apparent when horizontal roughness parameters were calculated.

6.5. Conclusions

The results obtained demonstrate the ability of both TLS and SfM techniques to measure surface roughness over agricultural soils. This is considered relevant since the experimental setting enabled a direct comparison of profiles measured with different techniques, due to the precise co-registration achieved. Also, the experimental plots represented different tillage classes and were larger than in other studies published on this topic, which adds value to the results obtained. The agreement between the elevation profiles obtained with TLS and SfM when compared to those obtained with a nadir-looking profilometer was reasonable and RMSE values were below 10 mm for smooth and intermediate roughness conditions. Rough soils (Mouldboard Plough) were more challenging and RMSE values as high as 20 mm were obtained for this class. Yet, these differences were not that relevant when different roughness parameters were computed. Parameter s and to a lesser extent l showed similar values when measured with the different techniques. However, some other roughness parameters, more sensible to the spatial arrangement of height variations like $\rho'(0)$, F or T_S showed a loss of high frequency elevation information in TLS and especially in SfM data. This smoothening effect seems to be inherent to the technique in the case of SfM surveys and related to occlusions due to the oblique viewing geometry in the TLS data. The latter could be avoided if a nadir-looking observation were available. Altogether, both TLS and SfM provide very powerful 3D information that enables a detailed analysis of surface roughness directionality, which is very relevant for applications like radar scattering or hydrology and soil erosion processes.

Acknowledgment

This work was supported in part by the Spanish Ministry of Economy and Competitiveness under Grant BES-2012-054521, Project CGL2011-24336, Project CGL2015-64284-C2-1-R, and Project CGL2016-75217-R (MINECO/FEDER, EU).

CONCLUSIONS

This thesis focused on the characterization of soil surface roughness over agricultural soils, considering different aspects such as roughness parameterization, in-situ measurement techniques and radar remote sensing sensitivity to roughness scale. These works needs to be contemplated in the context of the different fields of Earth science where soil surface roughness intervenes, in which different research questions have been posed in the last years with different and complementary points of view. This research effort has tried to answer some of these questions and hopes to contribute to a better understanding of the soil surface roughness phenomenon on agricultural soils.

On a first analysis, the most widely used roughness parameters proposed in the literature were evaluated in detail, in order to ascertain their ability to discriminate between different soil surface roughness classes typical on tilled soils. Roughness parameters values obtained for different classes showed that vertical and combined parameters took higher values as tillage became rougher, while horizontal parameters showed no clear pattern. On the contrary, fractal dimensions took lower values (more auto-affine behavior) as tillage became rougher. With all this, the best roughness parameters to discriminate between different tillage classes were the vertical parameter *LD* and the combined *MUD*. On the other hand, the parameters most sensitive to rainfall action were the horizontal parameter *LS* and the crossover lengths l_{SMV} and l_{RMS}. It is also important to note that some of the evaluated parameters were strongly correlated, and thus provided very similar information about surface roughness state. In this regard, it is recommended to select rather simple parameters (i.e., *s* or *MUD*) than more complex ones that might mostly provide the same information. On the contrary, some other parameters were poorly correlated with the majority (i.e., l_{SMV}, *LS* or l_{ACF}) offering complementary information which could, therefore, be interesting for particular purposes.

As already explained, surface roughness has a clear multi-scale behavior and, on the other hand, surface roughness strongly affects the backscattering observed by radar sensors. Therefore, in this thesis different scaling issues were analyzed to determine the roughness scales involved in the backscattering process. The results obtained confirm a clear dependence between roughness measurement scales and parameter

values, which suggests that the most relevant roughness components for C-band backscatter ranged between 5 and 100 cm. When roughness scales shorter than 5 cm and larger than 1 m were filtered out from the original profiles, roughness parameters obtained did not provide additional enhancement to the correlation with backscatter nor in the goodness-of-fit of the Oh model. It is remarkable that some roughness parameters (i.e., *D*, F and $\rho'(0)$) were more stable and more strongly correlated with backscatter than those commonly used in radar applications (i.e., *s* and *l* parameters). This fact could open new possibilities in surface roughness characterization for backscatter modelling in agricultural soils.

In relation to this, the sample size required for an accurate estimation of surface roughness parameters for radar applications on agricultural soils was also assessed in this thesis. The results obtained evidence the aforementioned correlation between roughness scales shorter than 1 m and C-band backscatter. To accurately characterize surface roughness a minimum of 10 samples (1-m-long profiles) were required for *s* parameter, while 20 samples might still be not enough for estimating *l* due to its large spatial variability. In relation to this, the lower spatial variability of *s* caused a better fit of the Oh model than that of the IEM and GOM because of a higher variability of *l*. All in all, for the retrieval of soil moisture with radar data it is recommended the Oh model as long as a minimum of 10-15 1-m-long roughness profiles are available per field.

Finally, recently developed Terrestrial Laser Scanner (TLS) and Structure from Motion (SfM) 3D roughness measurement techniques were evaluated and compared in this thesis with the most typically used laser profilometer 2D technique for surface roughness characterization on different agricultural soils. The results showed a reasonable agreement between the elevation profiles obtained with TLS and SfM and those obtained with the laser profilometer. Also, when estimating different roughness parameters, *s* and to a lesser extent *l* showed similar values with the three techniques. However, some parameters like $\rho'(0)$, F or T_S showed a high sensitivity to high frequency roughness components lost in TLS and especially in SfM data. In the light of the results obtained, it could be concluded that both TLS and SfM techniques are sufficiently accurate and provide very powerful 3D information for characterizing surface roughness directionality on agricultural soils. The latter is important, since

roughness directionality has been shown to be very relevant for fields like radar remote sensing or soil surface hydrology and erosion processes.

Altogether, some guidelines about the most convenient parameters for surface roughness characterization in agricultural soil were presented. Also, the surface roughness scales involved in radar backscattering and the sample size required for an accurate estimation of roughness parameters for radar remote sensing applications was also addressed. And finally, the feasibility of different 3D measurement techniques for surface roughness characterization was evaluated. It is expected that the results obtained throughout this thesis will contribute to a better understanding of the surface roughness phenomenon in agricultural soils.

upna
Universidad Pública de Navarra
Nafarroako Unibertsitate Publikoa

CONCLUSIONES

Esta tesis doctoral se ha centrado en la caracterización de la rugosidad superficial en suelos agrícolas, considerando diferentes aspectos como la parametrización de la rugosidad, las técnicas de medición in-situ y la sensibilidad de la teledetección radar a la escala de rugosidad. Estos trabajos deben de comprenderse en el contexto de los diferentes campos de las ciencias de la tierra donde interviene la rugosidad superficial del suelo, sobre la que se han planteado diferentes cuestiones en los últimos años con diferentes y complementarios puntos de vista. Este esfuerzo investigador ha intentado responder alguna de estas preguntas y espera contribuir a una mejor comprensión del fenómeno de la rugosidad superficial en suelos agrícolas.

En un primer análisis, se ha realizado una evaluación detallada de los parámetros de rugosidad más utilizados en la literatura, con el objetivo de determinar su capacidad para discriminar entre las diferentes clases de rugosidad superficial del suelo típicas en suelos laboreados. Los valores de los parámetros de rugosidad obtenidos para las diferentes clases han mostrado que los parámetros verticales y combinados han arrojado mayores valores a medida que el laboreo se hacía más rugoso, mientras que los horizontales no han mostrado un patrón claro. Por el contrario, las dimensiones fractales mostraron valores más bajos (comportamiento más auto-afín) cuanto más rugoso era el laboreo. Con todo ello, los mejores parámetros de rugosidad para discriminar entre diferentes clases de laboreo han sido el parámetro vertical *LD* y el combinado *MUD*. Por otro lado, los parámetros más sensibles a la acción de la precipitación han sido el parámetro horizontal *LS* y las longitudes de cruce l_{SMV} y l_{RMS}. También es importante tener en cuenta que algunos de los parámetros evaluados han estado fuertemente correlacionados, y por lo tanto han proporcionado una información muy similar sobre el estado de la rugosidad superficial. En este sentido, se recomienda seleccionar parámetros más simples (*s* o *MUD*) frente a los más complejos que podrían proporcionar la misma información. Por el contrario, algunos otros parámetros estaban muy poco correlacionados con la mayoría (l_{SMV}, *LS* o l_{ACF}), ofreciendo información complementaria que, por lo tanto, podría resultar interesante para fines particulares.

Como se ha explicado anteriormente, la rugosidad superficial tiene un claro componente multi-scala y, por otro lado, la rugosidad superficial afecta fuertemente la

retrodispersión observada por los sensores radar. Debido a esto, en esta tesis doctoral se han analizado diferentes cuestiones de la escala para determinar las escalas de rugosidad que intervienen en el proceso de retrodispersión. Los resultados obtenidos confirman una clara dependencia entre las escalas de medición de la rugosidad y los valores de los parámetros, lo que sugiere que las componentes de rugosidad más relevantes para la retrodispersión en banda C oscilan entre 5 y 100 cm. Cuando las escalas de rugosidad menores de 5 cm y mayores de 1 m se han filtrado de los perfiles originales, los parámetros de rugosidad obtenidos no han proporcionado una mejora adicional en la correlación con la retrodispersión ni en el grado de ajuste del modelo de Oh. Es notable que algunos parámetros de rugosidad (D, F and $\rho'(0)$) han sido más estables y han tenido una mayor correlación con la retrodispersión que los parámetros comúnmente utilizados en aplicaciones radar (s y l). Este hecho podría abrir nuevas posibilidades en la caracterización de la rugosidad superficial para el modelado de la retrodispersión en suelos agrícolas.

En relación a esto, en esta tesis doctoral también se ha abordado el tamaño de muestra requerido para una estimación precisa de los parámetros de rugosidad para aplicaciones radar en suelos agrícolas. Los resultados obtenidos evidencian la antes mencionada correlación entre escalas de rugosidad menores a 1 m y la retrodispersión en banda C. Para caracterizar con precisión la rugosidad superficial, se han necesitado un mínimo de 10 muestras (perfiles de 1 m de largo) para el parámetro s, mientras que 20 muestras podrían no ser suficientes para estimar l debido a su gran variabilidad espacial. En relación a esto, la menor variabilidad de s ha provocado un mejor ajuste del modelo de Oh que el de IEM y GOM debido a una mayor variabilidad de l. Con todo ello, para la estimación de la humedad del suelo con datos radar se recomienda el modelo de Oh, siempre que haya un mínimo de 10-15 perfiles de rugosidad de 1 m de largo disponibles por parcela.

Por último, en esta tesis doctoral se han evaluado y comparado las técnicas de medición de rugosidad 3D recientemente desarrolladas de láser escáner terrestre (TLS) y la denominada "Structure from Motion" (SfM) con la técnica 2D de perfilómetro láser, más utilizada para la caracterización de la rugosidad superficial en diferentes suelos agrícolas. Los resultados han mostrado un ajuste razonable entre los perfiles de elevación obtenidos con TLS y SfM y los obtenidos con el perfilómetro láser. Además, al estimar los diferentes parámetros de rugosidad, s y, en menor

medida, l han mostrado valores similares con las tres técnicas. Sin embargo, algunos parámetros como $\rho'(0)$, F o T_S han mostrado una alta sensibilidad a la pérdida de componentes de rugosidad de alta frecuencia en los datos obtenidos con TLS y, sobre todo, con SfM. En función de los resultados obtenidos, se podría concluir que ambas técnicas TLS y SfM son suficientemente precisas y proporcionan una poderosa información 3D para caracterizar la direccionalidad de la rugosidad superficial en suelos agrícolas. Esto último es importante, ya que se ha demostrado que la direccionalidad de la rugosidad es muy relevante para campos como la teledetección radar o los procesos hidrológico-erosivos de la superficie del suelo.

Con todo esto, se han presentado algunas pautas sobre los parámetros más apropiados para la caracterización de la rugosidad superficial en suelos agrícolas. Además, también se han abordado las escalas de rugosidad involucradas en la retrodispersión radar y el tamaño de muestra necesario para una precisa estimación de los parámetros en aplicaciones de teledetección radar. Y finalmente, se ha evaluado la viabilidad de diferentes técnicas de medición 3D para la caracterización de la rugosidad superficial. Se espera que los resultados obtenidos a lo largo de esta tesis doctoral contribuyan a una mejor comprensión del fenómeno de la rugosidad superficial en suelos agrícolas.

upna
Universidad Pública de Navarra
Nafarroako Unibertsitate Publikoa

ONDORIOAK

Doktore-tesi hau nekazal lurreko gainazalaren zimurtasuna ezaugarritzean zentratu da, alderdi desberdinak kontuan hartuz, hala nola, zimurtasunaren parametrizazioa, in-situ neurtzeko teknikak eta teledetekzioaren sentikortasuna zimurtasunaren eskalaren arabera. Lan horiek lur gainazalaren zimurtasunak esku hartzen duen lurreko zientzien alorreko testuinguruan ulertu behar dira, azken urteotan hainbat gai planteatu baitira ikuspuntu osagarri eta desberdinekin. Ikerketa ahalegin honek galdera horietako batzuei erantzun nahi izan die, nekazal lurreko gainazalaren zimurtasunaren fenomenoa hobeto uler dadin.

Lehenengo azterketan, literaturan gehien erabili izan diren zimurtasun parametroen ebaluazio zehatza egin da, nekazal lurretan ohikoak diren gainazalaren zimurtasun klase desberdintasunak bereizteko duten gaitasuna zehazteko helburuarekin. Klase desberdinetarako lortutako zimurtasun parametroen balioek erakutsi dute parametro bertikalek eta konbinatuek balio handiagoa eman dutela laborantza gero eta zimurragoa izatean, horizontalek, ordea, ez dute patroi argirik erakutsi. Dimentsio fraktalek, aldiz, balio baxuagoak erakutsi dituzte (auto-afinagoa den portaera) laborantza gero eta zimurragoa izatean. Horrekin guztiarekin, *LD* parametro bertikala eta *MUD* konbinatua izan dira parametrorik onenak, era bateko edo besteko laborantzak bereizteko. Bestalde, euriaren ondorioz *LS* parametro horizontala eta l_{SMV} eta l_{RMS} gurutze luzerak izan dira parametrorik sentikorrenak. Garrantzitsua da, halaber, aztertutako parametro batzuk biziki korrelazionatuta egon direla aintzat hartzea, eta, hortaz, gainazaleko zimurtasunaren inguruan emandako informazioa oso antzekoa izan dela. Horren harira, konplexuagoak beharrean, parametro sinpleagoak aukeratzea (*s* edo *MUD*) gomendatzen da, informazio bera eman baitezakete. Aitzitik, gehiengoarekin korrelazio gutxi duten beste hainbat parametrok (l_{SMV}, *LS* edo l_{ACF}) helburu partikularretarako interesgarria izan daitekeen informazio osagarria eskaintzen dute.

Aitzin aipatu moduan, gainazalaren zimurtasunak multi-eskala osagai argia du, eta, bestalde, gainazalaren zimurtasunak radar sentsoreek behatutako erretrodispertsioan eragin handia du. Hori dela eta, doktore-tesi honetan erretrodispertsioan parte hartzen duten zimurtasun eskalak zehazteko zenbait gai aztertu dira. Jasotako emaitzek zimurtasunaren neurketa eskalaren eta parametroen balioen arteko

menpekotasun argia egiaztatu dute, C bandako erretrodispertsioan zimurtasun osagairik nabarmenena 5 eta 100 cm artekoa dela iradokitzen dutelarik. Bestalde, 5 cm baino gutxiagoko eta 1 m baino gehiagoko zimurtasun eskalak jatorrizko profiletatik iragazi direnean, lortutako zimurtasun parametroek ez dute hobekuntza gehigarri bat eman erretrodispertsioaren korrelazioan, ezta Oh modeloko egokitze mailan ere. Nabarmena da zimurtasun parametro batzuk (D, F eta $\rho'(0)$) radar aplikazioetan erabili ohi diren parametroak (s eta l) baino egonkorragoak eta korrelazio altuagoa izan dutela. Horrek nekazal lurreko gainazalaren zimurtasuna ezaugarritzeko aukera berriak ireki ditzake erretrodispertsioa modelizatzeko nekazal lurretan.

Horrekin lotuta, doktore-tesi honetan nekazal lurretan radar aplikazioentzat zimurtasun parametroen estimazio zehatza lortzeko behar den laginaren tamainari heldu zaio. Lortutako emaitzek agerian utzi dute aurretik aipatutako 1 m baino gutxiagoko zimurtasun eskalak eta C bandako erretrodispertsioaren arteko korrelazioa. Gainazalaren zimurtasuna zehaztasunez ezaugarritzeko, gutxienez 10 lagin behar izan dira s parametroarentzat (1 m luzerako profilak), l estimatzeko, ordea, 20 lagin ez lirateke nahikoak izango, bere aldakortasun espazial handia dela eta. Horren arabera, s parametroaren aldakortasun txikiagoak Oh modeloaren doitzea ekarri du, IEM eta GOM modeloen gainetik, l parametroaren aldakortasun handiagoa dela medio. Horrekin guztiarekin, radar datuekin gainazalaren hezetasuna estimatzeko Oh eredua gomendatzen da, betiere, 1 m luzerako 10-15 profil partzela bakoitzeko eskuragarri baldin badira.

Azkenik, doktore-tesi honetan ebaluatu eta alderatu dira; alde batetik, berriki garatutako zimurtasuna neurtzeko “Terrestrial Laser Scanneer” (TLS) eta “Structure from Motion” (SfM) 3D teknikak; eta, bestetik, nekazal lurren gainazalaren zimurtasuna ezaugarritzeko gehien erabiltzen den laser profilometroa 2D teknika. Emaitzek doitze egokia erakutsi dute TLS eta SfM teknikekin lortutako altuera profilen eta laser profilometroarekin lortutakoen artean. Gainera, zimurtasun parametroak estimatzean, s parametroak eta, maila apalago batean, l parametroak balio berdintsuak erakutsi dituzte hiru teknikekin. Hala ere, parametro batzuek, $\rho'(0)$, F edo T_S, kasu, maiztasun handiko zimurtasun osagaien galerarekiko sentikortasun altua erakutsi dute TLS bidez jasotako datuetan, eta, batez ere, SfM teknikarekin jasotakoetan. Lortutako emaitzen arabera, ondoriozta daiteke biak ala biak, TLS eta

SfM, direla behar adina zehatz eta 3D informazio sendoa ematen dutela gainazalaren zimurtasuna nekazal lurretako norabidea ezaugarritzeko. Azken hori garrantzitsua da; izan ere, erakutsi dute zimurtasunaren norabidea oso esanguratsua dela teledetekzio radarraren alorrean edota lurreko higadura prozesu hidrologikoetan.

Horrekin guztiarekin, nekazal lurren gainazaleko zimurtasuna ezaugarritzeko parametro egokienen inguruko hainbat jarraibide aurkeztu dira. Horrez gain, landu dira, bai radar erretrodispertsioan parte hartzen duten zimurtasun eskalak, bai zimurtasun parametroen estimazio zehatz bat egiteko beharrezko lagina teledetekzio aplikazioetarako. Eta, azkenik, gainazaleko zimurtasuna ezaugarritzeko 3D teknika desberdinen bideragarritasuna ebaluatu da. Horrenbestez, doktore-tesian zehar lortutako emaitzek nekazal lurren gainazaleko zimurtasunaren fenomenoa hobeto ulertzen lagunduko dute.

upna
Universidad Pública de Navarra
Nafarroako Unibertsitate Publikoa

REFERENCES

Abdel-Messeh, M., Quegan, S., 2000. Variability in ERS scatterometer measurements over land. IEEE Transactions on Geoscience and Remote Sensing, 38 (4), 1767-1776.

Aguilar, M.A., Aguilar, F.J., Negreiros, J., 2009. Off-the-shelf laser scanning and close-range digital photogrammetry for measuring agricultural soils microrelief. Biosystems Engineering, 103 (4), 504-517.

Allain, S., Ferro-Famil, L., Pottier, E., 2003. Surface parameters retrieval from polarimetric and multi-frequency SAR data. In In Proceedings of the International Geoscience and Remote Sensing Symposium (IGARSS), 1417-1419, Toulouse, France.

Allmaras, R.R., Burwell, R.E., Larson, W.E., Holt, R.F., 1966. Total porosity and random roughness of the interrow zone as influenced by tillage. USDA Conservation Research Report, 7, 1-14.

Álvarez-Mozos, J., Casalí, J., González-Audícana, M., Verhoest, N.E.C., 2005. Correlation between ground measured soil moisture and RADARSAT-1 derived backscattering coefficient over an agricultural catchment of Navarre (North of Spain). Biosystems Engineering, 92 (1), 119–133.

Álvarez-Mozos, J., González-Audícana, M., Casalí, J., Larrañaga, A., 2008. Effective versus measured correlation length for radar-based surface soil moisture retraival. International Journal of Remote Sensing, 29 (17-18), 5397-5408.

Álvarez-Mozos, J., Verhoest, N.E.C., Larrañaga, A., Casalí, J., González-Audícana, M., 2009. Influence of surface roughness spatial variability and temporal dynamics on the retrieval of soil moisture from SAR observations. Sensors, 9 (1), 463–489.

Álvarez-Mozos, J., Campo, M.T., Gimenez, R., Casali, J., Leibar, U., 2011. Implications of scale, slope, tillage operation and direction in the estimation of surface depression storage. Soil and Tillage Research, 111 (2), 142–153.

Armstrong, A.C., 1986. On the fractal dimensions of some transient soil properties. European Journal of Soil Science, 37 (4), 641–652.

Arvidsson, J., Bölenius, E., 2006. Effects of soil water content during primary tillage - laser measurements of soil surface changes. Soil and Tillage Research, 90 (1-2), 222–229.

Baghdadi, N., Holah, N., Zribi, M., 2006a. Calibration of the Integral Equation Model for SAR data in C-band and HH and VV polarizations. International Journal of Remote Sensing, 27 (4), 805-816.

Baghdadi, N., Zribi, M., 2006b. Evaluation of radar backscatter models IEM, OH and Dubois using experimental observations. International Journal of Remote Sensing, 27 (18), 3831-3852.

Baghdadi, N., Cerdan, O., Zribi, M., Auzet, V., Darboux, F., Hajj, M.E., Kheir, R.B., 2008a. Operational performance of current synthetic aperture radar sensors in mapping soil surface characteristics in agricultural environments: application to hydrological and erosion modelling. Hydrological Processes, 22 (1), 9-20.

Baghdadi, N., Zribi, M., Loumagne, C., Ansart, P., Anguela, T., 2008b. Analysis of TerraSAR-X data and their sensitivity to soil surface parameters over bare agricultural fields. Remote Sensing of Environment, 112 (12), 4370–4379.

Baghdadi, N., Dubois-Fernandez, P., Dupuis, X., Zribi, M., 2013. Sensitivity of main polarimetric parameters of multifrequency polarimetric SAR data to soil moisture and surface roughness over bare agricultural soils. IEEE Geoscience and Remote Sensing Letters, 10 (4), 731-735.

Baghdadi, N., Zribi, M., Paloscia, S., Verhoest, N.E.C., Lievens, H., Baup, F., Mattia, F., 2015. Semi-empirical calibration of the integral equation model for co-polarized L-band backscattering. Remote Sensing, 7 (10), 13626-13640.

Bai, X., He, B., Li, X., 2016. Optimum Surface Roughness to Parameterize Advanced Integral Equation Model for Soil Moisture Retrieval in Prairie Area Using Radarsat-2 Data. IEEE Transactions on Geoscience and Remote Sensing. 54 (2), 2437-2449.

Barber, M.E., Grings, F.M., Álvarez-Mozos, J., Piscitelli, M., Perna, P.A., Karszenbaum, H., 2016. Effects of spatial sampling interval on roughness parameters and microwave backscatter over agricultural soil surfaces. Remote Sensing. 8 (6), 458.

Bauer, T., Strauss, P., Grims, M., Kamptner, E., Mansberger, R., Spiegel, H., 2015. Long-term agricultural management effects on surface roughness and consolidation of soils. Soil and Tillage Research, 151, 28–38.

Barneveld, R.J., Seeger, M., Maalen-Johansen, I., 2013. Assessment of terrestrial laser scanning technology for obtaining high-resolution DEMs of soils. Earth Surface Processes and Landforms. 38 (1), 90-94.

Beckmann, P., Spizzichino, A., 1987. The Scattering of Electromagnetic Waves From Rough Surfaces. Norwood, MA, USA: Artech House.

Bertuzzi, P., Rauws, G., Courault, D., 1990. Testing roughness indices to estimate soil surface roughness changes due to simulated rainfall. Soil and Tillage Research, 17 (1-2), 87–99.

Boiffin, J., 1984. La dégradation structurale des couches superficielles sous l'action des pluies. Thèse de Docteur Ingénieur, Paris INA-PG, 320pp.

Borgeaud, M., Attema, E., Salgado-Gispert, G., Bellini, A., Noll, J., 1995. Analysis of bare soil surface roughness parameter with ERS-1 SAR data. In proceedings of the Symposium on the Extraction of Bio and Geophysical Parameters from SAR Data for Land Applications, 307–316, Toulouse, France.

Bretar, F., Arab-Sedze, M., Champion, J., Pierrot-Deseilligny, M., Heggy, E., Jacquemoud, S., 2013. An advanced photogrammetric method to measure surface roughness: Application to volcanic terrains in the Piton de la Fournaise, Reunion Island. Remote Sensing of Environment, 135, 1-11.

Bryant, R., Moran, M.S., Thoma, D.P., Holifield Collins, C.D., Skirvin, S., Rahman, M., Slocum, K., Starks, P., Bosch, D., González Dugo, M.P., 2007. Measuring surface roughness height to parameterize radar backscatter models for retrieval of surface soil moisture. IEEE Geoscience and Remote Sensing Letters. 4 (1), 137-141.

Bruzzone, L., Roli, F., Serpico, S.B., 1995. Extension of the Jeffreys-Matusita distance to multiclass cases for feature selection. IEEE Transactions on Geoscience and Remote Sensing 33 (6), 1318–1321.

Burrough, P.A., 1983a. Multiscale sources of spatial variation in soil. I. The application of fractal concepts to nested levels of soil variation. European Journal of Soil Science, 34 (3), 577–597.

Burrough, P.A., 1983b. Multiscale sources of spatial variation in soil. II. A non-Brownian fractal model and its application in soil survey. European Journal of Soil Science, 34 (3), 599–620.

Callens, M., Verhoest, N.E.C., 2004. Analysis of soil roughness measurements using a 25 m laser profiler and a 4 m wide meshboard. In Proceedings of the International Geoscience and Remote Sensing Symposium (IGARSS), 1653-1656, Anchorage, AK, USA.

Callens, M., Verhoest, N.E.C., Davidson, M.W.J., 2006. Parameterization of tillage-induced single-scale soil roughness from 4-m profiles. IEEE Transactions on Geoscience and Remote Sensing. 44 (4), 878-887.

Casalí, J., Gastesi, R., Álvarez-Mozos, J., De Santisteban, L.M., Lersundi, J.D.V. d., Giménez, R., Larrañaga, A., Goñi, M., Agirre, U., Campo, M.A., López, J.J., Donézar, M., 2008. Runoff, erosion, and water quality of agricultural watersheds in central Navarre (Spain). Agricultural Water Management, 95 (10), 1111–1128.

Castillo, R.P., James, M.R., Quinton, J.N., Taguas, E.V., Gómez, J.A., 2012. Comparing the accuracy of several field methods for measuring gully erosion. Soil Science Society of America Journal, 76 (4), 1319-1332.

Chi, Y., Yang, J., Bogart, D., Chu, X., 2012. Fractal analysis of surface microtopography and its application in understanding hydrologic processes. Transactions of the American Society of Agricultural and Biological Engineers, 55 (5), 1781–1792.

Cierniewski, J., Kazmierowski, C., Królewicz, S., 2015. Evaluation of the Effects of Surface Roughness on the Relationship Between Soil BRF Data and Broadband Albedo. IEEE Journal of Selected Topics in Applied Earth Observations and Remote Sensing, 8 (4), 1528-1533.

Croft, H., Anderson, K., Kuhn, N.J., 2009. Characterizing soil surface roughness using a combined structural and spectral approach. European Journal of Soil Science, 60 (3), 431–442.

Croft, H., Anderson, K., Brazier, R.E., Kuhn, N.J., 2013. Modeling fine-scale soil surface structure using geostatistics. Water Resources Research, 49 (4), 1858–1870.

Currence, H.D., Lovely, W.D., 1970. Analysis of soil surface roughness. Transactions of the American Society of Agricultural Engineers, 13 (6), 710–714.

Dalla Rosa, J., Cooper, M., Darboux, F., Medeiros, J.C., 2012. Soil roughness evolution in different tillage systems under simulated rainfall using a semivariogram-based index. Soil and Tillage Research, 124, 226–232.

Davidson, M.W.J., Toan, T.L., Mattia, F., Satalino, G., Manninen, T., Borgeaud, M., 2000. On the characterization of agricultural soil roughness for radar remote sensing studies. IEEE Transactions on Geoscience and Remote Sensing. 38 (2), 630-640.

Davidson, M.W.J., Mattia, F., Satalino, G., Verhoest, N.E.C., Le Toan, T., Borgeaud, M., Louis, J.M.B., Attema, E., 2003. Joint statistical properties of RMS height and correlation length derived from multisite 1-m roughness measurements. IEEE Transactions on Geoscience and Remote Sensing, 41 (7), 1651–1658.

Dobriyal, P., Qureshi, A., Badola, R., Hussain, S.A., 2012. A review of the methods available for estimating soil moisture and its implications for water resource management. Journal of Hydrology, 458-459, 110-117.

Dong, L., Baghdadi, N., Ludwig, R., 2013. Validation of the AIEM through correlation length parameterization at field scale using radar imagery in a semi-arid environment. IEEE Geoscience and Remote Sensing Letters. 10 (3), 461-465.

Dubois, P.C., van Zyl, J., 1995. Measuring Soil Moisture with Imaging Radars. IEEE Transactions on Geoscience and Remote Sensing. 33 (4), 915-926.

D'Urso, G., Menenti, M., 1996. Performance indicators for the statistical evaluation of digital image classifications. ISPRS Journal of Photogrammetry and Remote Sensing, 51 (2), 78–90.

Eltz, F.L.F., Norton, L.D., 1997. Surface roughness changes as affected by rainfall erosivity, tillage, and canopy cover. Soil Science Society of America Journal, 61 (6), 1746–1755.

European Spatial Agenci, 2016. EO Portal Directory, Satellite Missions Database. [Online]. Available: http://directory.eoportal.org/web/eoportal/satellite-missions.

Famiglietti, J.S., Wood, E.F., 1994. Multiscale modeling of spatially variable water and energy balance processes. Water Resources Research, 30 (11), 3061-3078.

Favalli, M., Fornaciai, A., Isola, I., Tarquini, S., Nannipieri, L., 2012. Multiview 3D reconstruction in geosciences. Computers & Geosciences, 44, 168-176.

Fung, A.K., Li, Z., Chen, K.S., 1992. Backscattering from a Randomly Rough Dielectric Surface. IEEE Transactions on Geoscience and Remote Sensing. 30 (2), 356-369.

Fung, A.K., 1994. Microwave Scattering and Emission Models and Their Applications. Norwell, MA, USA: Artech House.

Fung, A.K., 2015. Backscattering From Multiscale Rough Surfaces With Application to Wind Scatterometry. Norwood, MA, USA: Artech House.

Gallant, J.C., Moore, I.D., Hutchinson, M.F., Gessler, P., 1994. Estimating fractal dimension of profiles: A comparison of methods. Mathematical Geology, 26 (4), 455–481.

Gilley, J.E., Kootwitz, E.R., 1995. Random roughness assessment by the pin and chain method. Applied Engineering in Agriculture, 12 (1), 39-43.

Gilliot, J.M., Vaudour, E., Michelin, J., 2017. Soil surface roughness measurement: A new fully automatic photogrammetric approach applied to agricultural bare fields. Computers and Electronics in Agriculture, 134, 63-78.

Glira, P., PfeifeR, N., Briese, C., ReSSl, C., 2015. A correspondence framework for ALS strip adjustments based on variants of the ICP algorithm. Photogrammetrie – Fernerkundung – Geoinformation, 2015 (4), 275-289.

Gneiting, T., Ševcíková, H., Percival, D.B., 2012. Estimators of fractal dimension: Assessing the roughness of time series and spatial data. Statistical Science, 27 (2), 247–277.

Gomez, C., Hayakawa, Y., Obanawa, H., 2015. A study of Japanese landscapes using structure from motion derived DSMs and DEMs based on historical aerial photographs: New opportunities for vegetation monitoring and diachronic geomorphology. Geomorphology. 242, 11-20.

Govers, G., Takken, I., Helming, K., 2000. Soil roughness and overland flow. Agronomie, 20 (2), 131–146.

Hansen, B., Schjønning, P., Sibbesen, E., 1999. Roughness indices for estimation of depression storage capacity of tilled soil surfaces. Soil and Tillage Research, 52 (1-2), 103–111.

Helming, K., Römkens, M.J.M., Prasad, S.N., 1998. Surface roughness related processes of runoff and soil loss: A flume study. Soil Science Society of America Journal, 62 (1), 243–250.

Helming, K., Roth, C.H., Wolf, R., Diestel, H., 1993. Characterization of rainfall - microrelief interactions with runoff using parameters derived from digital elevation models (DEMs). Soil Technology, 6 (3), 273–286.

Heng, B.C.P., Chandler, J.H., Armstrong, A., 2010. Applying close range digital photogrammetry in soil erosion studies. The Photogrammetric Record. 25 (131), 240-265.

Huang, C., Bradford, J.M., 1992. Applications of a laser scanner to quantify soil microtopography. Soil Science Society of America Journal, 56 (1), 14–21.

James, M.R., Robson, S., 2012. Straightforward reconstruction of 3D surfaces and topography with a camera: Accuracy and geoscience application. Journal of Geophysical Research Earth Surface, 117, F03017.

Jester, W., Klik, A., 2005. Soil surface roughness measurement—methods, applicability, and surface representation. Catena. 64 (2-3), 174-192.

Joseph, A.T., Van Der Velde, R., O'Neill, P.E., Lang, R.H., Gish, T., 2008. Soil moisture retrieval during a corn growth cycle using L-band (1.6 GHz) radar observations. IEEE Transactions on Geoscience and Remote Sensing. 46 (8), 2365-2374.

Kamphorst, E.C., Jetten, V., Guérif, J., Pitkänen, J., Iversen, B. V, Douglas, J.T., Paz, A., 2000. Predicting depressional storage from soil surface roughness. Soil Science Society of America Journal, 64 (5), 1749–1758.

Kornelsen, K.C., Coulibaly, P., 2013. Advances in soil moisture retrieval from synthetic aperture radar and hydrological applications. Journal of Hydrology, 476, 460-489.

Laliberte, A.S., Herrick, J.E., Rango, A., Winters, C., 2010. Acquisition, orthorectification, and object-based classification of unmanned aerial vehicle (UAV) imagery for rangeland monitoring. Photogrammetric Engineering & Remote Sensing, 76 (6), 661-672.

Le Hégarat-Mascle, S., Zribi, M., Alem, F., Weisse, A., Loumagne, C., 2002. Soil moisture estimation from ERS/SAR data: Toward an operational methodology. IEEE Transactions on Geoscience and Remote Sensing. 40 (12), 2647-2658.

Lehrsch, G.A., Whisler, F.D., Römkens, M.J.M., 1988. Spatial variation of parameters describing soil surface roughness. Soil Science Society of America Journal, 52 (2), 311–319.

Liang, Z., Feng, Z., Guangxiang, X., 2012. Comparison of Fractal Dimension Calculation Methods for Channel Bed Profiles. Procedia Engineering, 28, 252–257.

Lievens, H., Vernieuwe, H., Álvarez-Mozos, J., de Baets, B., Verhoest, N.E.C., 2009. Error in radar-derived soil moisture due to roughness parameterization: An analysis based on synthetical surface profiles. Sensors, 9 (2), 1067-1093.

Lievens, H., Verhoest, N.E.C., De Keyser, E., Vernieuwe, H., Matgen, P., Álvarez-Mozos, J., De Baets, B., 2011. Effective roughness modelling as a tool for soil moisture retrieval from C- and L-band SAR. Hydrology and Earth System Sciences, 15, 151-162.

Linden, D.R., Van Doren Jr, D.M., 1986. Parameters for characterizing tillage-induced soil surface roughness. Soil Science Society of America Journal, 50 (6), 1560–1565.

Linden, D.R., Van Doren, D.M., Allmaras, R.R., 1988. A model of the effects of tillage-induced soil surface roughness on erosion. In proceedings of the ISTRO 11th International Conference: Tillage and Traffic in Crop Production, 373-378, Edinburgh, Scotland.

Liu, H.H., Molz, F.J., 1996. Discrimination of fractional Brownian movement and fractional Gaussian noise structures in permeability and related property distributions with range analyses. Water Resources Research, 32 (8), 2601–2605.

Magunda, M.K., Larson, W.E., Linden, D.R., Nater, E.A., 1997. Changes in microrelief and their effects on infiltration and erosion during simulated rainfall. Soil Technology, 10 (1), 57–67.

Malinverno, A., 1990. A simple method to estimate the fractal dimension of a self-affine series. Geophysical Research Letters, 17 (11), 1953–1956.

Mallet, C., Bretar, F., 2009. Full-waveform topographic lidar: State-of-the-art. ISPRS Journal of Photogrammetry and Remote Sensing, 64 (1), 1-16.

Mandelbrot, B.B., 1977. Fractals. Encyclopedia of Statistical Science.

Manninen, A.T., 2003. Multiscale surface roughness description for scattering modelling of bare soil. Physica A: Statistical Mechanics and its Applications, 319, 535-551.

Martinez-Agirre, A., Álvarez-Mozos, J., Giménez, R., 2016. Evaluation of surface roughness parameters in agricultural soils with different tillage conditions using a laser profile meter. Soil and Tillage Research. 161, 19-30.

Martinez-Agirre, A., Álvarez-Mozos, J., Lievens, H., Verhoest, N.E.C., 2017a. Influence of Surface Roughness Measurement Scale on Radar Backscattering in Different Agricultural Soils. IEEE Transactions on Geoscience and Remote Sensing. 55 (10), 5925-5936.

Martinez-Agirre, A., Álvarez-Mozos, J., Lievens, H., Verhoest, N.E.C., Giménez, R., 2017b. Influence of surface roughness sample size for C-band SAR backscattering applications on agricultural soils. IEEE Geoscience and Remote Sensing Letters, 14 (12), 2300-2304.

Martinez-Agirre, A., Álvarez-Mozos, J., Milenkovic, M., Pfeifer, N., Giménez, R., Valle Melón, J.M., Rodríguez Miranda, A., 2017c. Evaluation of Terrestrial Laser Scanner and Structure from Motion techniques for quantifying soil surface roughness parameters over agricultural soils. ISPRS Journal of Photogrammetry and Remote Sensing. Under Review.

Marzahn, P., Ludwig, R., 2009. On the derivation of soil surface roughness from multi parametric PolSAR data and its potential fir hydrological modeling. Hydrology and Earth System Sciences, 13 (3), 381-394.

Marzahn, P., Rieke-Zapp, D., Ludwig, R., 2012a. Assessment of soil surface roughness statistics for microwave remote sensing applications using a simple photogrammetric acquisition system. ISPRS Journal of Photogrammetry and Remote Sensing, 72, 80-89.

Marzahn, P., Seidel, M., Ludwig, R., 2012b. Decomposing Dual Scale Soil Surface Roughness for Microwave Remote Sensing Applications. Remote Sensing. 4 (7), 2016-2032.

Matthias, A.D., Fimbres, A., Sano, E.E., Post, D.F., Accioly, L., Batchily, A.K., Ferreira, L.G., 2000. Surface roughness effects on soil albedo. Soil Science Society of America Journal, 64 (3), 1035-1041.

Mattia, F., Davidson, M.W.J., Le Toan, T., D'Haese, C.M.F., Verhoest, N.E.C., Gatti, A.M., Borgeaud, M., 2003. A comparison between soil roughness statistics used in surface scattering models derived from mechanical and laser profilers. IEEE Transactions on Geoscience and Remote Sensing. 41 (7), 1659-1671.

Milenkovic, M., Pfeifer, N., Glira, P., 2015. Applying terrestrial laser scanning for soil surface roughness assessment. Remote Sensing. 7 (2), 2007-2045.

Mirzaei, M., Ruy, M.S., Ziarati, T., Salehi, A., 2012. Monitoring of soil roughness caused by rainfall using stereo-photogrammetry. International Research Journal of Applied and Basic Sciences, 3 (2), 322-338.

Moreira, J.G., Da Silva, J.K.L., Kamphorst, S.O., 1994. On the fractal dimension of self-affine profiles. Journal of Physics A: Mathematical and General, 27 (24), 8079–8089.

Moreno, R.G., Álvarez, M.C.D., Alonso, A.T., Barrington, S., Requejo, A.S., 2008. Tillage and soil type effects on soil surface roughness at semiarid climatic conditions. Soil and Tillage Research, 98 (1), 35–44.

Mosbrucker, A.R., Major, J.J., Spicer, K.R., Pitlick, J., 2017. Camera system considerations for geomorphic applications of SfM photogrammetry. Earth Surface Processes and Landforms. 42 (6), 969-986.

Mushkin, A., Gillespie, A.R., 2005. Estimating sub-pixel surface roughness using remotely sensed stereoscopic data. Remote Sensing of Environment, 99 (1-2), 75–83.

Nouwakpo, S.K., Weltz, M.A., McGwire, K., 2016. Assessing the performance of structure-from-motion photogrammetry and terrestrial LiDAR for reconstructing soil surface microtopography of naturally vegetated plots. Earth Surface Processes and Landforms, 41 (3), 308-322.

Ogilvy, J.A., Foster, J.R., 1989. Rough surfaces: gaussian or exponential statistics?. Journal of Physics D: Applied Physics, 22 (9), 1243–1251.

Oh, Y., Sarabandi, K., Ulaby, F.T., 1992. An Empirical Model and an Inversion Technique for Radar Scattering from Bare Soil Surfaces. IEEE Transactions on Geoscience and Remote Sensing. 30 (2), 370-381.

Oh, Y., Kay, Y.C., 1998. Condition for precise measurement of soil surface roughness. IEEE Transactions on Geoscience and Remote Sensing. 36 (2), 691-695.

Otepka, J., Ghuffar, S., Waldhauser, C., Hochreiter, R., Pfeifer, N., 2013. Georeferenced point clouds: A survey of features and point cloud management. ISPRS International Journal of Geo-Information, 2 (4), 1038-1065.

Panciera, R., Tanase, M.A., Lowell, K., Walker, J.P., 2014. Evaluation of IEM, dubois, and oh radar backscatter models using airborne L-Band SAR. IEEE Transactions on Geoscience and Remote Sensing. 52 (8), 4966-4979.

Pardini, G., 2003. Fractal scaling of surface roughness in artificially weathered smectite-rich soil regoliths. Geoderma, 117 (1-2), 157–167.

Pauwels, V.R.N., Hoeben, R., Verhoest, N.E.C., De Troch, F.P., 2001. The importance of the spatial patterns of remotely sensed soil moisture in the improvement of discharge predictions for small-scale basins through data assimilation. Journal of Hydrology, 251 (1-2), 88-102.

Paz-Ferreiro, J., Bertol, I., Vidal Väzquez, E., 2008. Quantification of tillage, plant cover, and cumulative rainfall effects on soil surface microrelief by statistical, geostatistical and fractal indices. Nonlinear Processes in Geophysics, 15, 575–590.

Perez-Gutierrez, C., Martinez-Fernandez, J., Sanchez, N., Alvarez-Mozos, J., 2007. Modeling of soil roughness using terrestrial laser scanner for soil moisture retrieval. In Proceedings of the International Geoscience and Remote Sensing Symposium (IGARSS), 1877-1880, Barcelona, Spain.

Pfeifer, N., Mandlburger, G., Otepka, J., Karel, W., 2014. OPALS - A framework for Airborne Laser Scanning data analysis. Computers, Environment and Urban Systems, 45, 125-136.

Planchon, O., Esteves, M., Silvera, N., 1998. Micro-relief induced by ridging: Measurement, modelling, consequences on overland flow and erosion. In Proceedings of the 16th World Congress Soil Science, 477 (31), Montpellier, France.

Raju, G., 2008. Radar Engineering. New Delhi, India: I.K. International Publishing House Pvt. Ltd.

Rodríguez-Caballero, E., Afana, A., Chamizo, S., Solé-Benet, A., Canton, Y., 2016. A new adaptive method to filter terrestrial laser scanner point clouds using morphological filters and spectral information to conserve surface micro-topography. ISPRS Journal of Photogrammetry and Remote Sensing. 117, 141-148.

Römkens, M.J.M., Wang, J.Y., 1986. Effect of tillage on surface roughness. Transactions of the American Society of Agricultural Engineers, 29 (2), 429–433.

Saleh, A., 1993. Soil roughness measurement: chain method. Journal of Soil and Water Conservation, 48 (6), 527–529.

Skriver, H., 2007. Signatures of polarimetric parameters and their implications on land cover classification. In Proceedings of the International Geoscience and Remote Sensing Symposium (IGARSS), 4195–4198, Barcelona, Spain.

Smith, M.W., 2014. Roughness in the Earth Sciences. Earth-Science Reviews, 136, 202–225.

Smith, M.W., Vericat, D., 2015. From experimental plots to experimental landscapes: topography, erosion and deposition in sub-humid badlands from Structure-from-Motion photogrammetry. Earth Surface Processes and Landforms, 40 (2), 1656-1671.

Snapir, B., Hobbs, S., Waine, T.W., 2014. Roughness measurements over an agricultural soil surface with Structure from Motion. ISPRS Journal of Photogrammetry and Remote Sensing. 96, 210-223.

Su, Z., Troch, P.A., De Troch, F.P., 1997. Remote sensing of bare surface soil moisture using EMAC/ESAR data. International Journal of Remote Sensing, 18 (10), 2105-2124.

Swain, P.H., King, R.C., 1973. Two effective feature selection criteria for multispectral remote sensing. LARS Technical Reports, Paper 39, 536–540.

Taconet, O., Ciarletti, V., 2007. Estimating soil roughness indices on a ridge-and-furrow surface using stereo photogrammetry. Soil and Tillage Research, 93 (1), 64–76.

Thoma, D.P., Moran, M.S., Bryant, R., Rahman, M., Holifield-Collins, C.D., Skirvin, S., Sano, E.E., Slocum, K., 2006. Comparison of four models to determine surface soil moisture from C-band radar imagery in a sparsely vegetated semiarid landscape. Water Resources Research, 42, W01418.

Thomsen, L.M., Baartman, J.E.M., Barneveld, R.J., Starkloff, T., Stolte, J., 2015. Soil surface roughness: comparing old and new measuring methods and application in a soil erosion model. Soil, 1, 399-410.

Ulaby, F.T., Batlivala, P.P., Dobson M.C., 1978. Microwave Backscatter Dependence on Surface Roughness, Soil Moisture, and Soil Texture. Part I-Bare Soil. IEEE Transactions on Geoscience and Remote Sensing, 16 (4), 286-295.

Ulaby, F.T., Moore, R.K., Fung, A.K., 1982. Microwave remote sensing: active and passive. Volume II. Radar remote sensing and surface scattering and emission theory. Reading, MA, USA: Addison-Wesley.

Ulaby, F.T., Dubois, P.C., Van Zyl, J., 1996. Radar mapping of surface soil moisture. Journal of Hydrology, 184 (1-2), 57-84.

Vázquez, E. V, Vieira, S.R., De Maria, I.C., González, A.P., 2009. Geostatistical analysis of microrelief of an Oxisol as a function of tillage and cumulative rainfall. Scientia Agricola, 66 (2), 225–232.

Verhoest, N.E.C., Lievens, H., Wagner, W., Álvarez-Mozos, J., Moran, M.S., Mattia, F., 2008. On the soil roughness parameterization problem in soil moisture retrieval of bare surfaces from synthetic aperture radar. Sensors, 8 (7), 4213–4248.

Vericat, D., Smith, M.W., Brasington, J., 2014. Patterns of topographic change in sub-humid badlands determined by high resolution multi-temporal topographic surveys. Catena, 120, 164-176.

Vermang, J., Norton, L.D., Baetens, J.M., Huang, C., Cornelis, W.M., Gabriels, D., 2013. Quantification of soil surface roughness evolution under simulated rainfall. Transactions of the American Society of Agricultural and Biological Engineers, 56 (2), 505–514.

Vermang, J., Norton, L.D., Huang, C., Cornells, W.M., Da Silva, A.M., Gabriels, D., 2015. Characterization of soil surface roughness effects on runoff and soil erosion rates under simulated rainfall. Soil Science Society of America Journal, 79 (3), 903-916.

Vidal Vázquez, E., Vivas Miranda, J.G., Paz González, A., 2005. Characterizing anisotropy and heterogeneity of soil surface microtopography using fractal models. Ecological Modelling, 182 (3-4), 337–353.

Vidal Vázquez, E., Miranda, J.G. V, González, A.P., 2007. Describing soil surface microrelief by crossover length and fractal dimension. Nonlinear Processes in Geophysics, 14, 223–235.

Vivas Miranda, J.G., Paz González, A., Rubio, J.L., Morgan, R.P.C., Asins, S., Andreu, V., 2002. Fractal models for the description of soil surface roughness, in: Man and Soil at the Third Millennium. In Proceedings of the International Congress of the European Society for Soil Conservation, 2099–2112, Valencia, Spain.

Wagner, W., Blöschl, G., Pampaloni, P., Calvet, J.-., Bizzarri, B., Wigneron, J.-., Kerr, Y., 2007. Operational readiness of microwave remote sensing of soil moisture for hydrologic applications. Nordic Hydrology, 38 (1), 1-20.

Wegmüller, U., Santoro, M., Mattia, F., Balenzano, A., Satalino, G., Marzahn, P., Fischer, G., Ludwig, R., Floury, N., 2011. Progress in the understanding of narrow directional microwave scattering of agricultural fields. Remote Sensing of Environment, 115 (10), 2423-2433.

Woodget, A.S., Carbonneau, P.E., Visser, F., Maddock, I.P., 2015. Quantifying submerged fluvial topography using hyperspatial resolution UAS imagery and structure from motion photogrammetry. Earth Surface Processes and Landforms, 40 (1), 47-64.

Xingming, Z., Kai, Z., Xiaojie, L., Yangyang, L., Jianhua, R., 2014. Improvements in farmland surface roughness measurement by employing a new laser scanner. Soil and Tillage Research, 143, 137–144.

Zhao, L., Wang, L., Liang, X., Wang, J., Wu, F., 2013. Soil Surface Roughness Effects on Infiltration Process of a Cultivated Slopes on the Loess Plateau of China. Water Resources Management. 27 (14), 4759-4771.

Zhixiong, L., Nan, C., Perdok, U.D., Hoogmoed, W.B., 2005. Characterisation of soil profile roughness. Biosystems Engineering, 91 (3), 369–377.

Zobeck, T.M., Onstad, C.A., 1987. Tillage and rainfall effects on random roughness: A review. Soil and Tillage Research, 9 (1), 1–20.

Zobeck, T.M., Popham, T.W., 1998. Wind erosion roughness index response to observation spacing and measurement distance. Soil and Tillage Research, 45 (3), 311-324.

Zribi, M., Dechambre, M., 2003. A new empirical model to retrieve soil moisture and roughness from C-band radar data. Remote Sensing of Environment, 84 (1), 42–52.

Zribi, M., Baghdadi, N., Holah, N., Fafin, O., Guérin, C., 2005. Evaluation of a rough soil surface description with ASAR-ENVISAT radar data. Remote Sensing of Environment, 95 (1), 67-76.

Zribi, M., Sahnoun, M., Baghdadi, N., Le Toan, T., Ben Hamida, A., 2016. Analysis of the relationship between backscattered P-band radar signals and soil roughness. Remote Sensing of Environment, 186, 13-21.